2012

Strategies for real time reservoir management

Yuanyuan Shuai
Louisiana State University and Agricultural and Mechanical College

STRATEGIES FOR REAL TIME RESERVOIR MANAGEMENT

A Dissertation
Submitted to the Graduate Faculty of the
Louisiana State University and
Agricultural and Mechanical College
in partial fulfillment of the
requirements for the degree of
Doctor of Philosophy

in

The Craft & Hawkins Department of Petroleum Engineering

by
Yuanyuan Shuai
Bachelor in Marine and Offshore Engineering, China University of Petroleum, 2005
M.S. in Petroleum Engineering, China University of Geosciences, 2007
August 2012

Dedication

This dissertation is dedicated to my parents, for their unconditional love, to my husband, for the encouragement that he gave and the sacrifices he has made, to my son, who brightens up my life by coming into this world.

Acknowledgments

I would like to express the deepest appreciation to my advisor, committee chair, Dr. Christopher D. White, for his valuable guidance, unflinching encouragement and support. Without his supervision and persistent help this dissertation would not have been possible. Above all and most needed, he gave me the freedom to pursue my own research directions and encouraged me to be an independent researcher. I also thanks him for being so patient, understanding and comforting during the most difficult moment in my life. I am indebted to him more than he knows. I would also like to extend my appreciations to other committee members, Dr. Karsten Thompson, Dr. Mayank Tiyaki, Dr. Hongchao Zhang and Dr. Sam Bentley, who spent a lot of time reading and commenting on this dissertation.

Before I came to LSU, I had the opportunity to study in the petroleum department of University of Tulsa (TU). I would like to thanks all the teachers of LSU and TU from whom I had the privilege to learn something. Especially Professor Albert Reynolds, whose history matching class enabled me to develop a basic understanding on my research subject. I would also like to thank the departments of petroleum in LSU and TU for providing me the finical support.

In the past two years, I had opportunities to intern with Calpine Corporation and Shell Oil Company. I would like to thank Mr. Tim Conant, Mr. Julio Garcia, Mr. Fred Wadsen, Mr. Cox Bert and Mr. Inikori Solomon who made these internships possible.

Many thanks to all my colleagues and friends in LSU and TU for their company and help. I would especially thanks Ting Sun, Yin Feng, Chaohui Chen, Sy Do and Mei Han, for their valuable discussions and help on my research.

Finally, I would like to thank my parents and my parents in law, for their support, care and assistance.

Table of Contents

List of Tables

List of Figures

Abstract

Real–time reservoir management is developed to manage a shrinking labor force and rising demand on energy supply. This dissertation seeks good strategies for real–time reservoir management. First, two simulator–independent optimization algorithms are investigated: ensemble–based optimization (EnOpt) and bound optimization by quadratic approximation (BOBYQA). Multiscale regularization is applied to both to find appropriate frequencies for well control adjustment. Second, two gathered EnKF methods are proposed to save computational cost and reduce sampling error: gathered EnKF with a fixed gather size and adaptively gathered EnKF. Finally, oil price uncertainty is forecasted and quantified with three price forecasting models: conventional forecasting, bootstrap forecasting and sequential Gaussian simulation forecasting. The relative effect of oil price and its volatility on the optimization strategies are investigated.

A number of key findings of this dissertation are: (a) if multiscale regularization is not used, EnOpt converges to a higher net present value (NPV) than BOBYQA—even though BOBYQA uses second order Hessian information whereas EnOpt uses first order gradients. BOBYQA performs comparably only if multiscale regularization is used. Multiscale regularization results in a higher optimized NPV with simpler well control strategies and converges in fewer iterations; (b) gathering observations not only reduces the sampling errors but also saves significant amount of computational cost. In addition, adaptively gathered EnKF is superior to gathered EnKF with a fixed gather size when the prior ensemble mean is not near the truth; (c) it is shown that a good oil price forecasting model can improve NPV by more than four percent, and (d) instability in oil prices also causes fluctuation in optimized well controls.

Chapter 1
Introduction

A good understanding of reservoir management and its elements is important to the proper development and exploration of oil and gas reservoirs. This chapter gives a brief introduction to reservoir management and its major components, points out some problems existing in current real–time reservoir management and the approaches used in this study to solve these problems.

1.1 Introduction to reservoir management

Definition. Reservoir management has been defined by many authors. Fowler et al. (1996) summarized reservoir management as "a sequence of resource–deployment decisions made to maintain optimum economic recovery of petroleum." Gringarten (1998) defined reservoir management as "the application of available technology and knowledge to a reservoir system in order to control operations and maximize economic recovery within given management environment. " Thakur (1996) described reservoir management is to "rely on use of financial, technological, and human resources, while minimizing capital investments and operating expenses to maximize economic recovery of oil and gas from a reservoir." Overall, the whole purpose of reservoir management is to help oil companies make the best decisions to meet specific objective using all the available resources.

Process. The process of reservoir management generally begins with reservoir characterization or reservoir modeling. It requires construction of a single "most probable" simulation model, or an ensemble of simulation models to represent or estimate the real reservoir by integrating both static and dynamic knowledge about the reservoir. Once the reservoir model is constructed, verification is needed to make sure that the reservoir model is consistent with all the available information and can reproduce all the data used in characterization

process, including seismic, logs, well tests, and production data (Gringarten 1998). After the simulation model(s) are developed, they are used as input for subsequent development planning or decision making such as defining well counts, types, locations and production strategies. Once the field is developed and goes on production, data (such as geomechanics, traces, production logs, well tests data) are then collected and analyzed. These data are used as the feedback from the reservoir for calibrating the simulation models and revising plans and strategies. It is clear that reservoir management is an iterative process which must be repeated when new information is available.

Challenges. There has been a growing demand on energy due to the growing affluence as well as growing population. Because the "easy" oil fields are gone and existing fields are becoming more and more depleted, oil companies are starting to invest in complex and difficult fields. With the limited availability of finances and changing business needs, it becomes even harder to continue producing the existing field economically. Another challenge oil industry is facing is the shrinking labor force. The average oil worker is older than 50, and replacing the retirees becomes difficult as fewer and fewer people want to work in boom-and-bust business (Steinhubl and Klimchuk 2008). To manage the rising oil demand and shrinking labor force, integrating new technologies and strategies into conventional reservoir management is necessary.

1.2 Reservoir management in real time

To meet the rising demand on oil energy and manage the shirking labor force, the oil industry is making great effort to build the required infrastructure for managing the reservoir in real time. For example, with the implementation of permanent downhole gauges, information on pressure, temperature and other field conditions which were measured in days and months now are measured in seconds and minutes. Installation of inflow control valves on intelligent wells also provides flexibility to control each well segment independently—enabling improved recovery under complex reservoir conditions. Other examples include building onshore op-

eration rooms to remotely support drilling or production work process in realtime. Such infrastructure applications coupled with the advances in computers, internet and other information technologies make the real–time reservoir management within reach (Verma and Cline 2005).

The real–time reservoir management concept is also referred as closed–loop reservoir management, smart field, digital oil field, e-field, i-field and field of the future. Here, we use an E&P company's[1] smart field philosophy to illustrate the real time reservoir management concept. As it is shown in Fig. 1.1, the process of real–time reservoir management is a continuous cycle to optimize the the economic performance of the oil and gas field. It mainly integrates the following steps: (1) high frequency data are measured using downhole gauges and sensors and transmitted to the engineering office; (2) the measured data are used to update reservoir simulation models, which are then used to generate options for short and long term actions; (3) people from different disciplines are gathered to evaluate the options, and the decisions, and (4) the final decisions are implemented through intelligent well system. The intelligent well technology provides the capability to remotely monitor and manage multiple production zones independently through inflow control valves (ICV), reducing the cost of well interventions, accelerating the production and reducing the injection and production of water.

Compared with conventional reservoir management, real–time reservoir management has advantages such as (1) it can prevent hazardous outcomes and improve safely because problems can be identified and responded every quickly, and the remote sensors enable the operators to operate from a distance; (2) it helps the oil industry to manage the shrinking labor force by transforming oil operations from "labor intensive" to "technology driven" (Steinhubl and Klimchuk 2008); (3) most of all, the continuous reservoir model updating and optimization process is expected to improve the oil recovery and increase profit on developing complex reservoirs. Overall, real–time reservoir management is able to accelerate production through

[1]Shell Exploration & Technology Co.

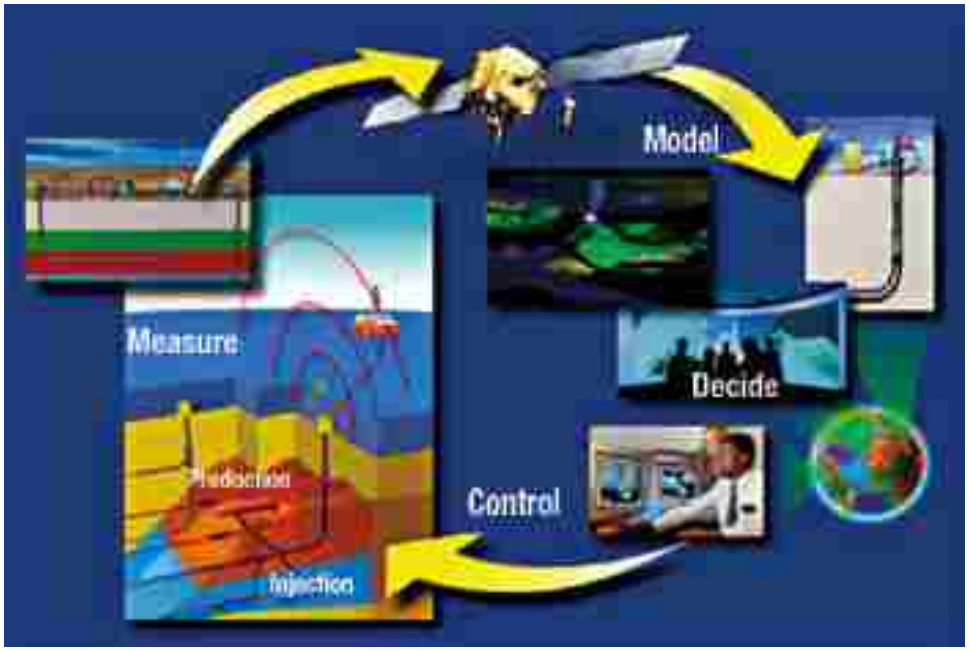

Figure 1.1: Shell's smart field philosophy includes the measure-model-decide-control loop (Dolle et al. 2006). First, high frequency data are measured using downhole gauges and sensors and transmitted to the engineering office; second, the measured data are used to update reservoir simulation models, which are then used to generate options for short and long term actions; third, people from different disciplines are gathered to evaluate the options, and the decisions, and, fourth, the final decisions are implemented through intelligent well system.

intelligent tools such as sensors, hardware, communication IT and software while reducing production costs and human resource requirements.

1.3 Computer assisted history matching

As mentioned earlier, the ultimate goal of reservoir management is to enable oil companies make the best decisions so that they can produce oil and gas reservoir effectively and profitability. The ability to make the best decisions relies predicting the consequence of implementing these decisions. The predication process is usually performed by running the plausible, estimated simulation model(s) on reservoir simulator. Thus, a good selection of reasonable simulation model(s) is one of the key components for a successful reservoir management. To better represent the actual reservoir, the estimated model(s) must be consistent with all available information. If not, the model(s) should be adjusted until it closely repro-

duces the past behavior of the reservoir. This process is defined as history matching. History matching can be carried out either manually or automatically on computers.

Traditionally, history matching has been done manually by adjusting model–input parameters until a good match of production data is obtained. Parameters commonly adjusted includes permeability, porosity, relatively permeability end points, water oil contact, fluids' viscosity. Manual history matching is a trial-and-error process. With the adjusted parameters high interacting with each other, it can be very time consuming and difficult especially when the reservoir model is complex.

Alternatively, computer–assisted history matching is done under the assistance of a computer program, combining with reservoir engineers' experience and skills. The computer assisted history matching does save significant amount of man power, especially with the increasing computational power and decreasing hardware cost. Multiple simulation jobs can be carried out simultaneously using multiple machines. Even a single job can be executed in parallel, for greater speed, using high performing computers. Thus the reservoir engineer has more time to analyze input and output data, interpret simulation results, and make necessary changes to the history match process (Maschio and Schiozer 2005; Yang, Nghiem, and Card 2007).

Reservoir history matching is an inverse problem with very large number of unknown parameters. History matching is typically an underdetermined inversion of a nonlinear system; such inverses are nonunique, which means that different combinations of model parameter values may yield nearly identical match to historical data. When it is done manually, only a few parameters can be adjusted, and due to the time limitation, the manual history matching usually leads only to a single matched model (Maschio and Schiozer 2005; Yang, Nghiem, and Card 2007). Unlike manual history matching, computer assisted history matching can consider a large number of unknowns by using efficient numerical optimization algorithms. In addition, reservoir model uncertainty can be better captured with computer assisted history matching. Commonly, reservoir model uncertainty is quantified using a Monte Carlo

approach, through which multiple realizations are sampled based on the prior knowledge of the reservoir model. The uncertainties are then reduced by conditioning the prior model to reservoir dynamic data such as production data and interpreted 4D seismic data.

In real–time reservoir management, the history matching process is repeated whenever new data are available to keep the reservoir model up–to–data. Therefore, this is also referred as "continuous reservoir model updating" in some publications. After the reservoir models are updated, they are then used for the optimization of economic life–cycle performance. This type of model–based life–cycle optimization is also referred to as "model–based production optimization" which is further introduced in next section.

1.4 Model–based production optimization

Production optimization aims to maximize the economic performance of a reservoir by making the best development decisions regarding the well count, well type, well trajectory, well location, well injection and production schedules and so on. Traditionally, this has been done by reservoir engineers using trail–and–error method. But in real–time reservoir management, this is done by combining numerical reservoir simulator with some optimization algorithms. The optimization algorithms are used to maximize or minimize some objective function $g(x)$ by manipulating some parameter x. The parameters x could be the well coordinates of each well; it can also be a set of well controls such as bottom hole pressures, flow rates of each well, etc. For a smart well system, well control valves allow control of the flow of each zone layer independently; therefore x can also be the bottom hole pressure or flow rate of each perforation layer. The objective function $g(x)$ to be maximized includes net present value of the reservoir, the cumulative oil production rate, the reservoir sweep efficiency, etc. The objective function is evaluated by running reservoir simulators using the reservoir simulation models obtained from history matching. The well count and well location optimization problems are more complicated than well control optimization problems because, unlike well control parameters which can be treated as real numbers, well count and location are usu-

ally treated as integral optimization problems. The well location optimization is treated as integral optimization because, with the standard commercial simulator, it is not possible to simulate off–center wells at arbitrary location accurately, resulting in discontinuity of the search space.

Because there are always uncertainties associated with the reservoir model parameters, an ensemble of reservoir simulation models is commonly used to describe the uncertainty. To incorporate reservoir model uncertainty, production optimization is done over multiple realizations. It is generally accepted that optimizing the objective function under reservoir model uncertainty results in better, more robust, decision. When uncertainty is quantified, a range of possible outcomes of uncertain events are considered and assigned probabilities to generate a probability-density function of the objective functions.

1.5 Two optimization problems

As explained above, real–time reservoir management contains two key components. One is continuous reservoir model updating using the production measurements. The other is life–cycle optimization based on the latest uncertain reservoir models. In fact, both of these components are ill–posed optimal problems with nonunique solutions. The reservoir model updating minimizes the objective function composed of the mismatch between prior model parameters and updated reservoir model parameters, plus the mismatch between model predicting data and the measured data. The production optimization maximizes the objective function composed of profitability of the hydrocarbon reservoir.

The common used optimization methods fall into two categories: nongradient–based and gradient–based optimizations. For nongradient–based optimization, algorithms such as simulated annealing and the genetic algorithm have been investigated for many years (Quenes et al. 1993; Quenes, Bhagavan, and Travis 1994; Huang and Kelkar 1994; Bukhamsin, Farshi, and Aziz 2010). Nongradient–based methods are simulator–independent and therefore easy to couple with commercial softwares. Moreover, most of them are often posed as global op-

timization while gradient based methods tend to get stuck in local optimum. However, for large–scale problems, non–gradient methods converge slowly and are therefore expensive. For gradient–based optimization, the gradient of the objective function is needed to design the optimization variables. The adjoint method of sensitivity analysis is commonly used to compute the gradient of the objective function with respect to the optimization variables (Gao, Rajeswaran, and Nakagawa 2007; Sarma 2006; Chen et al. 2010). Because it converges fast and the computational cost is nearly independent of the number of unknown parameters (the number of adjoins is independent of the number of unknowns), it has been widely used in history matching and production optimization. However, this method requires detailed knowledge of the reservoir simulator and the cost of gradient computations (especially Hessians) may be high. Alternatively, ensemble–based method generates an ensemble of perturbed variables to approximate the gradient, which is simulator–independent and may be of acceptably low computational cost (Chen 2008). However, the accuracy of this method strongly depends on the nonlinearity of the problems and the size of ensemble. Developing a cost efficient algorithm for simultaneous production optimization under reservoir model uncertainty is necessary.

1.6 Research objective

As field application of true real–time reservoir management is in its infancy, challenges remain on finding efficient and cost–effective methods to accelerate routine field application of real–time reservoir management. This dissertation explores the possible solutions to the following questions.

- **What is the optimal frequency for updating of reservoir models and production strategies?**

  The value of high frequency data streams can only be realized if we are able to use them efficiently and accurately to update the reservoir model and to make crucial reservoir

engineering decisions. However, transmission, archiving and integration of high frequency data streams received from permanent downhole gauges remains a challenge. Too–frequent model updating and production optimization will pose significant computational burden to the system. On the other hand, excessively low–frequency model updating and production optimization can not keep the reservoir management up–to–date and therefore may not help with real–time decision making.

- **What is the optimal frequency for adjusting production controls?**

  Similar problems exist in finding the control adjustment frequency; adjusting well controls too frequently imposes unrealistic control burdens on operations, increasing well management cost. Moreover, high–frequency control adjustment increases the risk of optimization algorithms being trapped at local optima as the problem is more underdetermined. On the other hand, excessively low–frequency control adjustment may not truly optimize oil recovery.

- **How does oil price uncertainty impact on the optimal production controls?**

  Although the optimal control strategy is strongly depend on the unknown reservoir properties, uncertainty in oil price will certainly also play a role on decision making. The oil price uncertainty is always significant and it can not be eliminated, an accurate forecast on the volatility of future oil price is as important as reservoir characterization and reserves determinations because it enable the oil companies to make better decisions and allocate their capital efficiently.

1.7 Dissertation outline

Chen (2008) introduced and ensemble–based closed–loop optimization method which combines ensemble based data assimilation methods, including Ensemble Kalman Filter (EnKF) and Ensemble Random Maximum Likelihood (EnRML) with Ensemble–based Optimization

(EnOpt) for production optimization. Her results showed that ensemble–based closed–loop optimization is suitable for large scale problems because the use of ensemble greatly reduced the dimensionality of both data assimilation and production optimization.

The ensemble–based methods are the focus of this dissertation. Modifications and improvements are made to address the problems listed in section 1.6. This dissertation contains 8 chapters. A brief summary of each chapter is given as following.

Chapter 2 compares two simulator–independent optimization algorithms on single reservoir model optimization: the ensemble based optimization (EnOpt) and bound optimization by quadratic approximation (BOBYQA). The application of multiscale regularization to find the best well control frequency is also tested on these two methods. Mutiscale regularization starts optimization from the coarsest control scale (and thus, with the fewest number of control parameters) and refines successively using the coarse–scale solution as the initial guess of controls for next finer scale optimization. The refining process is terminated when no further improvement on the objective function is obtained. Multiscale regularization aims to avoid too frequent control adjustment by adding well control parameters hierarchically. In a synthetic case study, if multiscale regularization is not used, then EnOpt converges to a higher net value of production than BOBYQA even though BOBYQA uses second order Hessian information (EnOpt uses first order gradients). BOBYQA performes comparably only if multiscale regularization is used. After multiscale regularization, both methods obtain net value of production (NVP) that equal or exceed unregularized optimization, with simpler well control strategies and convergence in fewer iterations.

Chapter 3 reviews ensemble Kalman filter as a data assimilation approach and proposes gathering observations as a way to improve the stability and save computational cost of standard EnKF. In gathered EnKF method, if there is no significant change in observations compared to previous ensemble predictions, the measurements are stored instead of assimilated. Model updating is done only if the gathered data volume exceeds a specified threshold, or if the observations diverge from prior ensemble predictions significantly. Due

to the finite size of ensemble, sampling errors are introduced to the Kalman gain both from prior ensemble covariance and the perturbed observation, resulting in a negative bias of estimated ensemble covariance. In this chapter, we theoretically prove that the sampling errors introduced from the prior ensemble have the same effect for gathered and standard EnKF. However, by gathering the observations less errors are introduced from the perturbed observation resulting in a better estimated of the ensemble covariance. More over, gathered EnKF also reduces the computational costs of simulation restarts, file transfers and reading and writing required at each EnKF assimilation step. This method is first tested on a scalar case and then on a 2D synthetic reservoir history matching case. Both cases show that gathered EnKF is more efficient and stable than standard EnKF.

Only 2D synthetic reservoir models are used in chapter 2 and chapter 3 to demonstrate how the proposed methods work. A more realistic, complex reservoir model is needed for the further testaments. The Brugge "field case is a 3D synthetic complex reservoir field made available to participants by Netherlands Organization for Applied Scientific Research (TNO) in the preparation for SPE Applied Technology Workshop (ATW) (Chen and Oliver 2010; Peters et al. 2009), a benchmark project for closed–loop reservoir management, held in Brugge in June 2008. Since the Brugge field is the most "realistic", complex, 3D synthetic case that has been widely used for comparative study of alternative methods for reservoir history matching and model–based production optimization; it is also chosen as illustrative example in this dissertation. The detailed description of the Brugge field is given in chapter 4.

Chapter 5 focuses on improving the gathered EnKF proposed in chapter 3 to an adaptively gathered EnKF. In fact, as it is shown in chapter 5 through the Brugge field example, the gathered EnKF with a fixed gather size does not always works better than the standard EnKF. If the initial ensemble mean is not very close to the truth, the gathered EnKF with a large gather size may result in a slower convergence than the standard EnKF. If the mean is not close to the truth, neither would be the estimated covariance from the ensemble

close to the true covariance due to the nonlinear characteristic of the dynamic model. In such case, recursive updates keep the model on track and close to the true solution and therefore converge more quickly. To overcome this problem, an adaptively gathered EnKF is proposed in chapter 5. The method starts with a small gather size. Then, if the mean ensemble prediction is converging on the observations after assimilation, the gather size is doubled until it reaches a specified maximum interval. If the mean ensemble prediction is diverging from the observations, we reduce our gather size by half. The adaptively gathered EnKF can also be used to determine the optimal frequency for updating reservoir model and optimizing the production controls. It is reasonable to update the model more frequently at the beginning (when the mean is not near the truth and the uncertainty is relatively large). When the mean is near the truth and the uncertainty is small, corrections to the prior model are smaller, and high–frequency model updating may destroy ensemble diversity and cause filter divergence. Therefore, a larger time interval can be used for model updating and production optimization to save computational cost. The adaptively gathered EnKF is tested on the Brugge field. Results shows it works better than standard EnKF and gathered EnKF with a fixed gather size in terms of time saving and convergence.

Chapter 6 applies the proposed methods on the closed–loop frame work. In addition, three price forecasting models are used to quantify the price uncertainty: conventional forecasting, sequential Gaussian simulation and bootstrap sampling methods. Price uncertainty is included into the closed–loop frame work and tested on Brugge field. This allows posing questions about relations among price uncertainty and volatility, reservoir uncertainty, and control strategy, including

- What are the relative effects of price and technical uncertainty on optimization and value?
- As the level of price volatility and/or imposed trends change, how does the optimized control strategy change?

- How does the discount rate affect the optimized control strategies?

All of these are addressed in Chapter 6.

Chapter 7 discusses some topics of particular interest for future study, including using Karhunen-Loeve expansion to save the computational cost of Kalman gain in gathered EnKF, optimizing well control with an adaptive multiscale regularization method in which well controls are adjusted with a changing time interval, and extending ensemble–based methods for well location optimization by integrating off–center well simulation to standard simulator.

Chapter 8 summarizes the whole dissertation.

Chapter 2

Using Mutiscale Regularization to Obtain Realistic Optimal Control Strategies[2]

2.1 Introduction

The benefits of smart wells have been demonstrated in theoretical studies and practical applications (Brouwer et al. 2001; Jansen et al. 2002; Ramakrishnan 2007; van Essen et al. 2009; Meshioye et al. 2010; van Essen et al. 2010). These benefits can summarized as two types: (1) for highly heterogeneous reservoirs, smart wells can help avoid early water or gas breakthrough from high permeability zones, and (2) for multilateral wells (or monobore wells with multiple segments), smart wells provide flexibility to control each branch (or segment) of the well independently. Smart wells can do this because, unlike conventional wells, smart wells have permanent downhole sensors and controls. Those sensors provide realtime rates, pressures and temperatures; the control valves allow control of flow in each reservoir interval. The data feedback and inflow control valves (ICVs) are the key components of smart well systems. Based on the feedback, the downhole control valves are adjusted to suppress unwanted fluid production and increase oil recovery.

Optimization algorithms can be used to find the optimum valve settings. These methods can be categorized into two classes, gradient–free methods and gradient methods. Gradient–free methods do not rely on gradient information to guide the optimization search. Their primary benefits are their potential to find the global optimum and the ability to handle discrete design variables. Because they are capable of discrete parameter optimization, gradient–free methods are also used in well placement optimization (Onwunalu and Durlofsky 2010). A considerable disadvantage of gradient–free methods is that they require more function evaluations than gradient methods and converge slowly. For instance, Isebor (2009) compared gradient–free methods (including a genetic algorithm, general pattern search, and

[2] Portions of this chapter appeared in 2011 SPE conference paper no. 142043.

Hooke-Jeeves direct search) with a gradient method (sequential quadratic programming) for constrained production optimization. Isebor found that the gradient–free methods tend to be about an order of magnitude slower than the gradient method with adjoint–computed gradients. To improve the efficiency of gradient–free methods, one should combine them with a local optimization method. Harding, Radcliffe, and King (1996) showed the combination of a genetic algorithm with sequential quadratic programming for local search outperforms the "pure" genetic algorithm. This was also observed by Isebor (2009).

In contrast, gradient methods take advantage of the gradient information to guide their search. Despite their inability to guarantee a global optimum, these methods converge much faster than gradient–free optimization. Common methods of this type used in production optimization are steepest ascent (Chen, Oliver, and Zhang 2009), conjugate gradient (Chaudhri et al. 2009), and sequential quadratic programming (Isebor 2009).

For gradient optimization, two approaches can be used to compute the gradients of objective function with respect to well control variables. One approach is to obtain the gradients using the adjoint equation. The other approach is to approximate the gradients using methods such as finite difference perturbation, simultaneous perturbation stochastic approximation, or EnOpt. Among all these methods, the adjoint method is the most robust and therefore the most efficient. For example, Chen et al. (2010) found that the adjoint method converges in less than 50 simulation runs if it was used to optimize production for a Brugge case with about 3600 well control variables. However, few commercial simulators provide adjoint gradients, and computing them requires detailed knowledge of the underlying simulator formulation. Unlike the adjoint method, approximate gradient methods can treat the simulator as a "black box." That is, it does not require the explicit knowledge of the dynamic fluid flow equations used in simulator source code. However, extra function evaluations — here, simulation runs — are required to approximate the gradients.

In this chapter, two simulator independent optimization algorithms were investigated: ensemble based optimization (EnOpt) and bound optimization by quadratic approximation

(BOBYQA). Multiscale regularization was applied to both to find appropriate frequencies for well control adjustment. Here, the properties of the reservoir simulation model are assumed to be known deterministically. Methods to incorporate uncertainty is discussed in subsequent chapters.

2.2 Optimization formulation and methods

2.2.1 Objective function.

As it is mentioned in the introduction chapter, the ultimate goal of reservoir management is to optimize some cost function $g(x)$ of the reservoir by adjusting the well control vectors x including, for example, well rates and bottom hole pressures (BHPs). The cost function can be the net present value (NPV) of the reservoir, the ultimate recovery and sweep efficiency, etc. The net present value is more common than others to be chosen as the the objective function (Wang, Li, and Reynolds 2009; Chen, Oliver, and Zhang 2009; Chaudhri et al. 2009). Assuming no cost for water injection, following Chaudhri et al. (2009), the formula for calculating NPV of a single two–phase (oil/water) reservoir model is given as:

$$g(x) = \sum_{i=1}^{N_t} \frac{P_o Q_{oi}(x) - P_w Q_{wi}(x)}{(1+r_\tau)^{\frac{t_i}{\tau}}}, \tag{2.1}$$

where, x is the N_x–long vector of control variables, and N_t is the number of control time steps; P_o and P_w are oil price and water disposal cost, respectively. The increments of oil and water production over time step i are Q_{oi} and Q_{wi}; r_τ is the discount rate for a time interval τ, and t_i is cumulative time at time step i. The objective function $g(x)$ gives NPV as a function of the well controls x. If the discount rate is set to zero, the denominator in Eq. 2.1 is unity and the objective function can be simplified to

$$g(x) = \sum_{i=1}^{N_t} \left[P_o Q_{oi}(x) - P_w Q_{wi}(x) \right]. \tag{2.2}$$

The objective function $g(x)$ in Eq. 2.2 is the net value of production (NVP), as no discount factor is considered.

2.2.2 Ensemble optimization.

EnOpt was first introduced in production optimization by Nwaozo (2006) and further investigated by Chen, Oliver, and Zhang (2009), Wang, Li, and Reynolds (2009), and Chaudhri et al. (2009). EnOpt can be applied for the optimization of a large number of well control settings. In addition, EnOpt can account for uncertain reservoir models without increasing the number of optimization parameters if an ensemble of reservoir models is available (as for EnKF history matches).

In Nwaozo (2006) and Wang, Li, and Reynolds (2009), the initial mean value of well controls of each well was randomly sampled from a uniform distribution with specified lower and upper bounds.The mean value was then perturbed to generate multiple realizations. With the mean value of each well available, the well control distribution of each well as a function of time was then generated by sampling a Gaussian distribution using the prescribed mean and a covariance function with a practical range of a. The covariance function is defined as:

$$C_{i,j} = \sigma^2 exp(\frac{-3|i-j|}{a}), \tag{2.3}$$

where σ is the standard deviation of the well control vector; a is the correlation range; i and j are the control step indices.

EnOpt (Chen, Oliver, and Zhang 2009) uses the steepest ascent method to iteratively update the well control vector x, and at each iteration uses the perturbed ensemble to approximate the gradients. At iteration l, after the N_e samples of well control vectors $x_{l,j}$ are randomly generated following the Gaussian distribution described in Eq. 2.3,N_e simulations are run, and then the net value of production $g(x_{l,j})$ is evaluated for all $j \in \{1 \dots N_e\}$ using Eq. 2.2; N_e is the number of models in the ensemble. Following Chen, Oliver, and Zhang (2009), the gradients of objective function NVP with respect to well controls can be approximated as

$$G_l^T \approx C_{x_l}^{-1} C_{x_l, g(x_l)}, \tag{2.4}$$

with

$$C_{x_l,g(x_l)} = \frac{1}{N_e - 1} \sum_{j=1}^{N_e} (x_{l,j} - \bar{x}_l)(g(x_{l,j}) - \bar{g}(x_l)), \tag{2.5}$$

and

$$C_{x_l} = \frac{1}{N_e - 1} \sum_{i,j=1}^{N_e} (x_{l,i} - \bar{x}_l)(x_{l,j} - \bar{x}_l)^T. \tag{2.6}$$

In Eq. 2.4, G_l is the vector of the gradients at iteration l. C_{x_l} is the covariance matrix of the well control variables x_l. $C_{x_l,g(x_l)}$ is the cross–covariance between well control variables $x_{l,j}$ and objective function $g(x_{l,j})$. In Eq. 2.5 and Eq. 2.6, $\bar{x}_l$ and $\bar{g}(x_l)$ indicate the mean values of well controls and the objective function for the ensemble at iteration l. They are

$$\bar{x}_l = \frac{1}{N_e} \sum_{j=1}^{N_e} x_{l,j},$$

and

$$\bar{g}(x_l) = \frac{1}{N_e} \sum_{j=1}^{N_e} g(x_{l,j}).$$

The steepest ascent equation for updating control variables x is

$$x_{l+1} = x_l + \frac{1}{\alpha_l} C_{x_l} C_{x_l} G_l^T, \tag{2.7}$$

where α_l is a tuning parameter to determine step size in the search direction at iteration l. Because the cross–covariance estimated using a perturbed ensemble may suffer from spurious correlation when the ensemble size is not sufficiently large, Chen, Oliver, and Zhang (2009) suggest using a matrix product of the covariance matrix of the control variables $R_{x_l} = C_{x_l} C_{x_l}$ for localization and smoothing. After substituting Eq. 2.4 to Eq. 2.7, the steepest ascent method used for ensemble optimization becomes

$$x_{l+1} = x_l + \frac{1}{\alpha_l} C_{x_l} C_{x_l,g(x_l)}.$$

2.2.3 Trust–region optimization.

BOBYQA is a package of Fortran subroutines written by Powell (2009). It is an iterative algorithm for solving bound–constrained problems in which the objective function can be

treated as a "black box" which evolves the reservoir state forward in time, and therefore these methods do not require modifications in the simulator to evaluate the objective function and its derivatives.The BOBYQA method (Powell 2009) applies a trust region optimization algorithm for bound–constrained nonlinear optimization. This method does not require derivative information for the objective function, nor does it explicitly approximate the derivatives. Instead, at each iteration it builds a local quadratic model $Q(x)$ of the objective function $g(x)$ by multivariate interpolation in combination with trust region techniques. The trust region is referred as a subset of the region of the objective function to be optimized using the approximate quadratic model. The region can either be expanded or contracted depending on the quality of the approximation of the quadratic function $Q(x)$ to $g(x)$. If the approximation is good, then the region is expanded; otherwise, the region is contracted.

The quadratic model employs the form,

$$Q(x+d) = Q(x) + d^T \bigtriangledown Q(x) + \frac{1}{2} d^T \bigtriangledown^2 Q(x) d,$$

which is solved by conditioning

$$Q(x_i) = g(x_i),\ \forall i \in \{1 \dots m\},$$

where d is the searching distance; $m \in \{(n+2) \dots (2n+1)\}$ and n is the total number of control variables. In our numerical experiments, $m = n + 2$ function evaluations are used to build the quadratic model $Q(x)$. The quadratic approximation Q is used to evaluate the needed derivatives.

The algorithm used by BOBYQA is an iterative algorithm that uses the least Frobenius norm updating strategy. For an $n \times n$ matrix A with entries $a_{ij}, i, j \in \{1 \dots n\}$, the Frobenius norm is

$$\|A\|_F = \sqrt{\sum_{i,j=1}^{n} a_{ij}^2}\ .$$

At each iteration, we solve the following optimization problem

$$\begin{aligned} \min \quad & \|\nabla^2 \ell_t\|_F \\ s.\,t. \quad & \ell_t(x^+) = 1,\ \ell_t(x) = 0, x \in \mathbf{X} \setminus x_t, \end{aligned} \tag{2.8}$$

where ℓ_t is a second order polynomial which needs to be determined, $\mathbf{X}$ is the current set of interpolation points, x^+ is a new point added to $\mathbf{X}$ and x_t is a point deleted from $\mathbf{X}$ (Powell 2009).

Then, the new model $Q^+(x)$ is updated by

$$Q^+(x) = Q(x) + \{g(x^+) - Q(x^+)\}\ell_t(x),$$

where $\ell_t(x)$ is the solution of (Eq. 2.8). Eq. 2.8 has a closed form solution, which can be computed by solving a linear system (Powell 2009).

Hence, only on the order of n function evaluations are needed to build the quadratic model, whereas normally $(n+1)(n+2)/2$ function evaluations are required for building a full quadratic model. Global convergence as well as the good local sampling for building the quadratic model are guaranteed by trust region techniques. Recent research (Moré and Wild 2009) in the computational optimization community indicates this trust region model method performs better than other optimization methods without explicit gradient computations.

Comparing with EnOpt, for small scale problems (less than a hundred control variables) we would expect BOBYQA to converge faster because it extracts local second order Hessian information, whereas EnOpt only uses first order gradient information. Moreover, at each iteration, it requires only one new function evaluation to update the local quadratic model whereas EnOpt requires an ensemble of function evaluations to update the gradients. However, BOBYQA is limited to medium scale optimization problems (a few hundred variables), because at least $n+2$ function evaluations are needed for building the first quadratic model; this is unacceptable for large scale problems (thousands of variables) with expensive function evaluations.

2.2.4 Multiscale regularization.

In production optimization, specifying the frequency of well control adjustment is a challenge. On one hand, high–frequency control adjustment imposes unrealistic control burdens on operations, increasing well management cost. In addition, high–frequency control implies many control variables, and many degrees of freedom increase the risk of an optimization algorithm being trapped at local optimum, as the problem is less well–determined. Moreover, some optimization algorithms can be computationally infeasible when the number of unknowns is large. On the other hand, excessively low–frequency control adjustment may not truly optimize oil recovery.

Multiscale regularization provides a way to address this problem. It starts optimization from the coarsest control scale (and thus, with the fewest number of control parameters) and refines successively using the coarse–scale solution as the initial guess of controls for next finer scale optimization. The refining process is terminated when no further improvement on the objective function is obtained.

In this chapter, we test the performance of ordinary multiscale regularization with the EnOpt and BOBYQA optimization methods. Lien et al. (2008) used adaptive multiscale regularization with an adjoint method for production optimization. Their method needs fine–scale gradients of the objective function as indicators to guide the refinement. We use ordinary multiscale regularization rather than gradient–based adaptive multiscale regularization for two reasons. First, the gradients calculated by both EnOpt and BOBYQA are approximate rather than true gradients, so that gradient adaptive multiscale regularization may not outperform ordinary multiscale regularization; we observed no improvement in our numerical experiments. Second, computing the fine–scale gradients at each refinement stage is expensive for BOBYQA method, requiring at least $n+2$ function evaluations to build the quadratic model.

The step–wise procedure for ordinary multiscale regularization is:

1. At scale $l = 1$ (the coarsest scale), one well control is used for each well; the number of unknowns is equal to the number of wells. The time step is set equal to the production (optimization) period. Initial values are assigned to each well control.

   START: DO WHILE LOOP (check stop criterion, see if further refinement improves NVP)

2. Find optimum solution for scale l using EnOpt or BOBYQA

3. $l = l+1$. Reduce time step by a factor of 2, and increase the number of control parameters by a factor of 2. Use the solution from step 2 as the initial well control for this scale.

   END: DO WHILE LOOP

Because both EnOpt and BOBYQA are iterative methods, in addition to the outer "DO WHILE" loop used for refinement, there is an inner loop for well control optimization at each control regularization scale l, which is not shown here. The change in NVP is also used as the stop criterion for the inner loop. The stop criterion for the inner loop is not kept constant. Instead, it is decreased as the scale is refined, because convergence at the coarse scale takes many simulation runs while NVP is only slightly increased.

2.3 Test case

The EnOpt and BOBYQA optimization methods are applied to a simple–but–interesting synthetic test case. Optimization is done with and without multiscale regularization, and the results for all cases are compared.

2.3.1 Case description.

We consider a two–dimensional two–phase synthetic reservoir model. It has 45 × 45 × 1 grid blocks with a uniform grid block size of 50 ft × 50 ft × 15 ft. To add heterogeneity, the reservoir model is "channelized" with three uniform high–permeability zones (5 D) and a low–permeability back ground (80 mD; Fig. 2.1). Reservoir porosity is uniform and equal to 0.2. Nine producers and four injectors are located in a repeated five–spot well pattern, with three producers and two injectors positioned at high permeability channel and others positioned at the low permeability background. This configuration is chosen to induce intuitively clear challenges in well control optimization (Discussion, later).

During the water flooding process, water is injected at 900 stb/day for each injector with a total injection rate of 3600 stb/day. Only fluid production rates for producers are considered as control variables for the NVP optimization. The time range for optimization is 960 days. The price of oil is 80 $/bbl and the cost for produced water disposal is 5 $/bbl. A total fluid production rate constraint of 3600 stb/day is imposed for the producers.

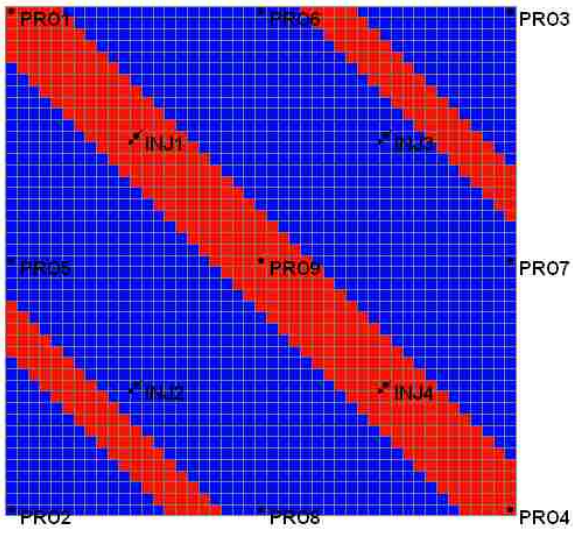

Figure 2.1: The permeability distribution of the channelized synthetic example: 5 D for three high permeability channels and 80 mD for the low permeability background.

2.3.2 Optimization parameters.

Before multiscale regularization, the time step for production optimization is 60 days. Thus, there are 16 control variables for each producer and 144 total unknowns. For multiscale regularized EnOpt and BOBYQA, the coarsest scale time step is 960 days, with one control variable for each producer. As regularization proceeds, the time step decreases by a factor of two whereas the total number of control variables increases by a factor of two for the next finer scale. The refinement is continued until the stop criterion is reached. An ensemble size of 30 is used for the ensemble–based method. A nonoptimized case is used as a reference case, in which the total production rate is equally distributed among the producers (400 stb/day for each producer). If not specified otherwise, this is also the initial value used for the optimized scenarios discussed in the next section.

2.3.3 Results.

The optimized NVPs for EnOpt, BOBYQA, multiscale regularized EnOpt and multiscale regularized BOBYQA range from 85.3 to 86.9 million dollars (Fig. 2.2). All optimized cases have higher NVPs compared with the nonoptimized case (NVP with constant rates). Multiscale regularized EnOpt (Fig. 2.2(a), upper curve) obtains the highest NVP among all these methods. Multiscale regularized BOBYQA (Fig. 2.2(b), upper curve) has a similar NVP to EnOpt (Fig. 2.2(a), lower curve), but with faster convergence. The BOBYQA (Fig. 2.2(b), lower curve) method is not as efficient as other methods. With $n+2$ ($n = 144$ before multiscale regularization) function evaluation runs to build the quadratic model, BOBYQA takes less than 20 simulation runs to converge because it uses second order gradients. However, it converges to a local optimum instead of the global one; for this particular system, BOBYQA may converge to a local optimum if the number of control variables is more than a hundred. In comparison, regularized BOBYQA has higher NVP even at the coarsest scale of regularization (scale 1). For EnOpt, the effect of multiscale regularization is not as significant as for BOBYQA, but the convergence speed and NVP are improved slightly. Moreover,

both multiscale regularized cases terminate at scale 4 with a total number of 72 (8 control variables $\times$ 9 wells) unknowns, which is 50 percent fewer than the total number of well controls (16 control variables $\times$ 9 wells = 144 unknowns) used in unregularized EnOpt and BOBYQA methods.

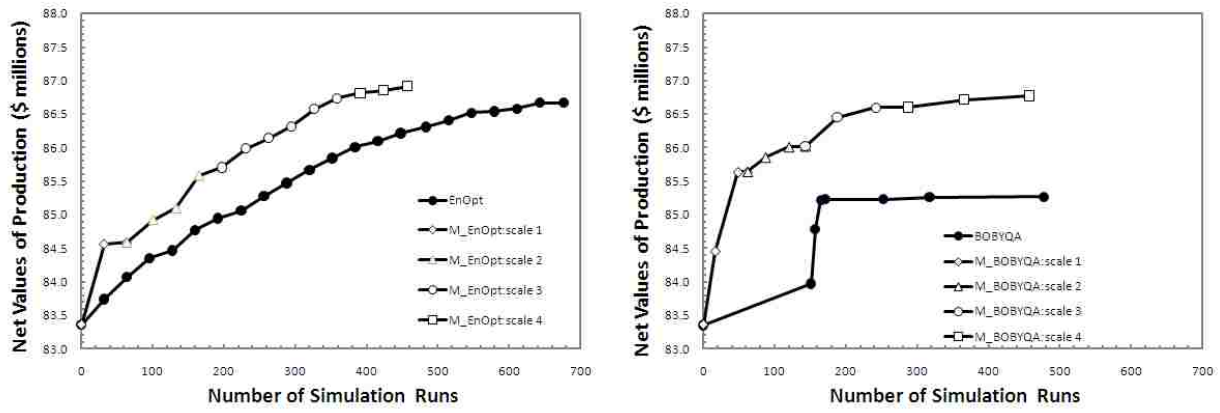

(a) EnOpt and multsicale regularized EnOpt

(b) BOBYQA and multsicale regularized BOBYQA

Figure 2.2: NVP as a function of number of simulation runs before and after multiscale regularization. Multiscale regularized methods converge to higher NVPs with fewer simulation runs and fewer control variables. (scale 1: 1 control variable for each producer each 960 days; scale 2: 2 control variables for each producer each 480 days; scale 3: 4 control variables for each producer each 240 days; scale 4: 8 control variables for each producer each 120 days; unregularized cases: 16 control variables for each producer each 60 days.)

2.4 Discussion

2.4.1 Improving sweep efficiency.

In the nonoptimized case (Fig. 2.3(a)), water is breaking through to producers 1 and 4 as they are connected to injectors 1 and 4 by high permeability channel, leaving unswept regions due to permeability heterogeity. After optimization (Fig. 2.3(b) to Fig. 2.3(e)), water breakthrough for producers 1 and 4 is delayed by all optimization algorithms and the unswept area is reduced. In addition, multiscale regularization (Fig. 2.3(c) and Fig. 2.3(e)) reduces the unswept area for both EnOpt and BOBYQA. Among all these methods, multiscale

regularized EnOpt works the best because it has a larger swept area (the darker blue regions) than all the other methods.

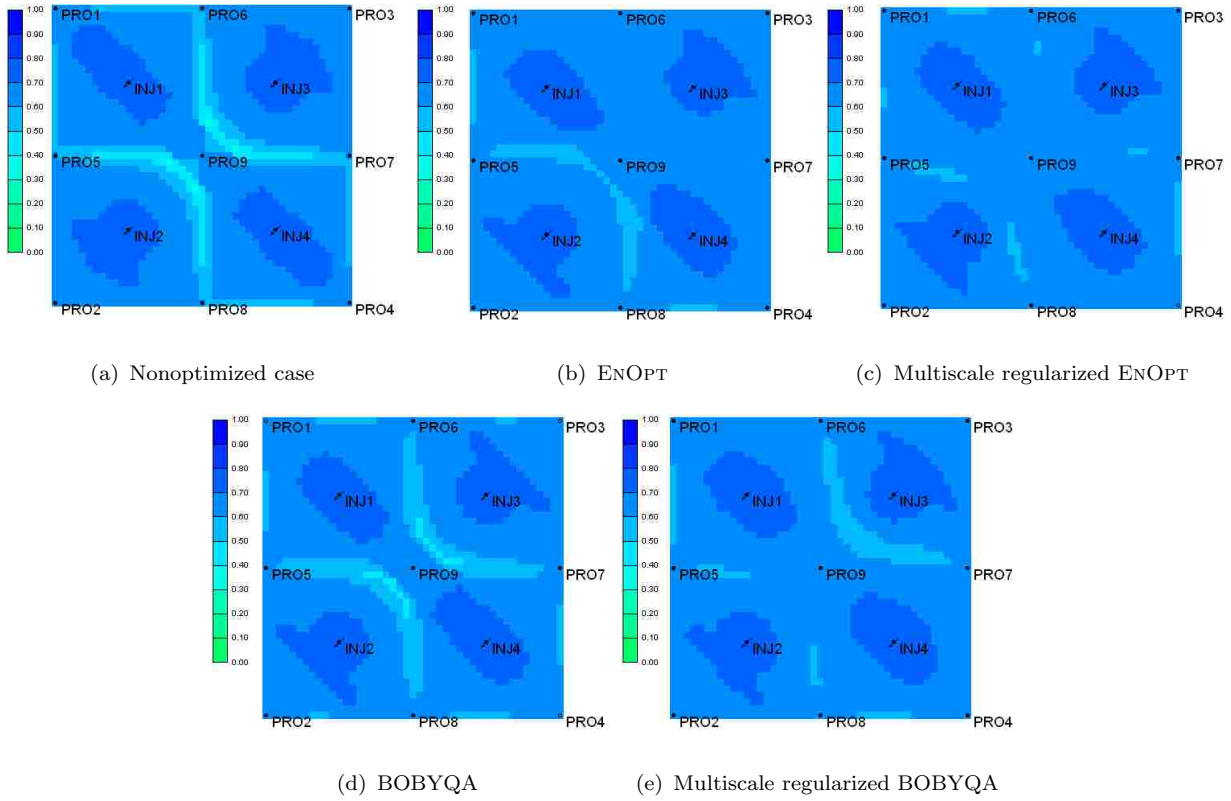

(a) Nonoptimized case (b) EnOpt (c) Multiscale regularized EnOpt

(d) BOBYQA (e) Multiscale regularized BOBYQA

Figure 2.3: Water saturation at the end of 32 months before and after multiscale regularization. Areas with darker blue have been swept. Thus, the relatively large extents of the cyan hues in the nonoptimized case indicate lower recovery. EnOpt improves recovery (less cyan); BOBYQA performs comparably only if multiscale regularization is used.

2.4.2 Sensitivity to initial controls.

Because this problem is nonlinear, the optimization is nonunique and may be sensitive to initial guesses of the control vector. When different initial guesses are used with unregularized methods (Table 2.1), there is a significant effect on the controls and the net value of production (differences up to 1.61 percent for EnOpt and 2.09 percent for BOBYQA). Regularization allows all methods to converge to consistent, higher optima regardless of differences in the initial controls (differences less than 0.35 percent and 0.23 percent for

regularized EnOpt and BOBYQA). This is important, because the initial controls may be difficult to specify for complex reservoir models. Three initial guesses used in Table 2.1 are:

- Initial 1 assigns the production rates from the coarsest scale of multiscale regularized BOBYQA optimization to the producers. For producers 1 to 9 these are 177, 249, 262, 206, 375, 887, 598, 413 and 433 stb/day, respectively.
- Initial 2 assigns 400 stb/day to each producer.
- Initial 3 uses the same production rates used as for initial 1, except the order of assignment is from producer 9 to 1. This initial estimate is farther from optimal than initial 1.

Table 2.1: The effect of initial guesses on optimized NVPs ($ millions) for different methods. MEnOpt and MBOBYQA stand for Multiscale regularized EnOpt and Multiscale regularized BOBYQA respectively.

Methods	Optimized NVP using initial 1	Optimized NVP using initial 2	Optimized NVP using initial 3	Difference[a] (%)
EnOpt	86.8	86.7	85.4	1.61
BOBYQA	85.8	85.3	84.0	2.09
MEnOpt	86.7	86.9	86.6	0.35
MBOBYQA	86.6	86.7	86.5	0.23

[a]The difference is computed as $\frac{\max NVP - \min NPV}{\max NVP} \times 100\%$.

2.4.3 Evolution of controls.

The changes of well controls as simulation runs are shown for producers 1 and 5 in Fig. 2.4 and Fig. 2.5. Producer 1 is located in a high permeability channel whereas producer 5 is located in the low permeability background. For both EnOpt and BOBYQA, multiscale regularized algorithms tend to have simpler control strategies but with more sudden changes in most cases (compare right figures in Fig. 2.4 and Fig. 2.5 with their left figures). Instead of specifying a fixed resolution and optimizing a large control set initially, multiscale regularization optimizes from a low resolution and sequentially increases resolution to avoid

high–dimensional local optima. Apparently (Fig. 2.4(b), Fig. 2.4(d), Fig. 2.5(b) and Fig. 2.5(d)), the coarse scale optimizes in some average sense, providing a good initial estimate for next finer scale. In addition, because producer 1 is located within the high permeability channel, it produces at high rates at early stage. The production rate gradually decreases as the water break through. This trend was captured by most of the methods except for multiscale regularized BOBYQA method. With the decreasing of production rate on producer 1, the production rate for producer 5 starts to increase to meet the total production rate constraints (Fig. 2.5). Although the control strategies are very different (Fig. 2.4), the recoveries values are very similar (Table 2.1).

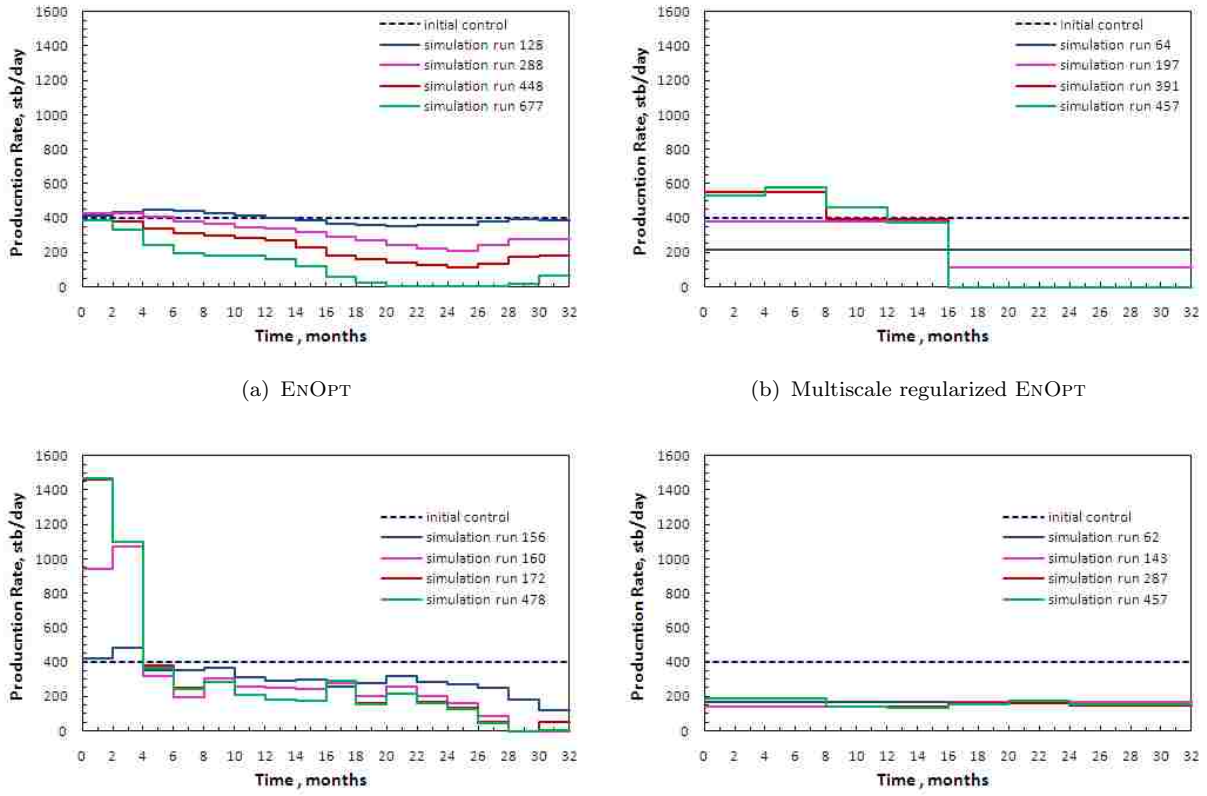

(a) EnOpt

(b) Multiscale regularized EnOpt

(c) BOBYQA

(d) Multiscale regularized BOBYQA

Figure 2.4: Change of control variables with simulation runs: producer 1. Multiscale regularized methods give simpler control strategies. The coarse scale optimizes in some average sense, providing a good initial estimate for next finer scale. Because producer 1 is located in the high permeability channel, it produces at high rates at early stage. The production rate gradually decreases as the water break through. This trend was captured by all the methods except for multiscale regularized BOBYQA method.

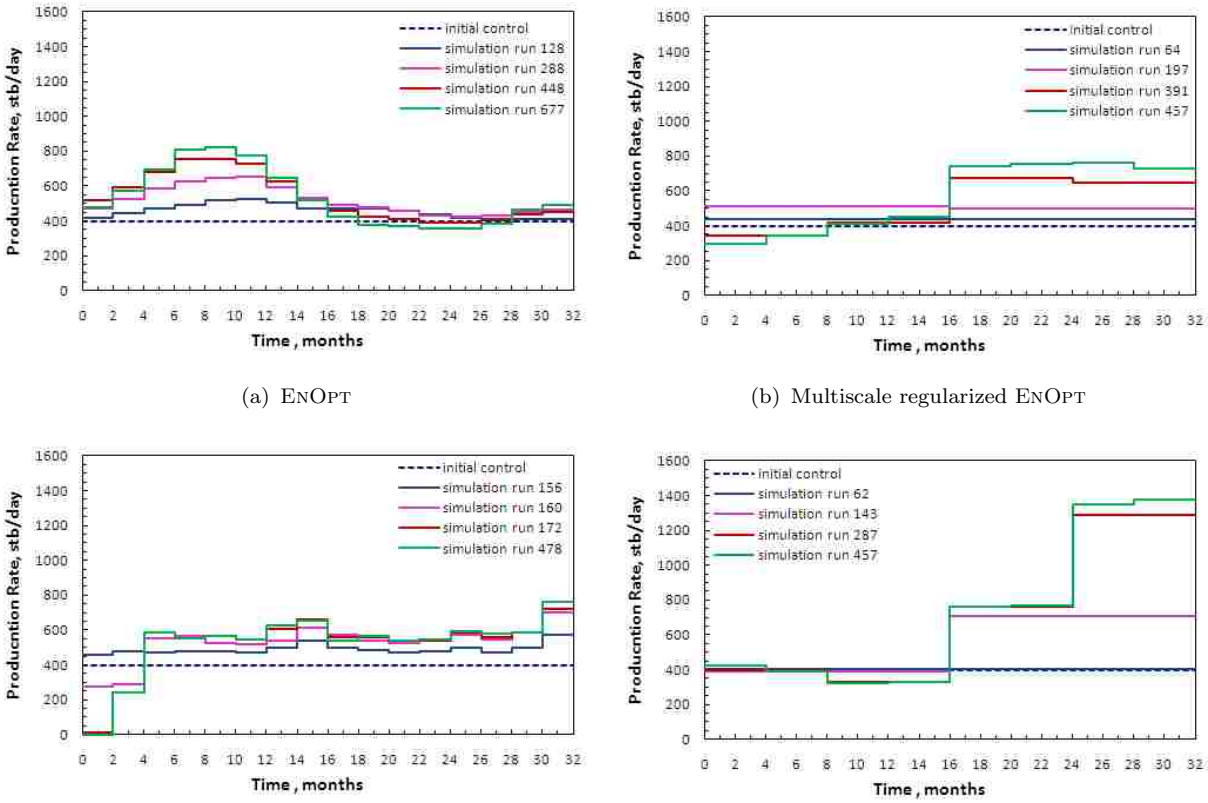

(a) EnOpt

(b) Multiscale regularized EnOpt

(c) BOBYQA

(d) Multiscale regularized BOBYQA

Figure 2.5: Change of control variables with simulation runs: producer 5. Multiscale regularized methods give simpler control strategies. The coarse scale optimizes in some average sense, providing a good initial estimate for next finer scale.With the decreasing of production rate on producer 1, the production rate for producer 5 starts to increase to meet the total production rate constraints.

Optimized well control trends from most methods are similar (Fig. 2.6). Because producer 1 is connected to injector 1 by a high permeability channel, the optimized controls from EnOpt, multiscale regularized EnOpt and BOBYQA tend to be higher at the beginning of production due to the better transmissibility, and then decrease gradually to reduce water production after water breakthrough (Fig. 2.6(a)). Similarly, as producer 5 is positioned in the low permeability background, it takes much longer for water to breakthrough comparing with producer 1. Therefore, this objective function is less sensitive to producer 5 than producer 1. However, to satisfy the total liquid production rate constraints (3600 stb/day), the optimized well controls from multiscale regularized EnOpt, BOBYQA and multiscale regularized BOBYQA increase at later time because of the rate reduction from wells (e.g., producer 1) in the high permeability channel (Fig. 2.6(b)).

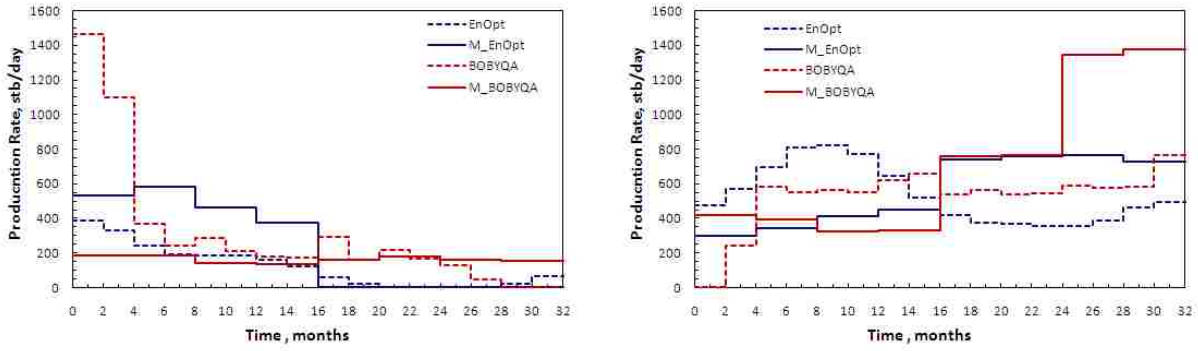

(a) Producer 1

(b) Producer 5

Figure 2.6: Comparison of optimized controls from EnOpt, multiscale regularized EnOpt, BOBYQA and multiscale regularized BOBYQA. Similar trends are obtained for different methods.

2.4.4 Nonuniqueness and optimality.

The optimized control trends from most methods are similar. However, some well control trends from different methods are different even though they have similar NVPs. In this example (Fig. 2.6), the EnOpt NVP is similar to multiscale regularized BOBYQA, but the estimated optimal controls for producers 1 and 5 are quite different. This can be further

explained by Fig. 2.7, where

$$\sigma_m = \sqrt{\frac{\sum_{i=1}^{N_x}(x_{i,m} - x_{i,best})^2}{N_x - 1}}.$$

The deviation of g_m (m indicates different methods) from g_{best} can be calculated as ($g_{best} - g_m$). The nonoptimized control variance σ_o and net value of production g_o are used for normalization. The loss in optimized g_m increases with the increase of deviation of x_m from x_{best}. However, the penalty in the value of production is small (less than 0.3 percent) for the optimized cases, even if there is a significant difference in control values (σ_m/σ_o =0.88). Such small differences in optimality for such markedly different control strategies (Figs. 2.4–2.5) are somewhat surprising.

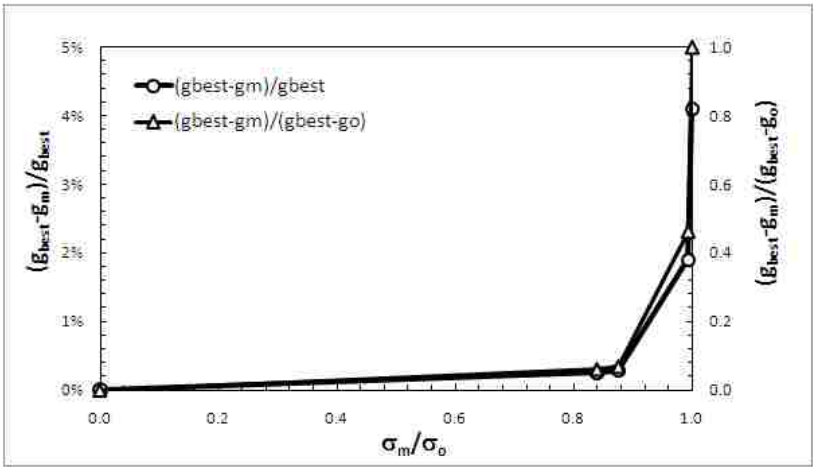

Figure 2.7: The deviation of optimized g_m from g_{best} increases with the deviation of well controls x_m from the best controls x_{best}. The penalty in the value of NVP is small (less than 0.3 percent), even when there is a significant difference in control values (σ_m/σ_o =0.88 with σ_o=275 stb/day)

2.4.5 Extensions.

Only time scale regularization is considered in our synthetic case. For life cycle production optimization with many wells or well segments, regularization both in time and space might be more efficient (Lien et al. 2008).

One disadvantage of ordinary multiscale regularization is that the refinement is carried out uniformly instead of adaptively, resulting in local over–parameterization and wasting

simulation runs in methods like BOBYQA. Examining Fig. 2.4(b) as an example, for the last 16 months, only one control variable is needed whereas four control variables are assigned at scale 8. Adaptive multiscale regularization may be a good way to solve this problem.

2.5 Conclusions

Two simulator–independent methods of smart well production optimization were investigated, EnOpt and BOBYQA. Multiscale regularization was tested on these two methods including examining effective control adjustment frequencies. The BOBYQA method is not as efficient as EnOpt method for optimization problems with more than a hundred unknowns because the BOBYQA method is prone to converging to local optima.

Multiscale regularization is promising for production optimization. The advantages of applying multiscale regularization on well control optimization include:

- Mutiscale regularized well control optimization is more efficient than direct fine–scale optimization.
- Regularizing the well controls makes the optimization problem for coarse scale less undetermined.
- The solution from the coarse scale appears to be less likely to converge to a local optimum.
- Coarse–scale early iterations provide a good starting point for the next finer scale, resulting in higher optima and better convergence speed.
- Instead of using a priori determined control adjustment frequency, mutiscale regularization finds the best control adjustment frequency by increasing control frequency successively until further refinement does not increase NVP.

Chapter 3
Application of Gathered EnKF for Continuous Reservoir Model Updating

3.1 Introduction

In the past decade, the petroleum industry has invested hundreds of millions of dollars to develop and install instrumentation and hardware such as permanent downhole gauges to provide continuous dynamic reservoir data. Reservoir observations which used to be recorded at intervals of months or days are now recorded at frequencies of minutes or seconds. The ultimate goal for obtaining these high frequency data observations is to enable continuous updating of reservoir models so that real–time decision–making can improve reservoir performance. In this chapter, we propose a gathered EnKF to handle high frequency data assimilation.

The Ensemble Kalman Filter (EnKF) is a recursive data assimilation method. It is well–suited to continuous reservoir model updating (Chen et al. 2010; Chen, Oliver, and Zhang 2009; Gu and Oliver 2006; Li 2008; Wen and Chen 2007). The EnKF was introduced by Evensen (1994) as an alternative to the Extended Kalman Filter (EKF) for weather prediction; it was introduced to petroleum engineering by Nævdal et al. (2005). Ease of implementation and increasing deployment of permanent sensors make the EnKF appealing for continuous reservoir model updating.

The value of high frequency data streams can only be realized if we can use them to update the reservoir model, and thereby inform reservoir management decisions. However, despite the strengths of the EnKF, integrating high frequency data streams received from permanent sensors remains a challenge. First, the EnKF requires simulator restarts of each realization at each assimilation point, entailing file transfer and input–output. High–frequency model updating may impose a significant computational burden. Second, too–frequent model updating increases the need for rapid model updating, because the new observations may be

available at intervals as small as a few seconds. However, it is difficult to update an ensemble of models in seconds; moreover, such frequent updates may not improve ensemble fidelity. Lastly, EnKF performance depends on ensemble size. The ensemble size is commonly on the order of 100 to balance adequate sampling with computational cost. This is far less than the dimension of the model parameter space. The limited ensemble size may cause errors in the estimated covariances and thus the Kalman gain. This degrades the EnKF forecast as more data are assimilated. High–frequency model updating may destroy ensemble diversity and lead to filter divergence.

The Ensemble Smoother (ES) is an alternative proposed by Leeuwen and Evensen (1996) as a linear variance minimizing analysis. The ES is similar to the EnKF except that it assimilates all observations simultaneously rather than sequentially as the EnKF does. An advantage of the ES is that computational cost may be reduced by avoiding recursive model updating.

However, the ES strictly applies only to linear dynamic models and Gaussian priors (Evensen 2009); if these assumptions are honored, ES and EnKF should get identical results. For nonlinear dynamic models, ES is expected to perform more poorly than EnKF, as illustrated by Evensen (1997) and Evensen and van Leeuwen (2000) using a nonlinear Lorenz model. Because reservoir models are typically nonlinear, ES has not been commonly used for reservoir model updating. Skjervheim et al. (2011) compare the EnKF and ES for reservoir dynamics models; they found that the two methods may obtain similar results, and the ES may require as little as 10 percent of the time used for EnKF. They attribute this good performance of ES for nonlinear models to the diffusive nature of some reservoir dynamics problems, compared to the chaotic and dynamic Lorenz system previously used to test ES (Evensen 1997; Evensen and van Leeuwen 2000).

We propose a gathered EnKF method, which can also be seen as a step–wise ES method. In this method, if there is no significant mismatch between the observations and the ensemble predictions, the observations are stored (or "gathered") instead of being assimilated

immediately. Model updating is done only if the gathered data volume exceeds a specified threshold, or if the observations diverge from prior ensemble predictions. The motivations for the new algorithm are to

1. provide an efficient ensemble based method for nonlinear model updating that is more computationally efficient than the standard EnKF, and

2. reduce sampling errors caused by the finite size of ensembles.

That is, the gathered EnKF is intended to overcome limitations of the standard EnKF (which may require too–frequent model updating) and the ES (which may not keep the model sufficiently up–to–date and is less robust for nonlinear problems).

In the next section, we review the EnKF and ES. In section 3.3, we prove that for a linear dynamic model, simultaneous data assimilation (ES) has less sampling error than sequential data assimilation (EnKF). In section 3.4, the effects of gathering are tested with a scalar case and then a 2D reservoir model updating case. The gathered method is further improved to a more flexible adaptive way for high frequency data in real–time reservoir management in chapter 5.

3.2 Ensemble methods

The ensemble–based is a Monte Carlo approach for Bayesian updating. It begins with an ensemble of realizations based on a priori model parameters; these realizations are then used to approximate the covariance of the augmented vector at each assimilation step. The models are typically evolved through time using numerical methods. In this way, computations to evolve the covariance matrix from step to step are avoided, making large scale model updating practical.

3.2.1 Ensemble Kalman filter

We adopt the notation from Chen (2008). Let m be a a vector comprising model parameters (e.g., permeability and porosity at each gridblock), elements of m are constant but their estimates change with time. Let f be a vector of state variables (e.g., pressure and phase saturation at each gridblock); elements of f usually vary with time. Model parameters m are sometimes called "static variables," and state variables f are sometimes called "dynamic variables." Finally, let d denote the predicted production observations (e.g., bottom hole pressure and water-oil ratio). In the EnKF, an augmented vector y combines all these variables. At assimilation step i,

$$y_i = [m_i^T, f_i^T, d_i^T]^T \,. \tag{3.1}$$

The initial realizations (at time zero) are based on a priori knowledge of the initial state, sampled into an ensemble

$$M_0 = [m_{1,0}, m_{2,0}, m_{3,0}, \ldots, m_{Ne,0}] \,,$$

with the subscript $\cdot_{Ne}$ indicating the last member of an ensemble with N_e members. The initial states

$$f_{j,0} \,,\; j \in \{1 \ldots N_e\}$$

may vary among members because of initialization of models with differing a priori parameters $m_{j,0}$.

The observations $d_{obs,i}$ are obtained at discrete time points t_i. Burgers (1998) proved that using the same observations for all ensemble members causes the updated ensemble variance to be too low; essentially such a treatment implies that the observations are exact and over tunes the ensemble to the observations. This is corrected by adding random perturbations with correct covariances to the observation $d_{obs,i}$. That is,

$$d_{obs,j,i} = d_{obs,i} + \xi_{j,i}, \quad j = 1, 2, \ldots, N_e \,, \tag{3.2}$$

with expected value $\left\langle \xi_{j,i}\xi_{j,i}^T \right\rangle = C_{Di}$ and $\langle \xi_{j,i} \rangle = 0$. Here $\xi_{j,i}$ is the observation error at time stept_i, which is commonly assumed to follow a Gaussian distribution.

At each step, the augmented vectors y_j ($j \in \{1 \dots N_e\}$) are updated using the prior reservoir states and the weighted differences between the perturbed observation data and predicted data as

$$\begin{aligned} y_{j,i}^u &= y_{j,i}^f + K_{e,i}(d_{obs,j,i} - d_{j,i}) \\ &= y_{j,i}^f + K_{e,i}(d_{obs,j,i} - H y_{j,i}^f)\,. \end{aligned} \tag{3.3}$$

The forecast state vector comprises the posterior model parameters $m_{j,i-1}$ along with calculated "observations" $d_{j,i}$ and dynamic variables $f_{j,i}$. Explicitly, the Kalman gain is

$$K_{e,i} = C_{Ye,i}^f H^T (H C_{Ye,i}^f H^T + C_{Di})^{-1}, \tag{3.4}$$

and

$$H = [0 \;\; I],$$

where $K_{e,i}$ is Kalman gain matrix approximated from the ensemble at time step i. The subscript e denotes ensemble and the superscripts u and f indicate update and forecast. H is a measurement operator which extracts simulated observation data from the augmented vector y^f; 0 is a $N_d \times (N_y - N_d)$ matrix with all zeroes as its entries. I is a $N_d \times N_d$ identity matrix. N_d is the number of observations and N_y is the number of variables in the augmented vector. $C_{Ye,i}$ is the covariance matrix of the augmented vector which is approximated as

$$C_{Y_{e,i}}^f = \left\langle \left(y_i^f - \left\langle {y_i}^f \right\rangle \right) \left(y_i^f - \left\langle {y_i}^f \right\rangle \right)^T \right\rangle , \tag{3.5}$$

where $\langle \cdot \rangle$ indicates the expected value.

One advantage of the EnKF is that computation of the full matrix $C_{Ye,i}$ is rarely necessary. If we expand some expressions in the previous equations,

$$C_{Ye,i}^f H^T = \begin{bmatrix} C_{m_i,m_i} & C_{m_i,f_i} & C_{m_i,d_i} \\ C_{f_i,m_i} & C_{f_i,f_i} & C_{f_i,d_i} \\ C_{d_i,m_i} & C_{d_i,f_i} & C_{d_i,d_i} \end{bmatrix} \begin{bmatrix} 0 \\ 0 \\ I \end{bmatrix} = C_{y_i,d_i}\,, \tag{3.6}$$

and

$$HC^{f}_{Ye,i}H^{T} = C_{d_i,d_i}\,. \tag{3.7}$$

Then the computation of Kalman gain can be simplified as

$$K_{e,i} = C_{yi,di}(C_{di,di} + C_{Di})^{-1}. \tag{3.8}$$

After each updating step, the augmented vector is advanced from time t_{i-1} to time t_i, commonly using a reservoir simulator. In the forecast step, the dynamic variables f (such as pressure) and the predicted observations d are updated, but the the model parameters m are not (Eq. 3.9).

$$(f_{j,i}, d_{j,i})^{f} = F(m_{j,i-1}, f_{j,i-1})^{u}, \tag{3.9}$$

where $F(\cdot)$ denotes the forward operator (e.g., a reservoir simulator).

3.2.2 Ensemble smoother

The ES differs from the EnKF by assimilating the observations simultaneously instead of sequentially. Thus the augmented vector for the ES can be modified from Eq. 3.1 as

$$y = [m^{T}, f^{T}, d_1^{T}, d_2^{T}, \cdots, d_{Nt}^{T}]^{T}\,, \tag{3.10}$$

where N_t is the total number of discrete observation times (indicated by $\cdot_{Nt}$ when subscripted). For the remainder of this section, the time step subscript i is dropped because ES only has one step of assimilation.

If we define

$$d^{T} = [d_1^{T}, d_2^{T}, \cdots, d_{Nt}^{T}] \tag{3.11}$$

and

$$C_D = \begin{bmatrix} C_{D1} & \cdots & . \\ \vdots & \ddots & \vdots \\ . & \cdots & C_{DNt} \end{bmatrix}, \tag{3.12}$$

then Kalman gain for ensemble smoother is modified from Eq. 3.8 to obtain

$$K_e = C_{y,d}(C_{d,d} + C_D)^{-1} \tag{3.13}$$

with

$$y_j^u = y_j^f + K_e(d_{obs,j} - d_j)\,. \tag{3.14}$$

Assume that the total number of observations for all times is N_d^S,

$$N_d^S = \sum_{i=1}^{N_t} N_{d,i}$$

From Eq. 3.13, the ensemble Kalman gain is a multiplication of a N_y by N_d^S matrix with another N_d^S by N_d^S matrix. The ES method saves computational cost by avoiding simulation, requeueing, file input–output, and transferring at each data assimilation step. However, the increased work of computing the Kalman gain for large numbers of observations ($N_d^S \gg \max N_{d,i}$) may offset these savings (further discussion see 3.6.4).

3.3 Sampling errors of ensemble based methods

The ensemble Kalman filter tends to underestimate the model covariance even if ensembles of perturbed observations are used in the analysis step. This is because unlike the Kalman filter and extended Kalman filter (in which the error covariances are evolved in time), the ensemble Kalman filter uses the ensemble covariance to approximate the error covariance. For any finite ensemble, sampling errors cause a negative bias in the estimated covariance from the ensemble (van Leeuwenan 1998; Sacher and Bartello 2008). There are two types of sampling errors in the EnKF: first, errors are introduced from the prior ensemble; second, errors are caused by the perturbed observations. Both van Leeuwenan (1998) and Sacher and Bartello (2008) only considered the errors introduced from the prior ensemble.

In this section, we show that the observation sampling errors induce an additional negative bias in the estimated covariance. In addition, we prove that — for linear dynamic

models with only prior sampling errors considered — sequential data assimilation (filters) and simultaneous data assimilation (smoothers) give identical results. On the other hand, if observation sampling error is included, simultaneous data assimilation (ES) provides better covariance and gain estimates than sequential data assimilation (EnKF). Essentially, the smoother has a larger sample of observations, reducing bias.

3.3.1 The need to use perturbed observations

An ensemble of observation should be generated at each assimilation step by adding random perturbations with correct statistics to the observations (Burgers 1998); otherwise, the covariance of the updated ensemble will be too low compared to the true covariance. Explicitly,

$$\begin{aligned} C_{Ye}^{u} &= \left\langle \left(y^{u} - \langle y^{u} \rangle\right) \left(y^{u} - \langle y^{u} \rangle\right)^{T} \right\rangle \\ &= (I - K_e H) C_{Ye}^{f} (I - H^{T} K_e^{T}) \\ &\quad + K_e \left\langle \left(d_{obs} - \langle d_{obs} \rangle\right) \left(d_{obs} - \langle d_{obs} \rangle\right)^{T} \right\rangle K_e^{T} \\ &= (I - K_e H) C_{Ye}^{f} (I - H^{T} K_e^{T}) + K_e \left\langle \xi \xi^{T} \right\rangle K_e^{T}. \end{aligned} \tag{3.15}$$

If the observation is not perturbed, the second term in Eq. 3.15 vanishes $\left(K_e \left\langle \xi \xi^{T} \right\rangle K_e^{T} \equiv 0\right)$; in the traditional Kalman filter this term should equal to $K C_D K^{T}$, which is positive definite.

However, even if an ensemble of perturbed observations is used, the updated ensemble covariance is unbiased only if the prior ensemble covariance and the perturbed observation error are unbiased ($C_{Ye}^{f} = C_{Y}^{f}$ with C_{Y}^{f} denoting the true prior covariance and $C_D = \left\langle \xi \xi^{T} \right\rangle$), which is not assured because of the finite ensemble size.

3.3.2 The effect of finite ensemble size

Neither the initial ensemble nor the perturbed observation errors lead to exact covariance estimates for finite ensembles. If we denote the difference between the prior ensemble covariance C_{Ye}^{f} and the true prior covariance C_{Y}^{f} by ϵ with $\langle \epsilon \rangle = 0$, then the estimated prior covariance can be expressed as $C_{Ye}^{f} = C_{Y}^{f} + \epsilon$. Similarly, let $\left\langle \xi \xi^{T} \right\rangle = C_D + \rho$, with ρ being the assimilated errors from the perturbed observation.

Assuming a linear dynamic model and a Gaussian observation error model, we outline how observation sampling errors ρ for sequential data assimilation (EnKF) induce a negative bias in the ensemble covariance.

We first consider two data assimilation cycles for sequential data assimilation (EnKF) and then compare it with simultaneous data assimilation (ES). Defining

$$y = \left[m^T, f^T, d_1^T, d_2^T\right]^T ,$$

$$d_{obs} = \left[d_{obs,1}^T, d_{obs,2}^T\right]^T ,$$

$$C_D = \begin{bmatrix} C_{D1} & 0 \\ 0 & C_{D2} \end{bmatrix} ,$$

and

$$H = [H_1, H_2]^T , \text{ with } H_1 = [0\ 0\ I\ 0] \text{ and } H_2 = [0\ 0\ 0\ I].$$

The extraction matrix H_1 differs from H_2 because different observation sets are extracted at each data assimilation step. The observation errors of the two data sets are assumed to be independent.

We use subscript ϵ to indicate that only initial sampling error ϵ is considered, whereas subscript E indicates that initial errors ϵ and assimilated errors ρ are considered. The true case bears no subscript. Similarly, subscripts 1 and 2 denote for data assimilation step 1 and step 2.

Sampling errors from the initial ensemble

Assume the perturbed observation error is unbiased, which means $\left\langle \xi_1 \xi_1^T \right\rangle = C_{D1}$ and $\left\langle \xi_2 \xi_2^T \right\rangle = C_{D2}$. If only sampling errors in the prior ensemble are considered, and the system is linear, then sequential data assimilation (EnKF) and simultaneous data assimilation (ES) yield identical updated ensemble covariances (details, Appendix A).

A theoretical justification of the "inbreeding" effect caused by prior covariance sampling error ϵ is given both in van Leeuwenan (1998) and Sacher and Bartello (2008). Here we briefly

summarize those results. Because there is no difference between sequential data assimilation and simultaneous data assimilation when sampling error from the perturbed observation is not considered, in this subsubsection the time step subscript i is suppressed.

Following Sacher and Bartello (2008), to simplify the algebra, we define $\Phi = (HC_Y^f H^T + C_D)^{-1}$, $\kappa_\epsilon = \epsilon H^T \Phi$, and $L = I - KH$. The ensemble Kalman gain and the updated ensemble covariance are (Sacher and Bartello 2008)

$$K_E = K + L(\kappa_\epsilon - \kappa_\epsilon H \kappa_\epsilon) + O(\parallel \kappa_\epsilon H \kappa_\epsilon \parallel) \quad \text{and} \tag{3.16}$$

$$C_{YE}^u = C_Y^u + L\epsilon L^T - L\kappa_\epsilon \Phi^{-1} \kappa_\epsilon^T L^T + O(\parallel \kappa_\epsilon \Phi^{-1} \kappa_\epsilon^T \parallel). \tag{3.17}$$

The expected value of C_{YE}^u is

$$\langle C_{YE}^u \rangle = C_Y^u - L\langle \kappa_\epsilon \Phi^{-1} \kappa_\epsilon^T \rangle L^T + O(\parallel \kappa_\epsilon \Phi^{-1} \kappa_\epsilon^T \parallel). \tag{3.18}$$

Because the second term $L\langle \kappa_\epsilon \Phi^{-1} \kappa_\epsilon^T \rangle L^T$ in Eq. 3.18 is positive definite, the updated ensemble covariance always underestimates the true covariance.

Sampling errors from the perturbed observation

Because of finite ensemble size, the covariance of randomly sampled observation errors $\langle \xi \xi^T \rangle$ differs from the covariance of the true observation error C_D. If we denote the errors at each data assimilation cycle by ρ_1 and ρ_2 ($\langle \rho_1 \rangle = \langle \rho_2 \rangle = 0$), then the relationship between the true and the estimated observation error covariances is

$$\langle \xi_1 \xi_1^T \rangle = C_{D1} + \rho_1 \quad \text{and} \quad \langle \xi_2 \xi_2^T \rangle = C_{D2} + \rho_2 \tag{3.19}$$

Sequential data assimilation (EnKF). Let $C_{Y\epsilon}$ and K_ϵ denote the covariance and Kalman gain in which only prior sampling errors are considered. If the data sets are assimilated sequentially, d_1 followed by d_2, at first step assimilation, because $C_{YE,1}^f = C_{Y\epsilon 1}^f$, the

Kalman gain is expressed as

$$\begin{aligned} K_{E,1} &= C^f_{YE,1}(H_1 C^f_{YE,1} H_1^T + C_{D1})^{-1} \\ &= C^f_{Y\epsilon,1}(H_1 C^f_{Y\epsilon,1} H_1^T + C_{D1})^{-1} \\ &= K_{\epsilon,1}\,. \end{aligned} \tag{3.20}$$

That is, the initial ensemble errors ϵ *are* introduced to the Kalman gain at first assimilation (Eq. 3.16), but observation biases ρ_1 *are not* (Eq. 3.20). Similarly, since $K_{E,1} = K_{\epsilon,1}$, after first step assimilation, Eq. 3.15 can be rewritten as,

$$\begin{aligned} C^u_{YE,1} &= (I - K_{\epsilon,1}H_1)C^f_{Y\epsilon,1}(I - H_1^T K_{\epsilon,1}^T) \\ &\quad + K_{\epsilon,1}(C_{D1} + \rho_1)K_{\epsilon,1}^T \\ &= C^u_{Y\epsilon,1} + K_{\epsilon,1}\rho_1 K_{\epsilon,1}^T\,. \end{aligned} \tag{3.21}$$

Because $\langle \rho_1 \rangle = 0$, this leads to

$$\langle C^u_{YE,1} \rangle = \langle C^u_{Y\epsilon,1} \rangle. \tag{3.22}$$

Eq. 3.22 indicates that at first assimilation step, the sampling errors ρ_1 introduced from the perturbed observations will not affect the expect value of updated ensemble covariance.

However, the observation error bias will appear if multiple assimilation steps are used. For example, when incorporating the second data set d_2, a forecast step is taken to forward the augmented vector from step 1 to step 2. Here we assume a linear relationship between the last step updated (posterior) augmented vector y_1^u and the current step forecast (prior) augmented vector y_2^f, which is expressed as $y_2^f = A y_1^u$. Then the forecast ensemble covariance at second step can be calculated as,

$$\begin{aligned} C^f_{YE,2} &= A C^u_{YE,1} A^T \\ &= A(C^u_{Y\epsilon,1} + K_{\epsilon,1}\rho_1 K_{\epsilon,1}^T)A^T \\ &= C^f_{Y\epsilon,2} + A K_{\epsilon,1}\rho_1 K_{\epsilon,1}^T A^T. \end{aligned} \tag{3.23}$$

To simplify the equations, we define $\eta = AK_{\epsilon,1}\rho_1 K_{\epsilon,1}^T A^T$, $\kappa_\eta = \eta H_2 \Phi_\epsilon$, $K_{\epsilon,2} = C_{Y\epsilon,2}^f H_2^T \Phi_\epsilon$. and $\Phi_\epsilon = (H_2 C_{Y\epsilon,2} H_2^T + C_{D2})^{-1}$. Then the ensemble Kalman gain at the second assimilation step can be written as (details, Appendix B)

$$\begin{aligned} K_{E,2} &= C_{YE,2}^f (H_2 C_{YE,2}^f H_2^T + C_{D2})^{-1} \\ &= K_{\epsilon,2} + L_{\epsilon,2}(\kappa_\eta - \kappa_\eta H_2 \kappa_\eta) + O(\| \kappa_\eta H_2 \kappa_\eta \|), \end{aligned} \tag{3.24}$$

where $L_{\epsilon,2} = I - K_{\epsilon,2} H_2$. Similarly the updated ensemble covariance at the second step, $C_{YE,2}$, is (Appendix B)

$$\begin{aligned} C_{YE,2}^u &= C_{Y\epsilon,2}^u + L_{\epsilon,2}\eta L_{\epsilon,2}^T - L_{\epsilon,2}\kappa_\eta \Phi_\epsilon^{-1} \kappa_\eta^T L_{\epsilon,2}^T \\ &\quad + K_{E,2}\rho_2 K_{E,2}^T + O(\| (\kappa_\eta \Phi_\epsilon^{-1} \kappa_\eta^T \|). \end{aligned} \tag{3.25}$$

The expected value of $C_{Ye,2}$ is

$$\begin{aligned} \langle C_{YE,2}^u \rangle &= \langle C_{Y\epsilon,2}^u \rangle - L_{\epsilon,2} \left\langle \kappa_\eta \Phi_\epsilon^{-1} \kappa_\eta^T \right\rangle L_{\epsilon,2}^T \\ &\quad + O(\| (\kappa_\eta \Phi_\epsilon^{-1} \kappa_\eta^T \|). \end{aligned} \tag{3.26}$$

Eq. 3.26 shows that the sampling errors introduced from previous step's perturbed observation data set induce a negative basis ($-L_{\epsilon,2} \left\langle \kappa_\eta \Phi_\epsilon^{-1} \kappa_\eta^T \right\rangle L_{\epsilon,2}^T$) in subsequent steps (in the κ_η term). An over–confident prior reduces the weight given to subsequent observations. This may eventually lead to filter divergence, in which the ensemble update is insensitive to the observations.

Simultaneous data assimilation (ES). If the two data sets are assimilated at the same time, then similarly we would get,

$$C_{YE}^u = C_{Y\epsilon}^u + K_\epsilon \rho K_\epsilon^T \tag{3.27}$$

with the expected value

$$\langle C_{YE}^u \rangle = \langle C_{Y\epsilon}^u \rangle . \tag{3.28}$$

Comparing Eq. 3.26 with Eq. 3.28, the ES is less biased than EnKF because only sampling errors in the prior ensemble are introduced to the Kalman gain.

Gathered EnKF. Based on the above discussion, it appears that gathering the observations can reduce the sampling errors compared to sequential data assimilation — at least for the linear case. Because ρ is a matrix composed of random numbers, the trace of $K_\epsilon \rho K_\epsilon^T$ can possibly be reduced by increasing the dimension of ρ (ρ has a dimension of $N_d \times N_d$).

This method is a compromise between the simultaneous ES and the sequential EnKF, with the aim of obtaining some of the desirable properties of each method. Multiple EnKF assimilation points are "gathered" into a single assimilation for stability, accuracy, and efficiency.

3.4 A scalar case

Here we test our proof with a scalar case in which the forecast and observations are taken from a normal distribution with zero mean and unit variance, $N(0,1)$. 10^5 realizations are generated (MathWorks Inc. 2010) and divided to equal sized subsets for different ensemble sizes

$$N_e \in \{5, 20, 100, 1000\} \ .$$

The results discussed below are the expected value of all the subsets, each case using 10 observations.

In sequential data assimilation (EnKF), the 10 observations are assimilated sequentially with one observation at each time; in simultaneous data assimilation (ES), all the observations are assimilated at one time. The expected values of the RMSE (root mean square error) of the mean from the truth $\langle \delta \rangle$ and the spread of the samples $\langle \sigma \rangle$ are used to evaluate the performance of EnKF, ES and gathered EnKF. These statistics are defined as

$$\delta = \sqrt{\frac{\sum_{i=1}^{N_m} (m_{true,i} - \bar{m}_i)^2}{N_m}} \text{ and} \tag{3.29}$$

$$\sigma = \sqrt{\frac{\sum_{j=1}^{N_e} \sum_{i=1}^{N_m} (m_{j,i} - \bar{m}_i)^2}{N_m N_e}} \ , \tag{3.30}$$

with N_m being the dimension of m (here $N_m = 1$).

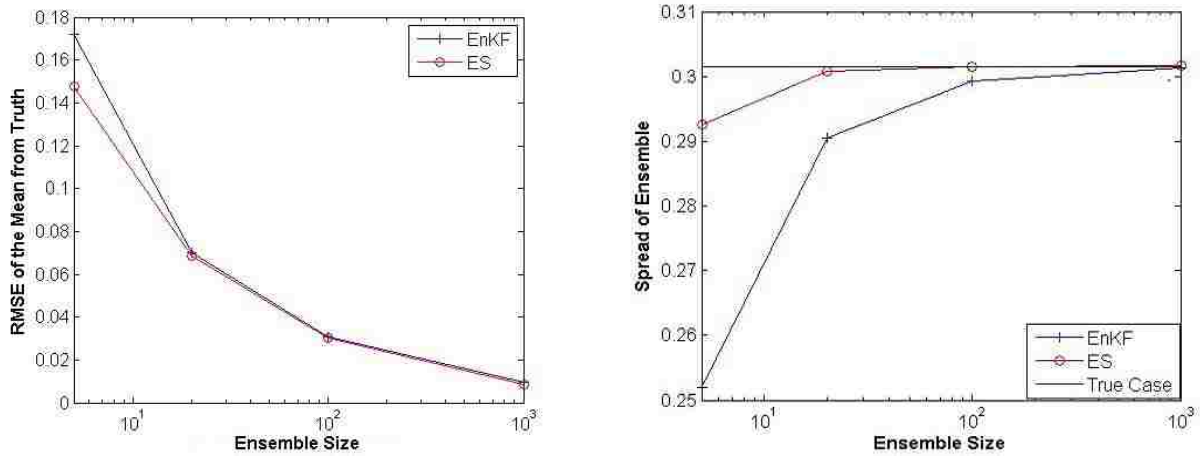

(a) Departure of the ensemble mean from the true mean (RMSE, $\langle\delta\rangle$).

(b) Updated ensemble spread, $\langle\sigma\rangle$.

Figure 3.1: Comparing ES with EnKF for various ensemble sizes for a linear, Gaussian scalar system. Means are performed over 10^5 realizations. The ES always outperforms the standard EnKF; ES and standard EnKF both converge to correct results as ensemble size N_e increases.

If the ensemble size is small (less than 20), ES has a lower RMSE $\langle\delta\rangle$ (Fig. 3.1(a)). As ensemble size increases, the difference between ES and EnKF decreases, with both becoming more accurate. Similar results observed for the updated ensemble spread (standard deviation) $\langle\sigma\rangle$ (Fig. 3.1(b)). For $N_e < 100$, the standard deviations of ensembles ($\langle\sigma\rangle$) from ES are more accurate than EnKF. As expected, updated standard derivation ($\langle\sigma\rangle$) of both ES and EnKF converge to the true standard derivation as N_e increases.

The effect of gather size is also tested with the scalar case. For small ensemble sizes (e.g., $N_e = 5$), the gathered EnKF with different gather sizes outperforms standard EnKF (equivalent to a gather size $N_g = 1$; Fig. 3.2). The wider the gather, the better the performance.

3.5 A 2D reservoir model updating case

3.5.1 Case description

We consider a 2D water flooding of synthetic case with 45 × 45 × 1 grid and cell size 30 ft × 30 ft × 10 ft. Only two phases, oil and water, are present. The porosity of the field is

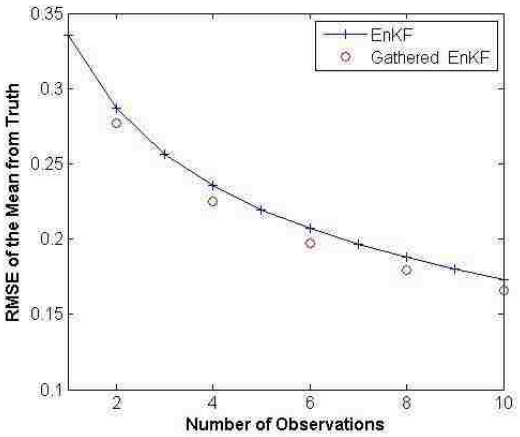

(a) Gather size = 2

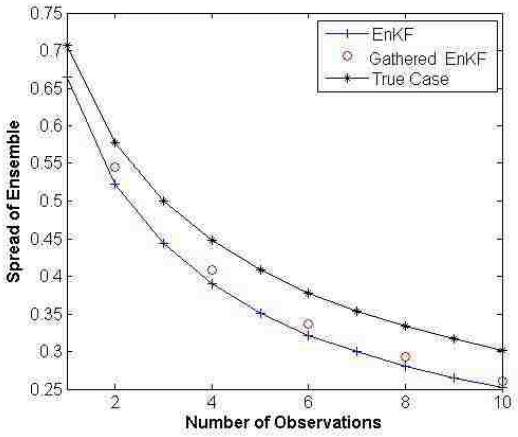

(b) Gather size = 2

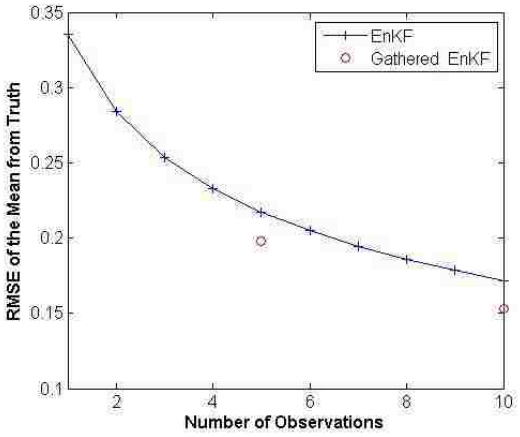

(c) Gather size = 5

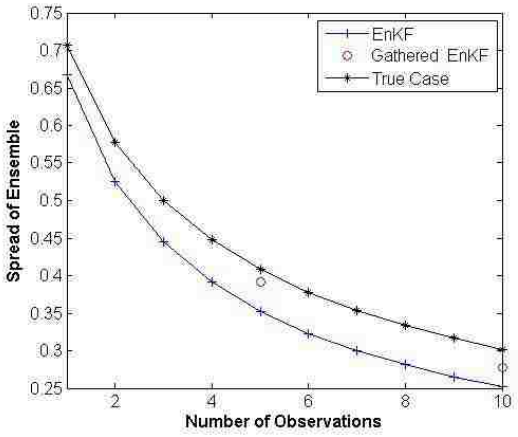

(d) Gather size = 5

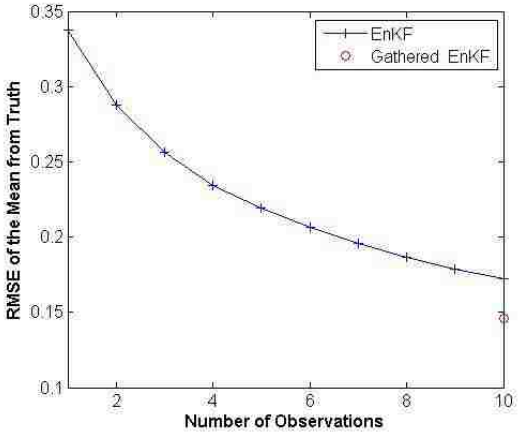

(e) Gather size = 10

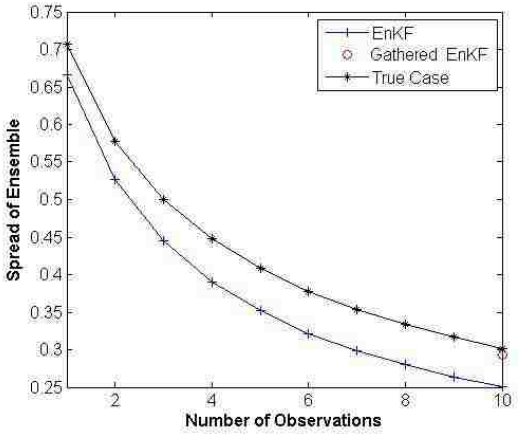

(f) Gather size = 10

Figure 3.2: Effect of gather size on sampling error for a linear, Gaussian scalar system with $N_e = 5$. Subfigures on the left shows the departure of the ensemble mean from the true mean (RMSE, $\langle \delta \rangle$ and the subfigures on the right shows the updated ensemble spread, $\langle \sigma \rangle$. Means are performed over 10^5 realizations. The departure from the true mean and reproduction of ensemble spread are always superior for the gathered EnKF. The advantage increases as gather size increases (from top to bottom).

assumed to be 0.2 through out the reservoir. The permeability in each gridlock is the only unknown model parameter to be estimated. The reservoir has a horizontal injector at the west side and a horizontal producer at the east side. Both the injector and the producer are composed of 15 equal-length segments with rate controls on every segment. The horizontal injector has a water injection rate of 60 stb/day per segment and the horizontal producer has a uniform pressure of 5780 psi. The true $\ln k$ distribution is Gaussian with mean 7.21 and variance of 1.12 respectively (permeability in mD). The semivariogram is elliptical with an west–east range of 810 ft and an north–south range of 405 ft.

Assuming the permeability at each well segment and the histogram of the permeability are known (and used to condition the prior ensemble), an initial ensemble with 500 realizations is generated using conditional sequential Gaussian simulation. Unless stated otherwise, the ensemble size is $N_e = 50$ to keep computational costs moderate. The observations of oil production rate and water cut of each producer segment, and bottom hole pressure of each injector segment are posted every 5 days until 180 days. The standard derivations of observations are assumed to be 5 stb/day for oil rate, 2 percent for water cut, and 7 psi for bottom hole pressure. A perturbation vector with the the same standard deviations as the observation errors is added to the observation to create the ensemble of observation data. There are 45 observations at each time step: 15 producer segments $\times$ 2 observations (q_o, f_w) + 15 injector segments $\times$ 1 observation (p_{wf}). For the standard EnKF, data assimilation takes place every 5 days, so there are 36 assimilation steps. For the gathered EnKF, three different gather sizes $N_g \in \{3, 6, 9, 18\}$ are examined.

3.5.2 Results

Similar to the scalar case, we use the RMSE of the mean from the truth (δ) and the spread of the samples (σ) to evaluate the performance of standard EnKF and gathered EnKF (Eqs. 3.29–3.30). For the sequential data assimilation after 180 days, the variance of the ensemble σ reduces to 0.2 whereas the RMSE of mean from the truth δ is as large as 0.4

(Fig. 3.3). In contrast, the gathered EnKF with $N_g = 18$ obtains a better RMSE ($\delta = 0.31$) and a more diverse ensemble ($\sigma = 0.29$); as in the linear case, the ensemble is both more diverse *and* more accurate. However, δ decreases more slowly for the gathered method than sequential EnKF at early time; this may due to the nonlinearity of the reservoir model. Both standard (Fig. 3.4(c)) and gathered (Fig. 3.4(d); $N_g = 18$) methods capture the basic

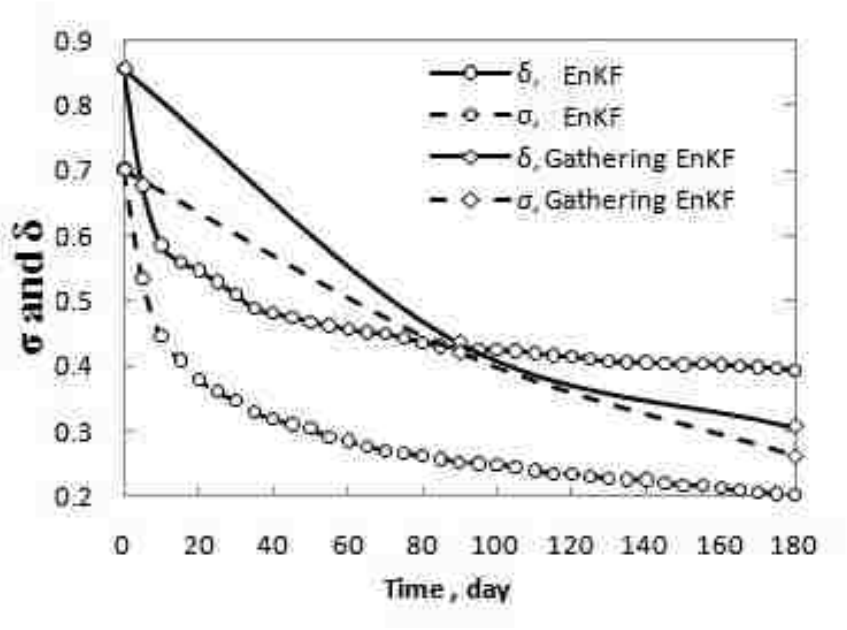

Figure 3.3: Comparison of RMSE of ensemble mean from the truth (δ) and ensemble spread (σ) for $\ln k$. At the end of the simulated time interval, the gathered EnKF has less error compared to the true mean (δ) and more diversity (σ)

features of the true average $\ln k$ field (Fig. 3.4(a)) at 180 days. Fig. 3.5 and Fig. 3.6 shows the production predictions by running the simulator forward from time zero to 600 days. Both methods match the production observation well; the gathered EnKF works slightly better than standard EnKF.

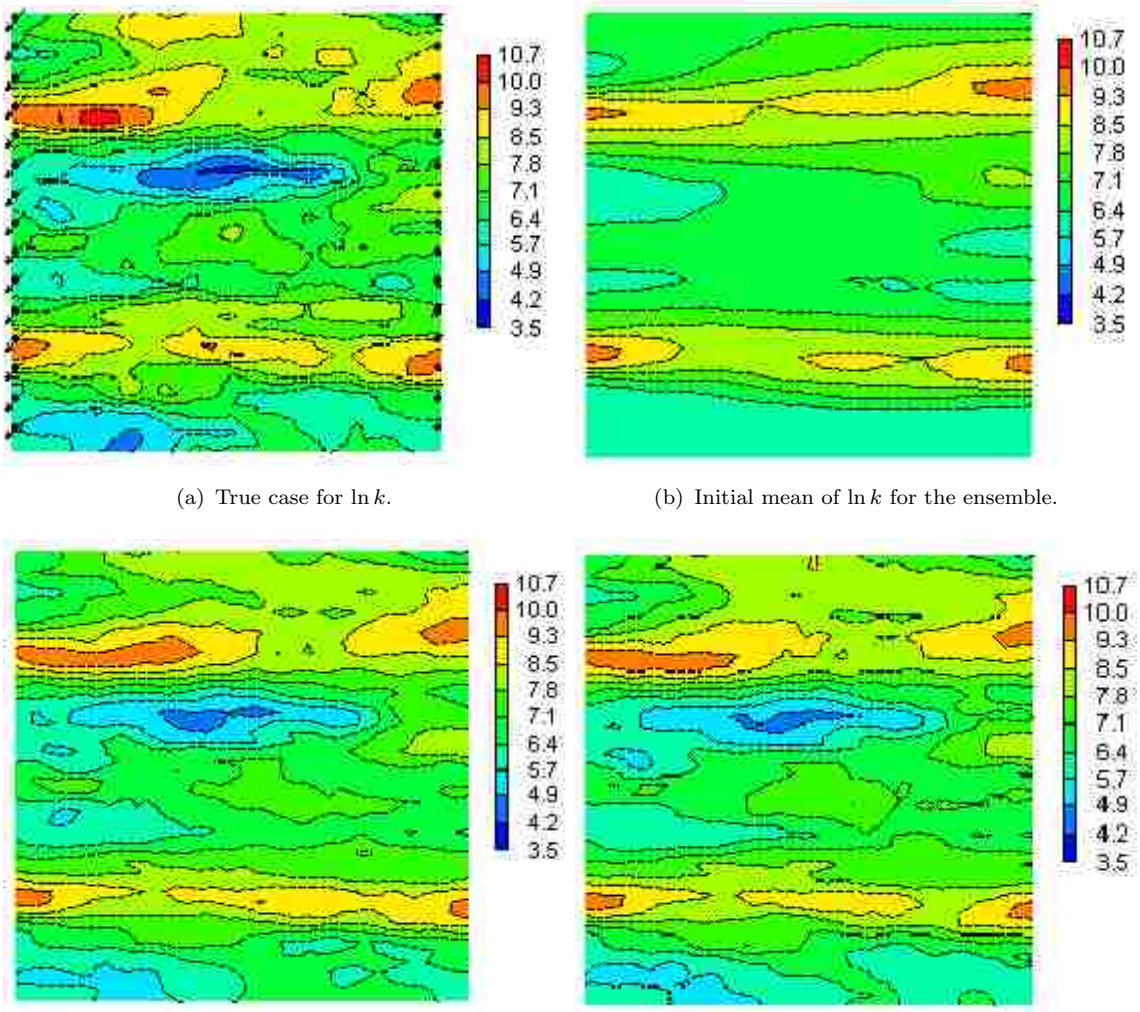

(a) True case for $\ln k$.

(b) Initial mean of $\ln k$ for the ensemble.

(c) Mean $\ln k$ after EnKF.

(d) Mean $\ln k$ after gathered EnKF.

Figure 3.4: Mean horizontal $\ln k$ distribution before and after data assimilation. The standard EnKF and gathered EnKF evolve to similar mean distributions.

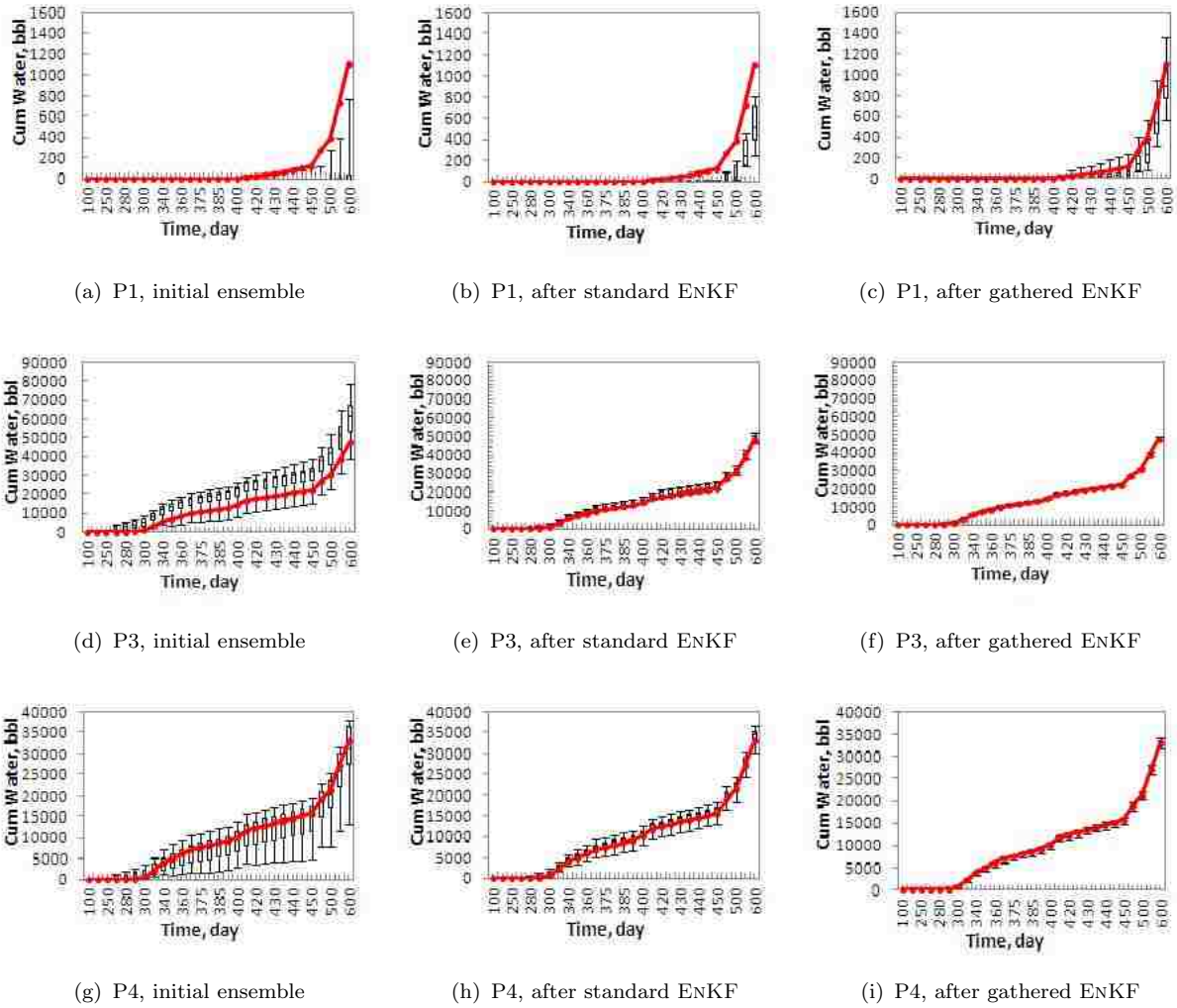

(a) P1, initial ensemble (b) P1, after standard EnKF (c) P1, after gathered EnKF

(d) P3, initial ensemble (e) P3, after standard EnKF (f) P3, after gathered EnKF

(g) P4, initial ensemble (h) P4, after standard EnKF (i) P4, after gathered EnKF

Figure 3.5: Comparison of cumulative water predictions before and after data assimilation. Box plots show the prediction of the realizations and red curve indicates the observation. Both methods match the production observations well; the gathered EnKF works slightly better than standard EnKF

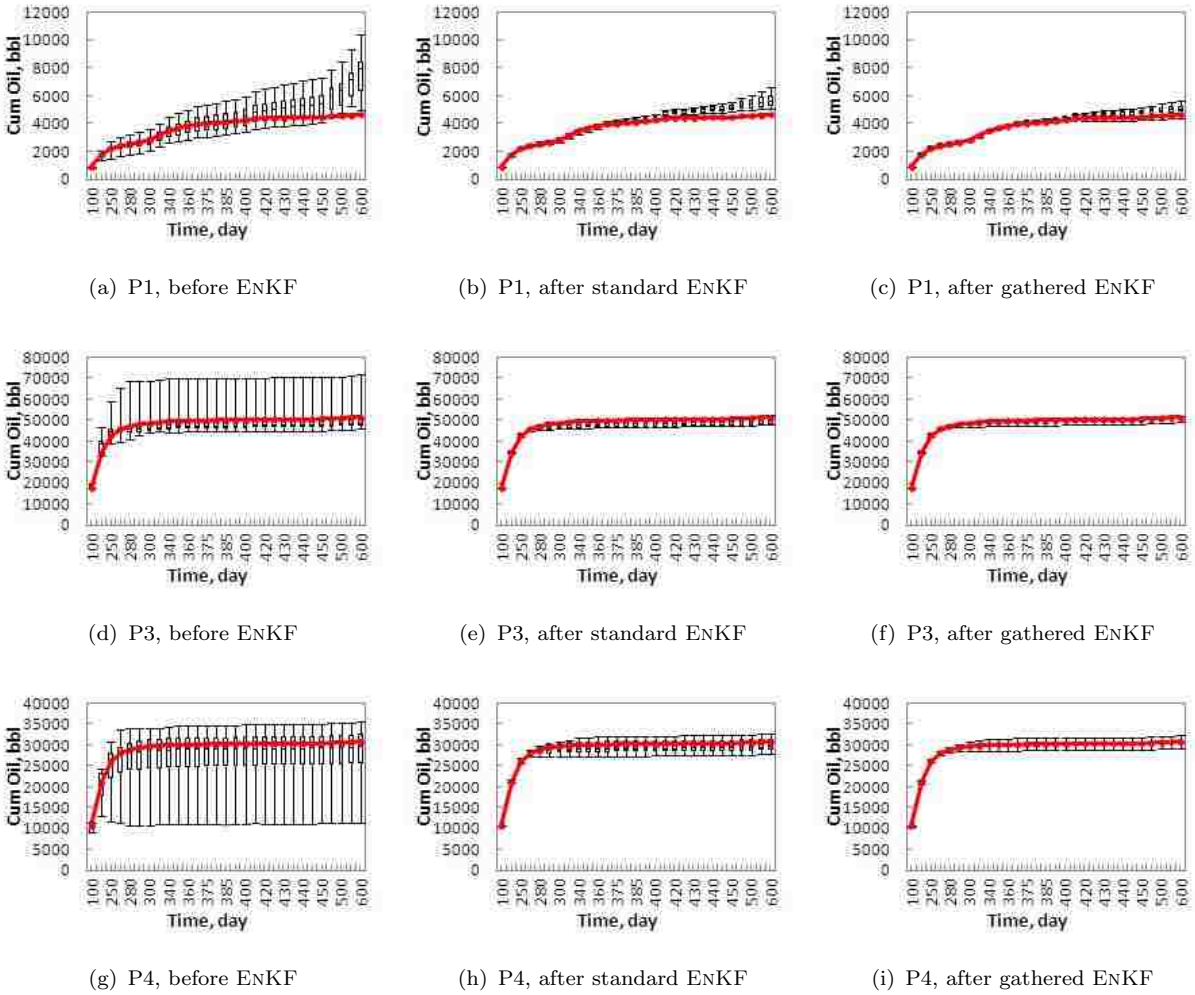

(a) P1, before EnKF (b) P1, after standard EnKF (c) P1, after gathered EnKF

(d) P3, before EnKF (e) P3, after standard EnKF (f) P3, after gathered EnKF

(g) P4, before EnKF (h) P4, after standard EnKF (i) P4, after gathered EnKF

Figure 3.6: Comparison of cumulative oil predictions before and after data assimilation. Box plots show the prediction of the realizations and red curve indicates the observation. Both methods match the production observations well; the gathered EnKF works slightly better than standard EnKF

3.6 Discussion

3.6.1 Effects of ensemble size.

The ensemble size effect is now assessed using a gather size of $N_g = 6$. To control bias, each case is repeated with the same ensemble 10 times, with differently perturbed observations. The RMSEs of the mean from the truth (δ) for each individual run are shown as diamonds and the ensemble standard derivations (σ) are shown as circles (Fig. 3.7). The expectation of these two values ($\langle\delta\rangle$ and $\langle\sigma\rangle$) are shown as solid and dashed lines respectively. The δ of the

standard EnKF (Fig. 3.7(a), Fig. 3.7(c) and Fig. 3.7(e)) are more dispersed than the gathered EnKF (Fig. 3.7(b), Fig. 3.7(d) and Fig. 3.7(f)). This shows that gathering the observations reduces the observation sampling errors introduced to the Kalman gain, making the model more stable. In addition, for small ensembles, the gathered EnKF obtains a smaller mean error $\langle\delta\rangle$ and greater diversity $\langle\sigma\rangle$ than standard EnKF. As expected, increasing ensemble size causes these two methods to converge.

3.6.2 Effects of gather size

The effect of gather size on sampling errors is also examined and the results are shown in Fig. 3.8 and Fig. 3.9. Increasing the gather size reduces the dispersion of σ and δ for different runs thus making the model more stable (Fig. 3.8). As the gather size N_g increases, the mean of the departure from the true mean (δ) decreases and mean of ensemble standard deviation σ is estimated more accurately (Fig. 3.9). This is consistent with the scalar case as well as the proof.

3.6.3 The effect of initial ensemble and time interval

A good initial ensemble ($||\epsilon|| \ll ||C_Y||$) is one of the key components for the successful EnKF data assimilation. In a *good* ensemble, the forecasts of the ensemble members should cover the true forecast and the mean of the ensemble should close to the truth (Fig. 3.10(a)). However, in some cases *bad* initial ensembles may generated due to the low resolution of the samples or small size of the ensemble, the ensemble forecasts may away from the truth and relatively close to each other (Fig. 3.10(b)). In this case, reservoir model updating could fail since the lack of ensemble spread would cause an overconfidence on the prior model(s).

To demonstrate this, we divide the 500 initial realizations to 10 equal–sized subsets. We forecast the performance of these 10 subsets by running the simulator forward from time zero to 600 days. A good and bad ensembles are then selected based on the RMSE of the forecast ensemble mean from the true observation. The smaller the RMSE, the higher the

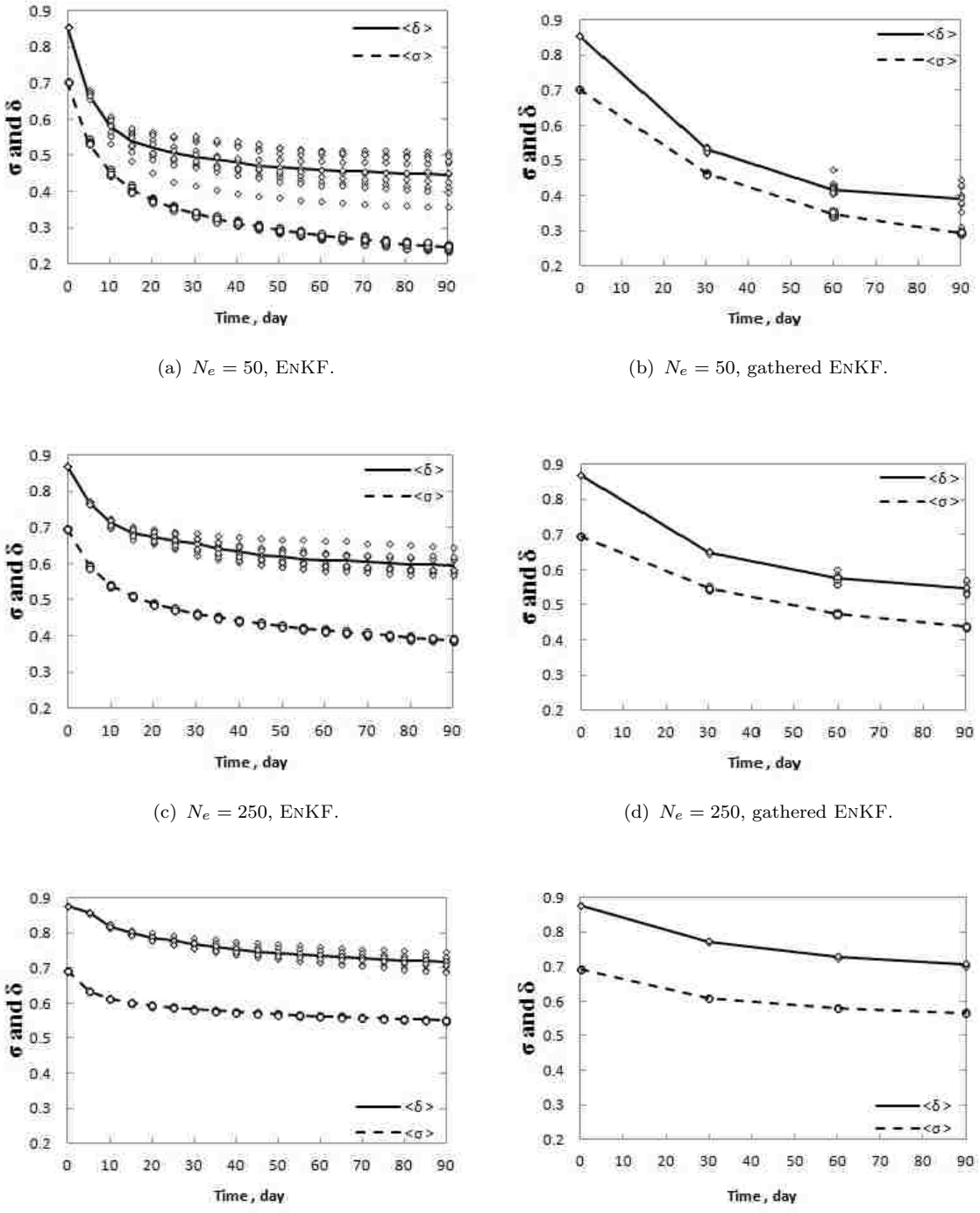

(a) $N_e = 50$, EnKF.

(b) $N_e = 50$, gathered EnKF.

(c) $N_e = 250$, EnKF.

(d) $N_e = 250$, gathered EnKF.

(e) $N_e = 500$, EnKF.

(f) $N_e = 500$, gathered EnKF.

Figure 3.7: Comparison of standard EnKF with gathered EnKF for different ensemble size, 2D synthetic waterflood case. All estimates improve with time and with increasing N_e. The gathered EnKF generally outperforms the standard EnKF, especially at late time: the estimate has smaller mean error and greater diversity.

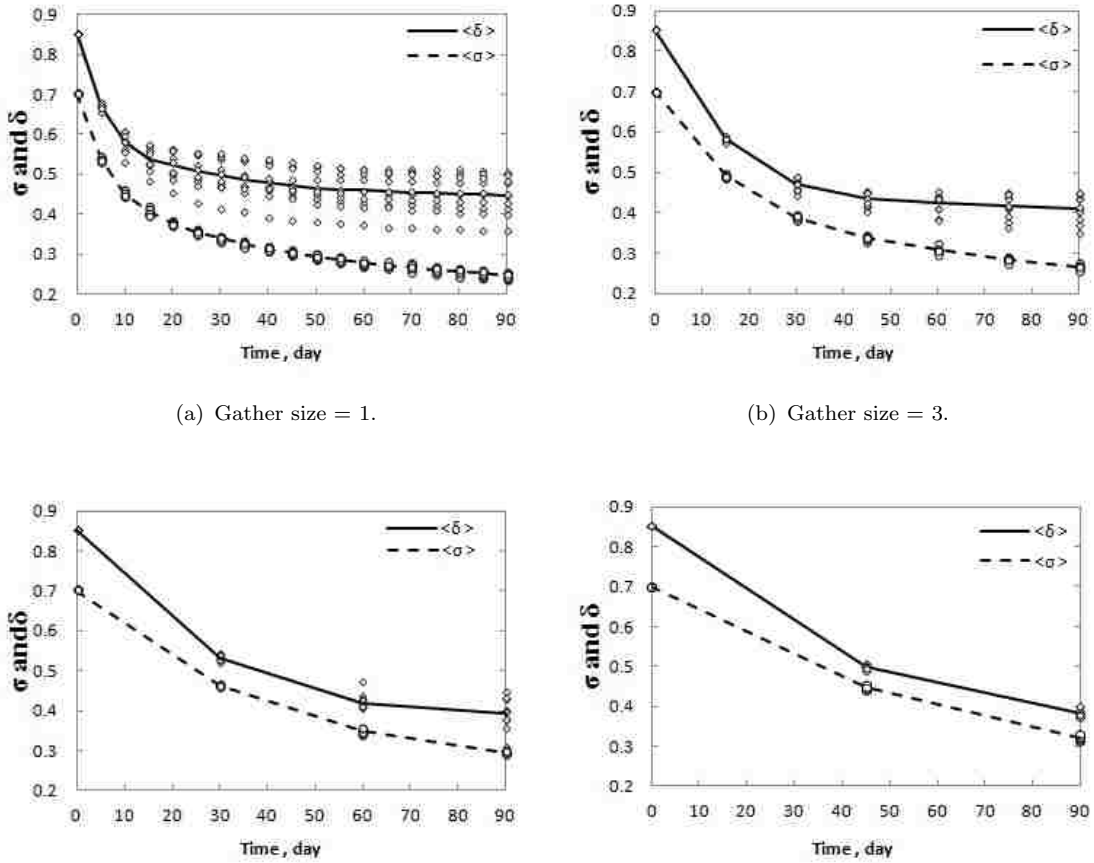

(a) Gather size = 1.

(b) Gather size = 3.

(c) Gather size = 6.

(d) Gather size = 9.

Figure 3.8: The effect of gather size on sampling errors for reservoir model updating case, 2D synthetic waterflood case. Increasing gather size reduces the dispersion of σ and δ for different runs, making the model more stable.

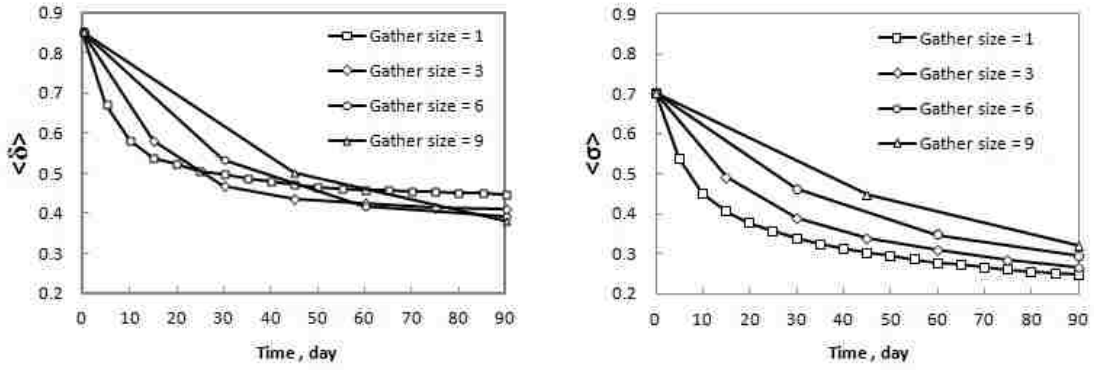

(a) $\langle\delta\rangle$ for different gather sizes.

(b) $\langle\sigma\rangle$ for different gather sizes.

Figure 3.9: Comparison of $\langle\delta\rangle$ and $\langle\sigma\rangle$ for different gather sizes, 2D synthetic waterflood case. The RMSE $\langle\delta\rangle$ decreases and ensemble standard derivation $\langle\sigma\rangle$ is estimated more accurately with the increasing gather size.

sample quality. When a good ensemble is used, the more observations assimilated (or the smaller the data assimilation time interval), the closer the the ensemble mean from the truth (Fig. 3.11(a)). However, if a bad ensemble is used, increasing the number of observations or reducing the time interval may not help to get the estimated mean close to the truth (Fig. 3.11(b)). If the prior ensemble is poor, the ensemble prediction can not cover the truth, and the forecast ensemble covariance ($C^f_{Y_E}$) may be relatively far away the true covariance (C^f_Y) due to large sampling errors (ϵ). This may cause a slower reduction of RMSE of the ensemble mean from the truth at early time. The ensemble may diverge from the truth at late time if ensemble diversity σ collapses to too small a value (Fig. 3.11(c)). The gathered EnKF can not solve this problem because it only reduces sampling errors from the perturbed observations. Thus, gathered EnKF outperforms standard EnKF only if a good initial ensemble is used. Methods to improve initial ensemble qualities was discussed by Oliver and Chen (2008) and Evensen (2009).

3.6.4 Computational efficiency

Gathering the observation data reduces data assimilation time and saves computational cost because of avoided restarts, file transfers, and reading and writing required at each EnKF assimilation step. The main cost save are from avoiding restarts, this is further discussed in chapter 5. However, increasing the number of observations assimilated at one time, increases the cost of computing the Kalman gain:

$$K_e \approx C_{y,d}(C_{d,d} + C_D)^{-1}\,.$$

Because the Kalman gain is a product of N_y by N_d^S matrix and N_d^S by N_d^S matrix, the cost of computing it increases exponentially with the increases of N_d^S. When the number of observations is small, the increase of Kalman gain computational cost is small compared with other costs.

For moderate values of observation count N_d^S and gather size N_g, computation costs decrease with increasing N_g (N_g is the number of discrete observation intervals gathered into a

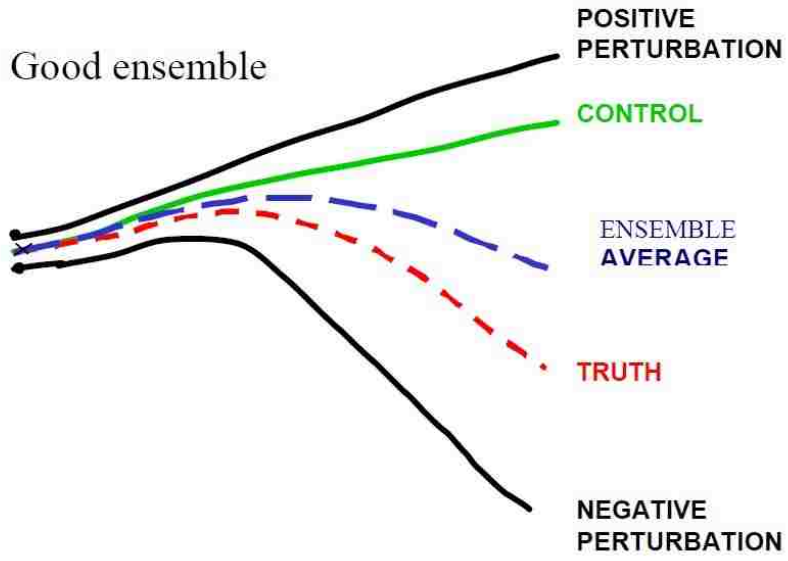

(a) Good ensemble

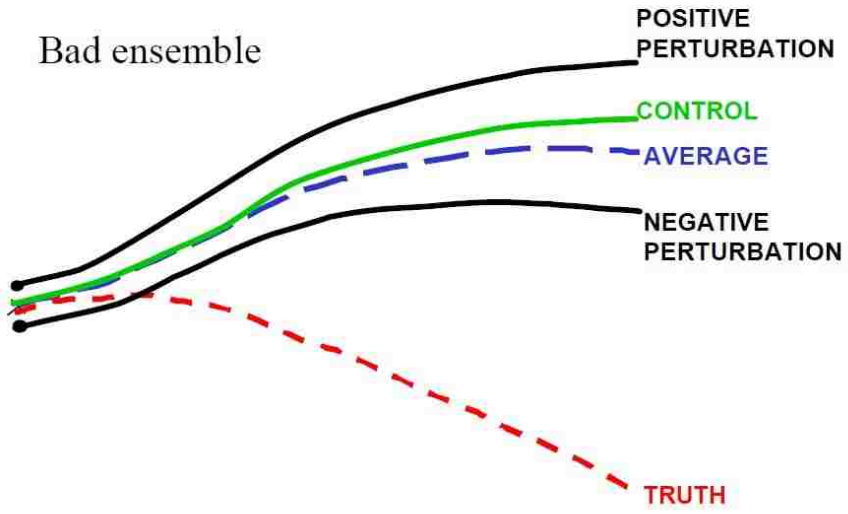

(b) Bad ensemble

Figure 3.10: Schematic of the essential components of an ensemble of forecasts: The analysis (a cross) which constitutes the initial conditions for the control forecast (in green); the initial perturbations (a thick dot) around the analysis, which in this case are chosen to be equal and opposite; the perturbed forecasts (in black); the ensemble average (in blue); and verifying analysis or truth (in red). The first schematic is that of a "good ensemble" in which truth is a plausible member of the ensemble. The second is a bad ensemble, quite different from the truth, pointing to the presence of a problem in the forecasting system such as deficiencies in the analysis, in the ensemble of perturbations and/or in the model, Kalnay (2006).

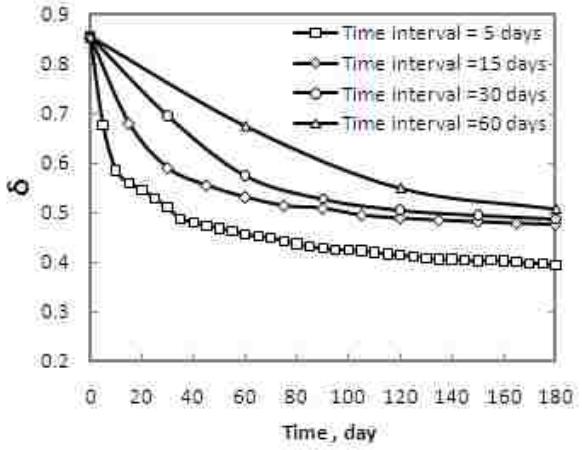

(a) Good ensemble

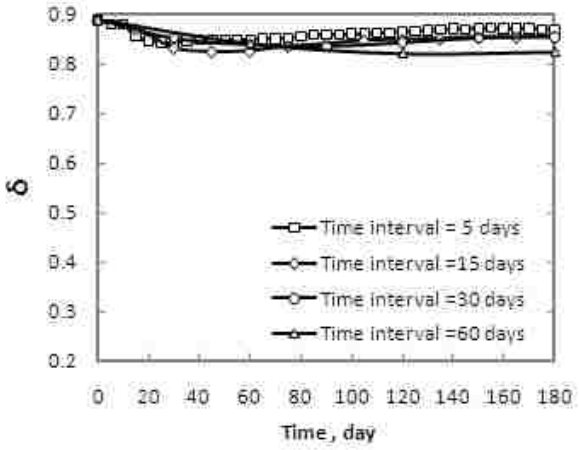

(b) Bad ensemble

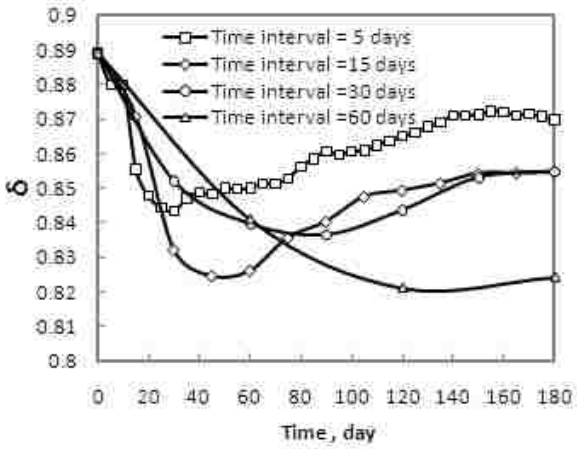

(c) Early–time detail of bad ensemble

Figure 3.11: The effect of initial ensemble.When a good ensemble is used, the more observations assimilated (or the smaller the data assimilation time interval), the closer the the ensemble mean from the truth. However, if a bad ensemble is used, increasing the number of observations or reducing the time interval may not help to get the estimated mean close to the truth.

single assimilation). However, for larger N_d^S, the cost of the Kalman gain increases steeply. If the increment of Kalman gain computation is bigger than the time saved on simulation restarts and data movement, then gathering the observations does not reduce the computational cost. Hence, there is an optimum gather size, N_g. For different ensemble sizes, model sizes, and model dynamics, the optimum gather size will be different. The bigger the en-

semble size N_e, the larger the value N_g, that minimizes computation work (Fig. 3.12). For $N_e = 50$, computation time is a minimum at $N_g = 9$; for $N_e = 500$, computation time is still decreasing at $N_g = 36$.

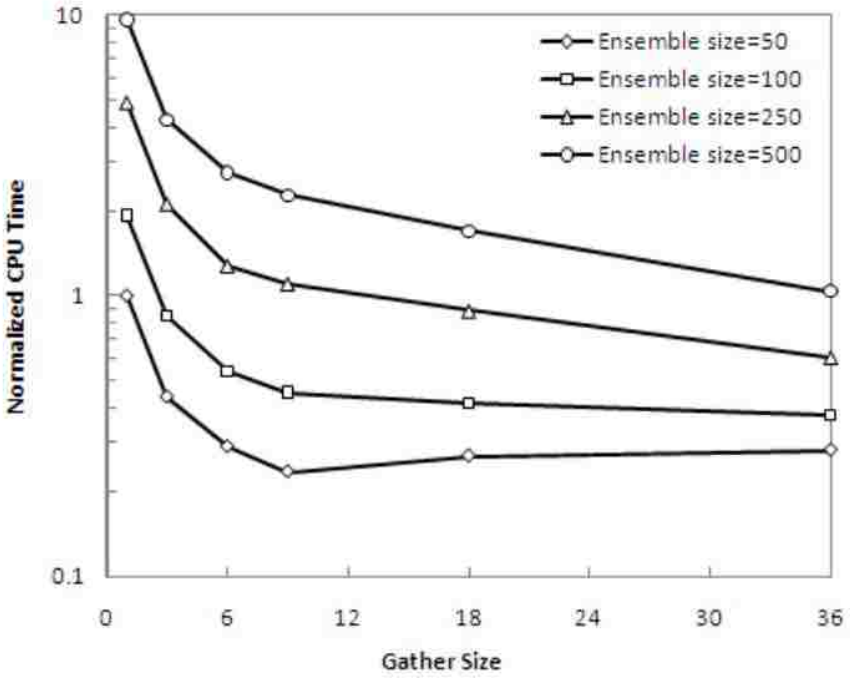

Figure 3.12: Normalized CPU time changes with gather size for different ensemble size, 2D synthetic waterflood case. An optimum gather size exists in terms of time saving. However, for different ensemble sizes, the optimum gather size will be different. The bigger the ensemble size used, the more we can gather. As shown in this figure, for $N_e = 50$, CPU time is a minimum at $N_g = 9$; for $N_e = 500$, CPU time is still decreasing at $N_g = 36$.

3.7 Conclusions

A gathered EnKF method is investigated in this chapter.

1. Gathering the observations was proven to reduce sampling errors in the Kalman gain, reducing bias in the ensemble covariance.

2. The gathered EnKF was tested with scalar and 2D reservoir history matching cases. These verified the improved estimation of the ensemble covariance and suggested improved estimation of the ensemble mean.

3. Improved estimation of the ensemble mean and the more diverse ensembles provided by gathering imply greater stability compared with the standard EnKF.

Chapter 4
The Brugge Field Description

Only 2D synthetic reservoir models are used in chapter 2 and chapter 3 to demonstrate how the proposed methods work. A more realistic, complex reservoir model is needed for the further testing and demonstration. Because the Brugge field is the most "realistic", complex, 3D synthetic case that has been widely used for comparative study of alternative methods for reservoir history matching and model–based production optimization; it is also chosen as illustrative example in this dissertation. A detailed description of the Brugge field is given in this chapter.

4.1 Introduction

The Brugge field case is a 3D synthetic complex reservoir field made available to participants by Netherlands Organization for Applied Scientific Research (TNO) in the preparation for SPE Applied Technology Workshop (ATW), a benchmark project for closed–loop reservoir management, held in Brugge in June 2008. The goal of the project was to test the different combined use of optimization and history matching methods in closed–loop reservoir management (Peters et al. 2009).

The original Brugge field model is a high–resolution model which consists of 20 million grid cells. This high resolution model was upscaled to a 450,000 grid cell model which was used as the true case. 104 further upscaled realizations containing 60,000 grid blocks were then generated using data extracted from the true case including well logs, geological facies classifications and maps. Each realization contains seven types of parameters needed to be history matched: facies, net–to–gross, porosity, permeability in X, Y, Z directions and the initial water saturation. The structure of the field (fault position and throws, top of structure map, zone thickness , grid cell geometry) was identical for all the realizations. These

104 realizations along with upscaled structure model, well log data, 10 years of production history data and inverted time–lapse 4D seismic data generated from the true case were provided to the participants. With all these information, participants are required to history match for the first 10 years and provide a history matched model (or a matched ensemble set) for production optimization for the next 20 years. The field contains 10 injectors and 20 producers. For the next 20 years, all these wells are assumed to be smart wells that each well segment can be controlled independently by inflow control valves. The economic parameters including oil price, water disposal cost as well as discount rate were also provided by TNO. Their strategies were then sent to TNO to be tested on the "true case" to get production observations for years 10–20. The observations were then sent back to participants with which they used to update their reservoir model and revise their optimization strategies for years 20–30.

Nine groups participated in the workshop and the results are reviewed by Peters et al. (2009). The combination of history matching and production optimization methods used by the participants varied considerably. For history matching, methods used by participants include EnKF, EnRML (Ensemble random likelihood), streamline–based generated travel time inversion, sequential quadratic program and so on. For production optimizations, methods used include EnOpt, sequential experimental design, adjoint–based gradients optimization and so on. The root mean square error (RMSE) for the production data and the realized NPV for the next 20 years are used to check the quality of history matching and production optimization respectively. The RMSE obtained by participants ranges from 574 to 58 for years 0–10 and from 1820 to 239 for years 10–20 years. Note here RMSE are the summation of water rate, oil rate and BHP. Even though they have different units (water, oil rate in bbl/day, BHP in psi), in this case, they are in the same order. The realized NPV ranges from \$4.01–\$4.46 billion for years 10–20 and \$4.12–\$4.50 billion for years 20–30. Among the nine groups, Chen and Oliver (2010) obtains the highest NPV (\$4.5 billion) which was only three percent lower than the optimized NPV (\$4.63 billion) on the true model.

Two lessons from the benchmark study which are also pointed out by Peters et al. (2009) are:

- A good history matched model or a set of good matched models are necessary to obtain a high realized NPV; none of the participants with high RMSE obtains high realized NPV. However, it is not sufficient. The quality of the optimization algorithm is equally important.

- Increasing the optimization and reservoir model updating frequency using the field feedback and increasing the uncertainty on the reservoir model parameters could improve the performance of closed–loop reservoir management.

In this chapter, we give detailed description of the Brugge field. In chapter 5, we propose an adaptively gathered EnKF method and test it on Brugge field. In chapter 6, we test the whole closed–loop reservoir management concept on the Brugge field.

4.2 Geology structure and simulation model

The Brugge reservoir consists of an E–W elongated half–dome with a large boundary fault and one internal fault. The reservoir extent is about 328,000 $\times$ 98,400 $\times$ 200 ft^3. The initial oil in place is about 775 MMstb. From top to bottom, the Brugge field consists of four main reservoir formations, Schelde, Maas, Waal and Schie. The characteristic of each zone are summarized in Table 4.1. The lithology for Schelde formation is discrete sand bodies in shale, for Maas formation is carbonate concretions and for Schie formation is the irregular carbonate patches. Schelde and Waal formations have higher permeability and porosity and more heterogenous than Maas and Schie formations. Out of these four formations, Waal formation has the most favorable reservoir properties.

The simulation model provided by TNO contains 60,000 gridblocks with $N_m = 44,550$ active gridblocks. It has 9 simulation layers. Layers 1–2 belong to the Schelde formation, layers 3–5 belong to Maas, layer 6–8 belongs to Waal, and layer 9 belongs to Schie. Each of

Table 4.1: Properties of the Brugge field formation

Formation	Average thickness (ft)	Average porosity	Average permeability (md)	Average net–to-Gross	Depositional environment
Schelde	32.8	0.207	1105	60	Fluvial
Maas	65.6	0.190	90	88	Lower shoreface
Waal	85.3	0.241	814	97	Upper shoreface
Schie	16.4	0.194	36	77	Sandy shelf

this 9 layers contains 139×48 grid blocks. The field is completed with 20 producers and 10 injectors (Fig. 4.1) with the producer surrounding by injectors.

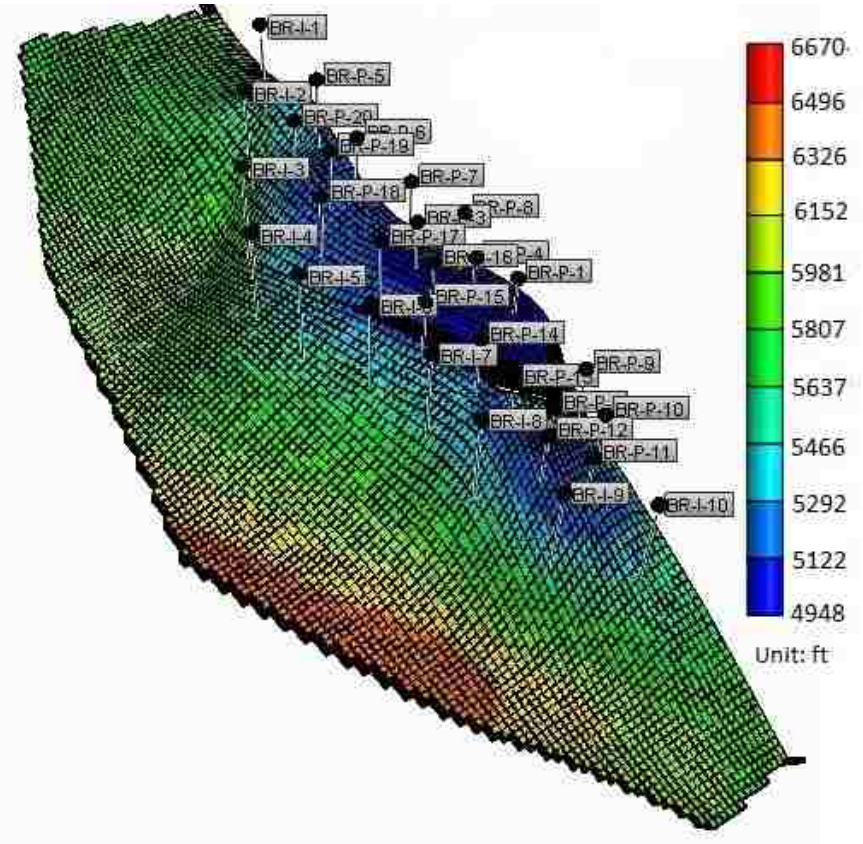

Figure 4.1: The top of the Brugge field. Injectors are indicated with I and producers with P. Areal extent is approximately 328,000 by 98,400 ft^2, and the model has 9 layers and 44,550 active blocks.

4.3 Prior realizations

A total of 104 realizations were generated using different geostatistical methods (Peters et al. 2009). The described properties are facies, net–to–gross, porosity, water saturation and permeability in the X, Y and Z directions. 78 of the realizations have facies modeling enabled (FY) while 26 of the realizations facies are ignored (FN). For half of the realizations with facies modeling enabled, the top formation (Schelde; fluvial depositional environment) is modeled using channel objects in a shale background (SF). The left half is modeled using sequential indicator simulation (SS). For the realizations without facies, only sequential indicator simulation (SS) is considered for all realizations. The porosity is generated using sequential Gaussian simulation for all the realizations. The permeability for realizations with facies enabled is generated either using single poroperm regression (KS) (Fig. 4.3, upper graph), or using different poroperm regression for different facies (KM) (Fig. 4.3, lower graph), or with cokriging on porosity (KP). When facies is ignored, only the first two methods are used to create permeability. Overall, the realization either has a combination of FN-SS-KS, or FN-SS-KP, or FY-SS-KS, or FY-SS-KP, or FY-SS-KM, or FY-SF-KS, or FY-SF-KP, or FY-SF-KM. Each type of combination has 13 realizations.

4.4 Reservoir simulation parameters of the true model

PVT data. Table 4.2 lists all the PVT data at reference pressure of 2465 psi. Because the reservoir is an undersaturated oil reservoir, the oil–water two–phase reservoir model is used simulate the reservoir model in this dissertation.

Table 4.2: PVT data of the Brugge field at reference pressure of 2465 psi.

	Density lb/ft^3	Compressibility 1/psi	Viscosity cp
Water	62.6	3.00×10^{-6}	0.320
Oil	56.0	9.26×10^{-6}	1.294
Pore	-	3.50×10^{-6}	-

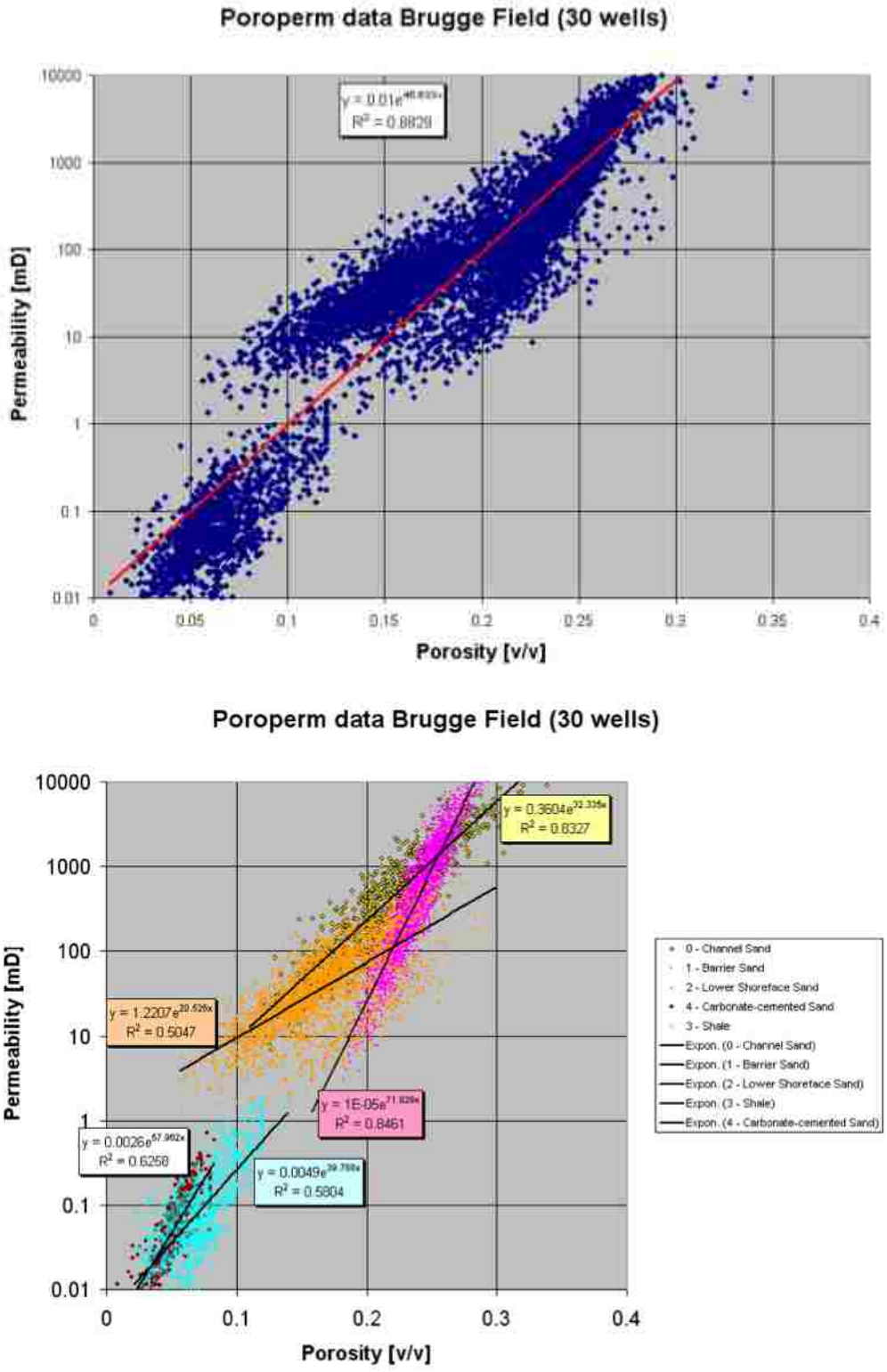

Figure 4.2: Porosity and permeability relations derived from all wells of the Brugge field. Upper graph shows the results for all facies. Lower graph shows the results for each individual facies (image from TNO).

Relative permeability and capillary pressure curves. The reservoir model is divided to seven different rock types based on the porosity (Table 4.3). For different rock types different relative permeability and capillary curves are used. The Corey permeability model is used to calculate the permeability curve with the same exponents for different rock types which are $n_w = 3$, $n_o = 5$, $K^e_{rw} = 0.6$ and $K^e_{ro} = 0.4$. The end points for water saturation are different for different rock types whereas the end points for oil saturation are the same. The relative permeability curves and capillary curves are shown in Fig. 4.3 and Fig.4.4 respectively.

Table 4.3: Relative permeability of the Brugge field for the Corey models

Rock type	Porosity (ϕ) range	S_{wc}	S_{or}
1	≥ 0.225	0.252	0.15
2	0.200–0.225	0.257	0.15
3	0.175–0.200	0.266	0.15
4	0.150–0.175	0.286	0.15
5	0.125–0.150	0.304	0.15
6	0.075–0.125	0.516	0.15
7	≤ 0.075	0.850	0.15

Initialization data. The reference pressure is about 2465 psi at 5578 ft depth and the free water level used in the true reservoir model is at depth 5505 ft. Besides free water level, TNO also provided 104 realizations of initial water saturations. Instead of using the free water level, we can also use the initial water saturation to initialize our reservoir models.

4.5 Producers and injectors

The field case has 20 vertical producers and 10 vertical peripheral water injectors. The well completions are summarized in Table 4.4. The injectors are completed in all the formations while some of the producers are only completed in the top layers to avoid completing under initial oil water contact. One well is turned on each month. The starting sequence for all the wells are as following: BR-P-5, BR-P-10, BR-P-11, BR-P-12, BR-P-13, BR-P-14, BR-P-15, BR-P-16, BR-P-17, BR-P-18, BR-P-19, BR-P-20, BR-P-1, BR-P-2, BR-P-3, BR-P-4,

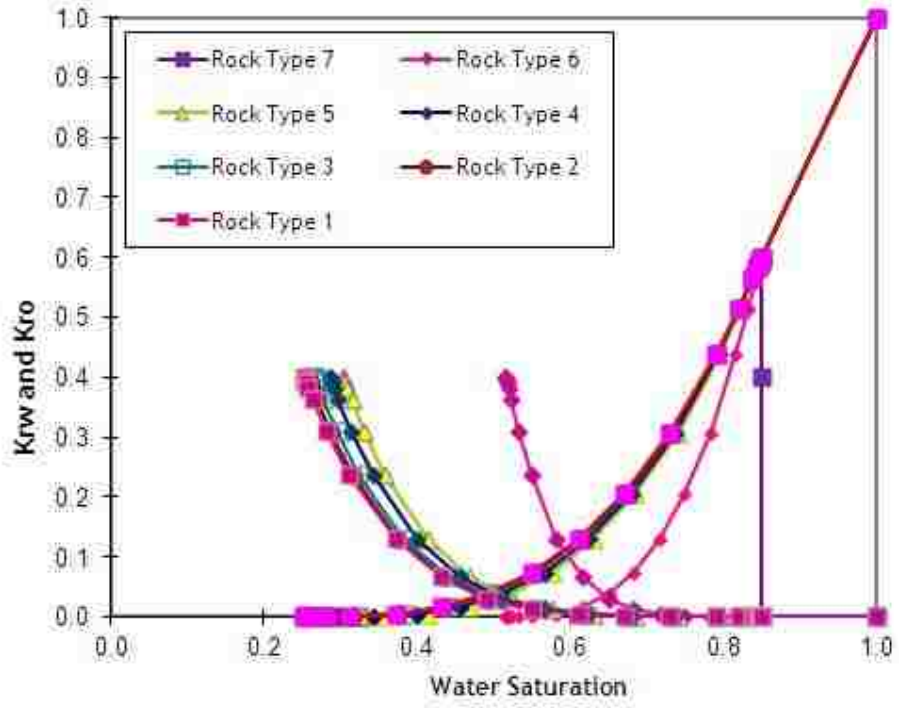

Figure 4.3: Relative permeability curves for seven rock types of the Brugge field. Rock types 1–5 have similar relative permeability curves.

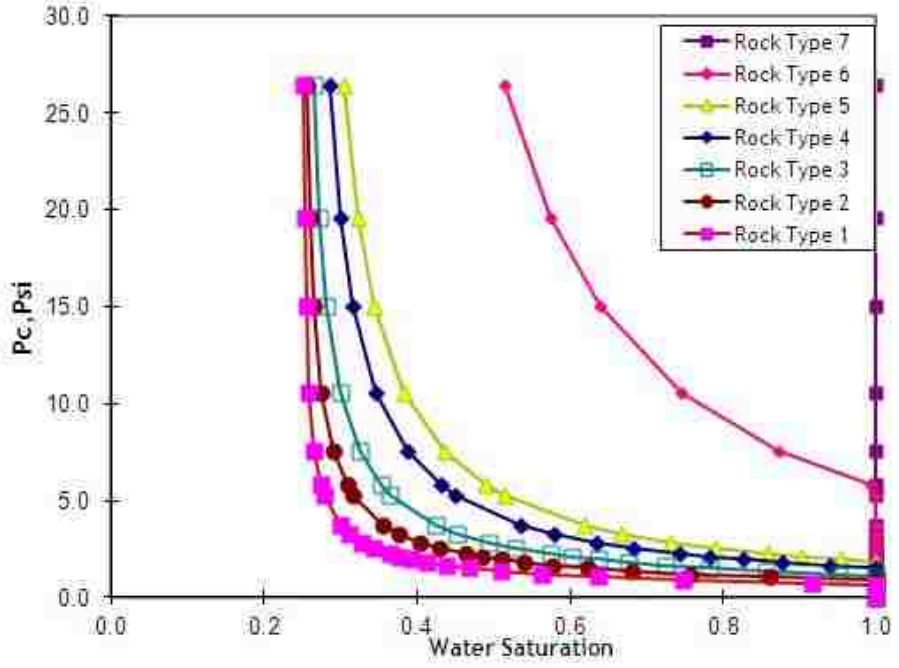

Figure 4.4: Capillary pressure curves for seven rock types of the Brugge field

BR-P-6, BR-P-7, BR-P-8, BR-P-9, BR-I-1, BR-I-2, BR-I-3, BR-I-4, BR-I-5, BR-I-6, BR-I-7, BR-I-8, BR-I-9 and BR-I-10. The first turned on well is BR-P-5 which begins producing on day 0 and the last well on production is BR-I-10, beginning on day 870. The producers are controlled by a fluid production rate of 2000 stb/day and a maximum water cut of 90 percent. The injectors are controlled by water injection rate of 4000 stb/day. Monthly production observations are provided for the first 10 years (bottom hole pressure for all wells, and oil rate and water rate for each producer). Production history data provided by TNO shows most of the wells can meet the target production rate 2000 stb/day except BR-P-9. BR-P-9 starts with a liquid production rate about 1300 stb/day and it keeps on dropping to about 600 stb/day at the end of year 10.

Table 4.4: Brugge field well perforations. Yes stands for perforated, no standards for not perforated.

	Layer 1, 2 Schelde Fm	Layer 3, 4, 5 Maas Fm	Layer 6,7,8 Waal Fm	Layer 9 Schie Fm
Producers 1-4, 6-8, 11-13 and 16-20	Yes	Yes	Yes	Yes
Producers 5, 10 ,14 and 15	Yes	Yes	No	No
Producer 9	Yes	No	No	No
All injectors	Yes	Yes	Yes	Yes

4.6 Initial ensemble performance

As I discussed in chapter 3, a good ensemble is needed for a good history match. In order to know how accurate the initial ensemble captures the true field, we forecast the production for the first ten years using the initial ensemble. The performance of the initial realizations are reviewed in terms of match qualities to the observations from the true field.

4.6.1 Production data

The predictions of water cuts for selected producers and the bottom hole pressure for selected producers and injectors are shown in Fig. 4.5 and Fig. 4.6 respectively. Here, we only

show the prediction of bottom hole pressure for one injector; because, the performance for all the injectors are quite similar. The initial ensemble prediction for most of the wells are biased and the ensemble mean is not near to the observations. Despite the bias, the spread of ensemble is moderate. For wells close to the free water level, water break through within 10 years (eg. BR-P-12, BR-P-18 and BR-P-20; Fig. 4.5). Generally, adjusting free water contact would be a good solution to match water cuts. However, in our case, the ensemble overestimates the water cuts of some wells while underestimates the water cuts of the others. Thus adjusting free water level may not be the ideal solution. In addition, the predictions of bottom hole pressures (Fig. 4.6) show that, the ensemble overestimates the bottom hole pressure for injectors and underestimates the bottom hole pressure for producers. This indicates an underestimation of permeability when the viscosities of water and oil are the same as the true case.

4.6.2 Inverted 4D seismic data

4D seismic is an important source of information for the reservoir monitoring and improvement of the geological model. The averaged seismic data, which inverted as time–lapse differences in pore pressure and water saturation changes for the first ten years is also provided by TNO as another type of observation data. However, because the data from TNO is for a finer scale model (450,000 gridlocks), we cannot assimilate it for history matching without down scaling; it can be used to check the quality of initial and updated realizations.

As it is shown in Fig. 4.7 and Fig. 4.8, the water swept area of the initial mean for Shelde zone and Waal zone are smaller than these of the inverted 4D seismic data, indicating the transmissibilities between injectors and producers are underestimated. This is further confirmed with the pressure changes which are shown in Fig. 4.8. Comparing with the inverted 4D seismic data, the initial ensemble mean has larger pressure drops at production area and smaller pressure drops in other area.

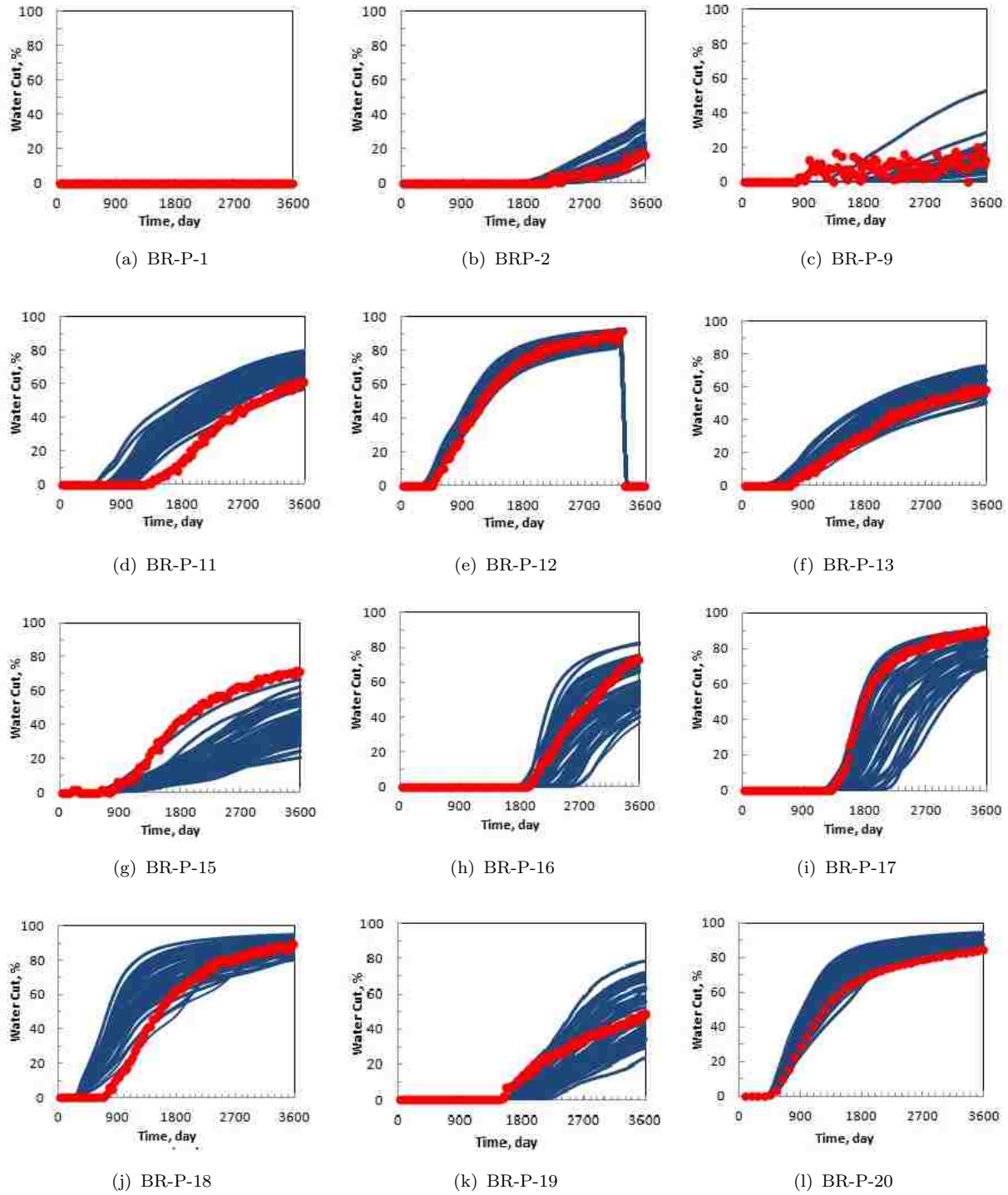

(a) BR-P-1 (b) BRP-2 (c) BR-P-9

(d) BR-P-11 (e) BR-P-12 (f) BR-P-13

(g) BR-P-15 (h) BR-P-16 (i) BR-P-17

(j) BR-P-18 (k) BR-P-19 (l) BR-P-20

Figure 4.5: Prediction of the water cuts from the initial ensemble for selected wells. Red dots indicate the observations. The initial ensemble forecasts for most of the wells are biased.

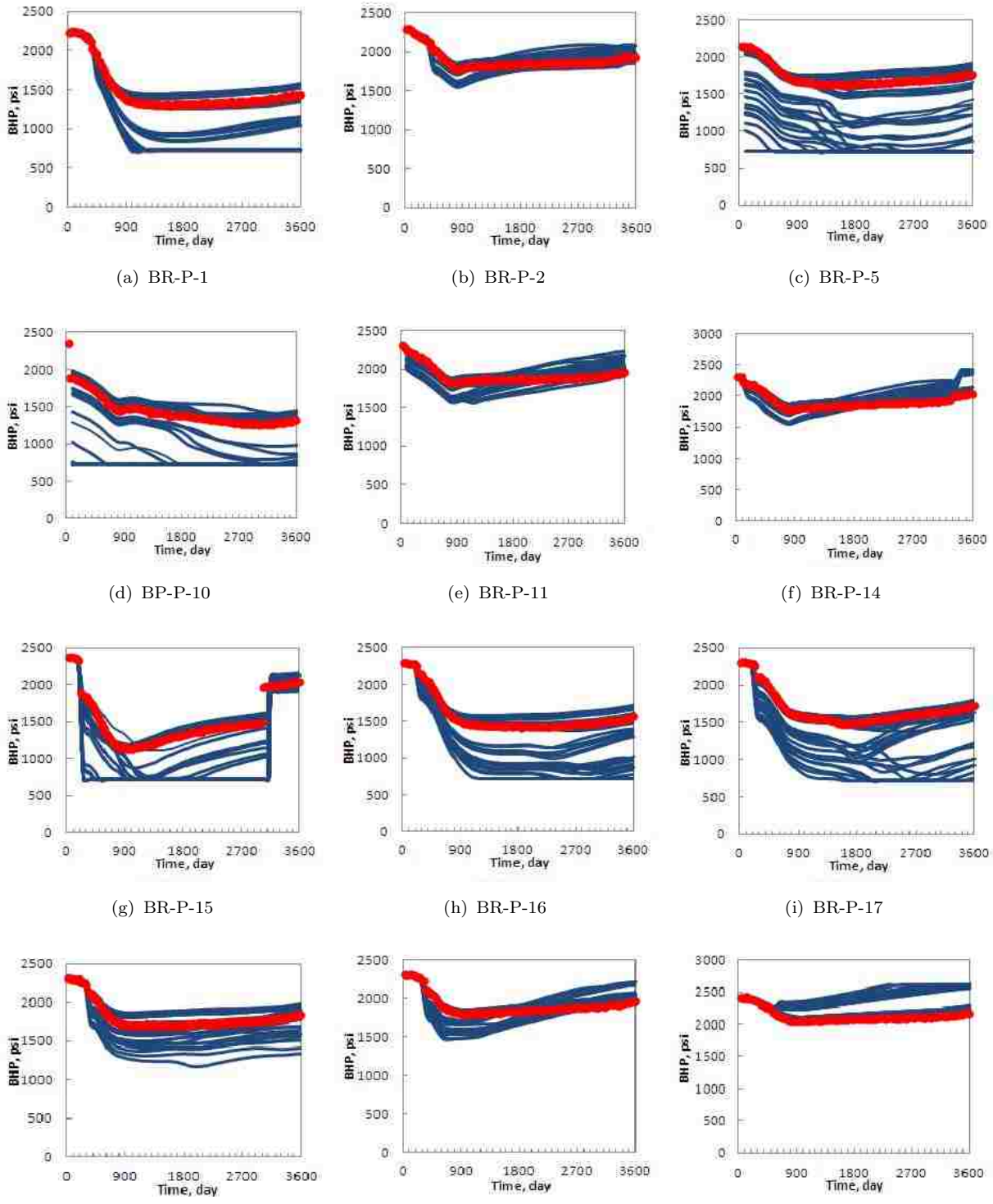

(a) BR-P-1 (b) BR-P-2 (c) BR-P-5

(d) BP-P-10 (e) BR-P-11 (f) BR-P-14

(g) BR-P-15 (h) BR-P-16 (i) BR-P-17

(j) BR-P-19 (k) BR-P-20 (l) BR-I-1

Figure 4.6: Prediction of the bottom hole pressure from the initial ensemble for selected wells. Red dots indicate the observations. The prediction of bottom hole pressure for most producers are lower than the observation; whereas the prediction of bottom hole pressure for most injectors are higher than the observation.

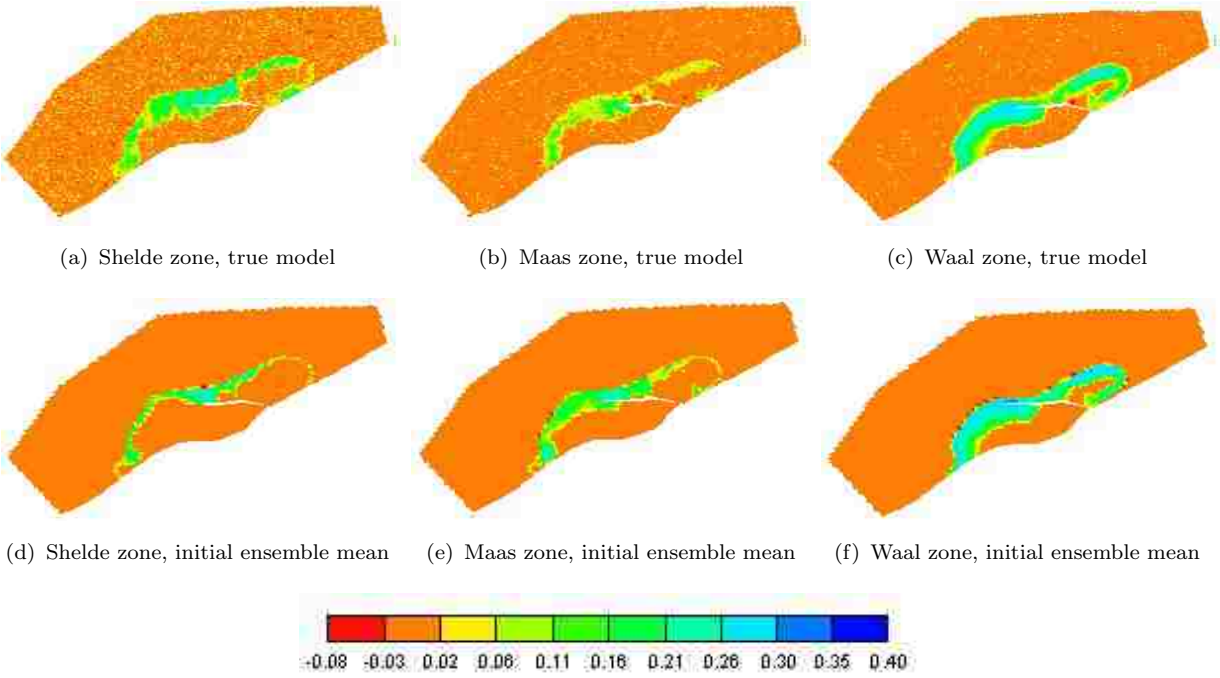

(a) Shelde zone, true model (b) Maas zone, true model (c) Waal zone, true model

(d) Shelde zone, initial ensemble mean (e) Maas zone, initial ensemble mean (f) Waal zone, initial ensemble mean

Figure 4.7: Water saturation changes for selected formations. Upper graphs show the 4D inverted seismic data from the true model. Lower graphs are the predictions from initial ensemble mean.

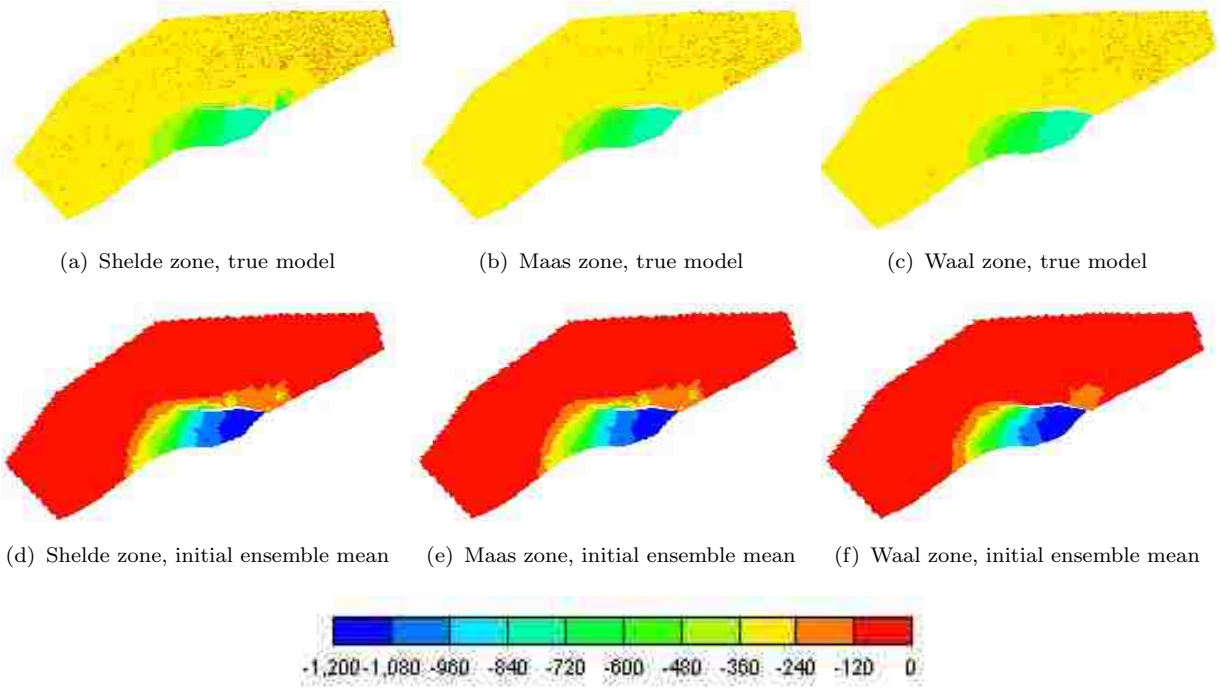

(a) Shelde zone, true model (b) Maas zone, true model (c) Waal zone, true model

(d) Shelde zone, initial ensemble mean (e) Maas zone, initial ensemble mean (f) Waal zone, initial ensemble mean

Figure 4.8: Pressure changes (unit in psi) for selected formations. Upper graphs show the 4D inverted seismic data from the true model. Lower graphs are the predictions from initial ensemble mean.

Chapter 5

An Adaptively Gathered EnKF for Brugge Field Model Updating

5.1 Introduction

Chapter 3 discussed the gathered EnKF with a fixed gathered size and tested it with a scalar and 2D cases. In this chapter, we apply it on a large and complex, synthetic reservoir model–the Brugge field (chapter 4). We demonstrate that the gathered EnKF with a fixed gather size may not work well if the ensemble mean is not very close to the truth. To address this problem, we propose an adaptively gathered EnKF method. The method starts with a small gather size. Then, if the ensemble mean prediction is converging on the observations after assimilation, the gather size is doubled until it reaches a specified maximum interval. If the mean ensemble prediction is diverging from the observations, we reduce our gather size by half. The adaptively gathered EnKF is compared with standard EnKF and gathered EnKF with a fixed gather size. Results are analyzed in terms of convergence and computational cost.

5.2 Numerical experiments description

TNO provided monthly water production rate and oil production rate for all the 20 producers, and bottom hole pressure for all the 10 injectors and 20 producers for years 1–10. For each time step, there are about 70 observations available and totally there are bout $70 \times 120 = 8400$ observations available. In our numerical experiments, the water cut and bottom hole pressure of the producers and the bottom hole of the injectors are used as observations. Because the observations do not change significantly from month to month, we assume the observations are available in a 3-month interval, thus the total number of observations used in our numerical experiments are $50 \times 40 = 2000$. TNO does not provide measurement errors for the observations, we assume the measurement error for water cut is 3 percent and for

bottom hole pressure is 15 psi. $Ne = 52$ realizations are used in our numerical experiments to save simulation time. To keep the diversity of the realizations, the 52 realizations are picked up from every two of the 104 realizations instead of being randomly selected.

Five different senerios are tested in this chapter: standard EnKF, gathered EnKF with$N_g = 3$, $N_g = 5$ and $N_g = 10$, and an adaptively gathered EnKF. The step–wise procedure for the adaptively gathered EnKF is:

1. At assimilation step $l = 1$, $N_g = 2$, updating ensembles with EnKF.

   START: DO WHILE LOOP (check stop criterion, see if more observations are available)

2. Forecast the performance of ensemble mean by forward running of simulation from year 0 to year 10. Calculate the least square error $\delta_{obs,l}$ between the ensemble mean prediction and the real observations.

3. $l = l + 1$. If $\delta_{obs,l-1} < \delta_{obs,l-2}$ and $N_g < N_{g,max}$, $N_g = N_g \times 2$, Else if $\delta_{obs,l-1} < \delta_{obs,l-2}$ and $N_g = N_{g,max}$, $N_g = N_g$, Else $\delta_{obs,l-1} > \delta_{obs,l-2}$, $N_g = N_g/2$, updating ensembles with EnKF.

   END: DO WHILE LOOP

The maximum gather size $N_{g,max}$ varies from case to case depending on the number of observations available at each time step and the ensemble size. In this chapter, we choose $N_{g,max} = 8$ because if we set $N_{g,max} = 16$ then it takes much longer to calculate the Kalman gain.

5.3 Results

5.3.1 Comparison of RMSE for production data

RMSE for water rate, oil rate and bottom hole pressure (BHP) for the history matching period of the first 10 years are used to show the quality of history match. They are calculated using Eqs. 5.1–5.3.

$$RMSE_{BHP} = \sqrt{\frac{1}{N_t(N_P+N_I)}\sum_{t=1}^{N_t}\sum_{i=1}^{N_P+N_I}(BHP_{t,i} - BHP_{obs,t,i})^2} \tag{5.1}$$

$$RMSE_{water} = \sqrt{\frac{1}{N_t N_P}\sum_{t=1}^{N_t}\sum_{i=1}^{N_P}(Q_{w,t,i} - Q_{wobs,t,i})^2} \tag{5.2}$$

$$RMSE_{oil} = \sqrt{\frac{1}{N_t N_P}\sum_{t=1}^{N_t}\sum_{i=1}^{N_P}(Q_{o,t,i} - Q_{oobs,t,i})^2} \tag{5.3}$$

where N_I is the number of injectors and N_P is the number of producers. N_t indicates total number of time step at which observations are available. Q_w and Q_o are the predicted water and oil production rates using updated ensemble. Q_{wobs} and Q_{oobs} are the water and oil rates from the true field.

RMSE results for the five different scenarios are summarized in Table 5.1. RMSEs have been significantly reduced compared with the initial ensemble for all cases. In addition, we notice that the gathered EnKF with a fixed gather size works better than standard EnKF only when small gather size is used ($N_g = 3$). The RMSEs increase with the increase of gather size. This is because, when the prior ensemble mean is not near the truth, a smaller gather size updating keeps the model on track and close to the true solution. However, if the gather size is too small, the frequent model updating may destroy ensemble diversity and lead to filter divergence; this explains why standard EnKF does not work as well as gathered EnKF with $N_g = 3$. In such case, gathering observations adaptively could be a good choice. In adaptively gathered EnKF, if the mean is not near the truth, a smaller gather size is chosen. The gather size increases when the ensemble mean gets more and more

close to the truth until it reaches to a specified maximum interval. The specified maximum interval is the optimum value at which computational cost is minimum. In this case, the adaptively gathered EnKF works slightly worse than gathered EnKF with $N_g = 3$ (better than $N_g = 10$) but with 18 percent reduction on computational cost (see 5.3.3).

Table 5.1: Quality of the history match (RMSE) with production data for years 0–10.

	RMSE water stb/day	RMSE oil stb/day	RMSE BHP psi
Initial ensemble	354	394	451
Standard EnKF	46	73	78
GEnKF $N_g = 3$	46	64	34
GEnKF $N_g = 5$	50	68	46
GEnKF $N_g = 10$	70	102	45
AGEnKF $N_g \in \{2, 4, 8\}$	55	70	39

Comparing with nine participated groups in the benchmark workshop (Table 5.2), our results obtained from AGEnKF is only higher than that of two groups (IRIS and OU groups). This may because we only use 52 realizations while these two groups used 104 realizations.

Table 5.2: History match results for years 0–10 from the Brugge benchmark study (Peters et al. 2009).

	RMSE water stb/day	RMSE oil stb/day	RMSE BHP psi
Halliburton	178	61.0	209
IRIS	19.4	25.1	13.2
OU/Chevron	41.3	47.3	18.4
Roxar	NA	NA	NA
SLB	118	181	275
TAMU	104	95.5	47.3
Tulsa	87.3	90.0	25.6
SIEP	135	161	165
Stanford/Chevron	213	130	82.4

5.3.2 Updated ensemble performance

Both the updated ensemble of adaptively gathered EnKF and standard EnKF are rerun from time zero. The performance of each updated realization for both methods are shown in Fig. 5.1 and Fig. 5.2. Both methods match the water cut very well (Fig. 5.1). The only thing different is that the updated ensemble spread of adaptively gathered EnKF is wider than standard EnKF for some wells (e.g. BR-P-17, BR-P-19). For bottom hole pressure, the results from adaptively gathered EnKF is less biased than standard EnKF for most of the wells.

The water saturation and pressure changes for the first 10 years are also plotted and compared with the 4D inverted seismic data. Because the standard EnKF and adaptively gathered EnKF obtain similar results, only the results of adaptively gathered EnKF is shown here. The water saturation (Fig. 5.3) and pressure (Fig. 5.4) changes after adaptively gathered EnKF match the 4D seismic data very well compared with the predictions using initial ensemble (Fig. 4.7 and Fig. 4.8).

5.3.3 Comparison of CPU time

The computation time for different senerios are summarized in Table 5.3. Increasing the gather size can save the total simulation time used for history matching. For example, comparing with standard EnKF, a gathered EnKF can reduce computational cost by more than 50 percent. Less than 20 percent of the total time saved is from avoiding time consumed by tasks like file reading, writing, transferring, calculating of the covariance matrix and so on (time used for i/o, etc). More than 80 percent is saved by avoiding restarts for simulation runs (Fig. 5.5). If we simulate the Brugge field for 10 years in one run, it requires less than 200 seconds; but if we cut it to 40 equalized runs (0.25 year per run), it takes more than 1000 seconds. Therefore, increasing the gather size can significantly save simulation run time, especially for large ensemble size (assuming all the realizations are running sequentially). However, with the increase of gather size, the time used for calculating Kalman

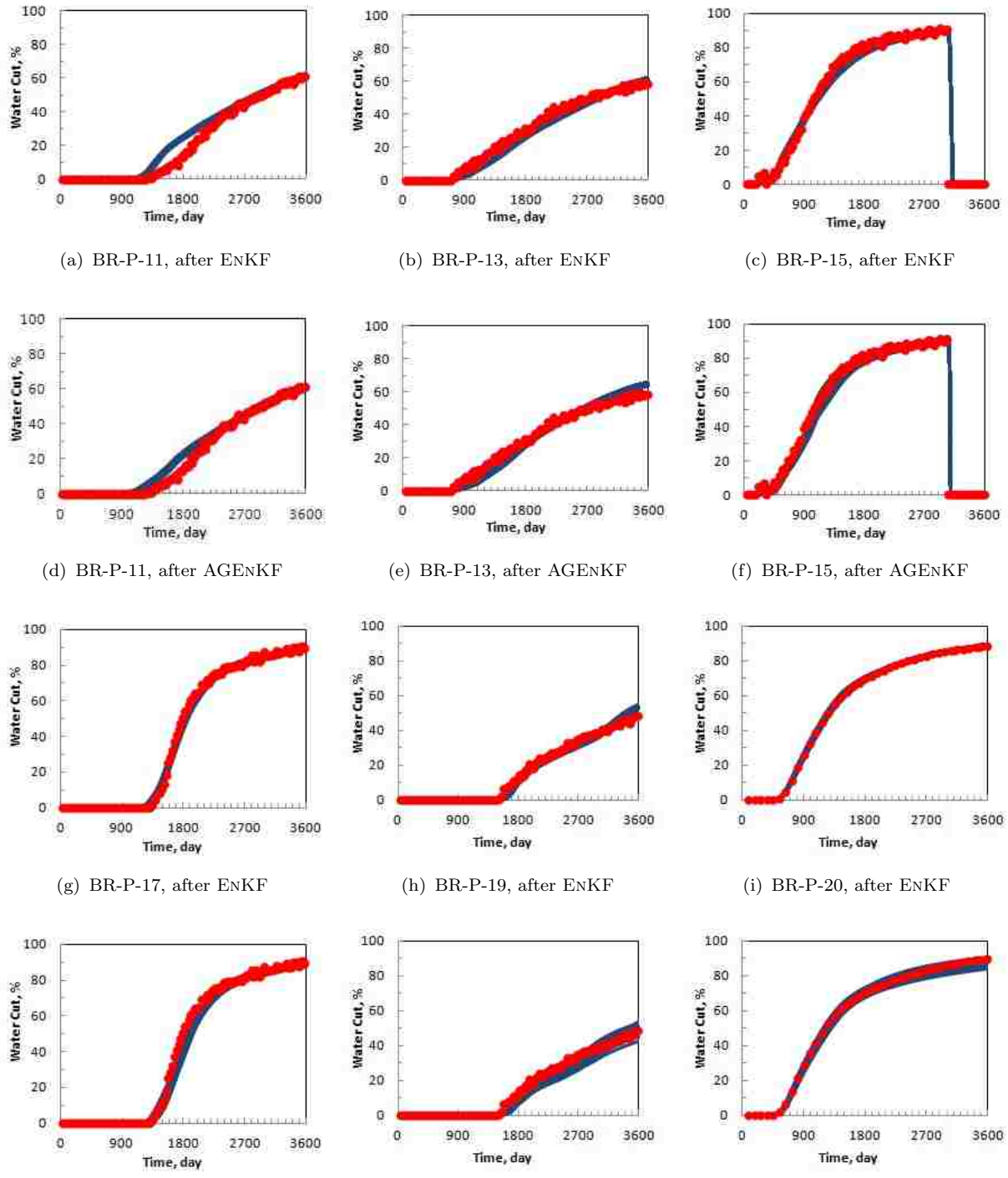

(a) BR-P-11, after EnKF (b) BR-P-13, after EnKF (c) BR-P-15, after EnKF

(d) BR-P-11, after AGEnKF (e) BR-P-13, after AGEnKF (f) BR-P-15, after AGEnKF

(g) BR-P-17, after EnKF (h) BR-P-19, after EnKF (i) BR-P-20, after EnKF

(j) BR-P-17, after AGEnKF (k) BR-P-19, after AGEnKF (l) BR-P-20, after AGEnKF

Figure 5.1: History match of water cut for selected wells using EnKF and adaptively gathered EnKF (AGEnKF). Red dots are the observations from the true case. Both methods match the observations well. The updated ensemble spread of adaptively gathered EnKF is wider than standard EnKF for some wells (e.g. BR-P-17, BR-P-19 and BR-P-20).

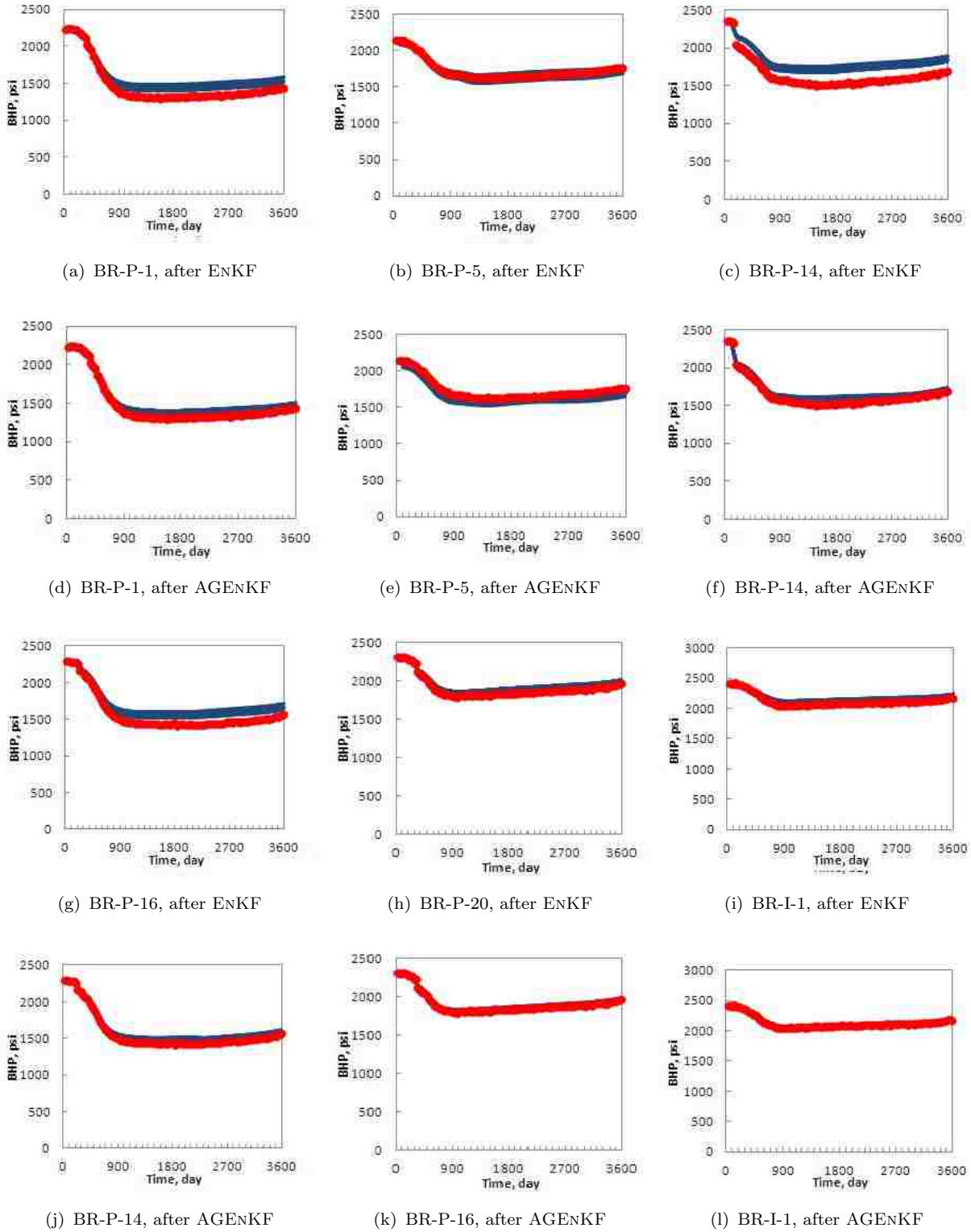

(a) BR-P-1, after EnKF (b) BR-P-5, after EnKF (c) BR-P-14, after EnKF

(d) BR-P-1, after AGEnKF (e) BR-P-5, after AGEnKF (f) BR-P-14, after AGEnKF

(g) BR-P-16, after EnKF (h) BR-P-20, after EnKF (i) BR-I-1, after EnKF

(j) BR-P-14, after AGEnKF (k) BR-P-16, after AGEnKF (l) BR-I-1, after AGEnKF

Figure 5.2: History match of bottom whole pressure for selected wells using EnKF and adaptively gathered EnKF (AGEnKF). Red dots are the observations from the true case. Both methods match the observations well. The results of the adaptively gathered EnKF is less biased than the standard EnKF.

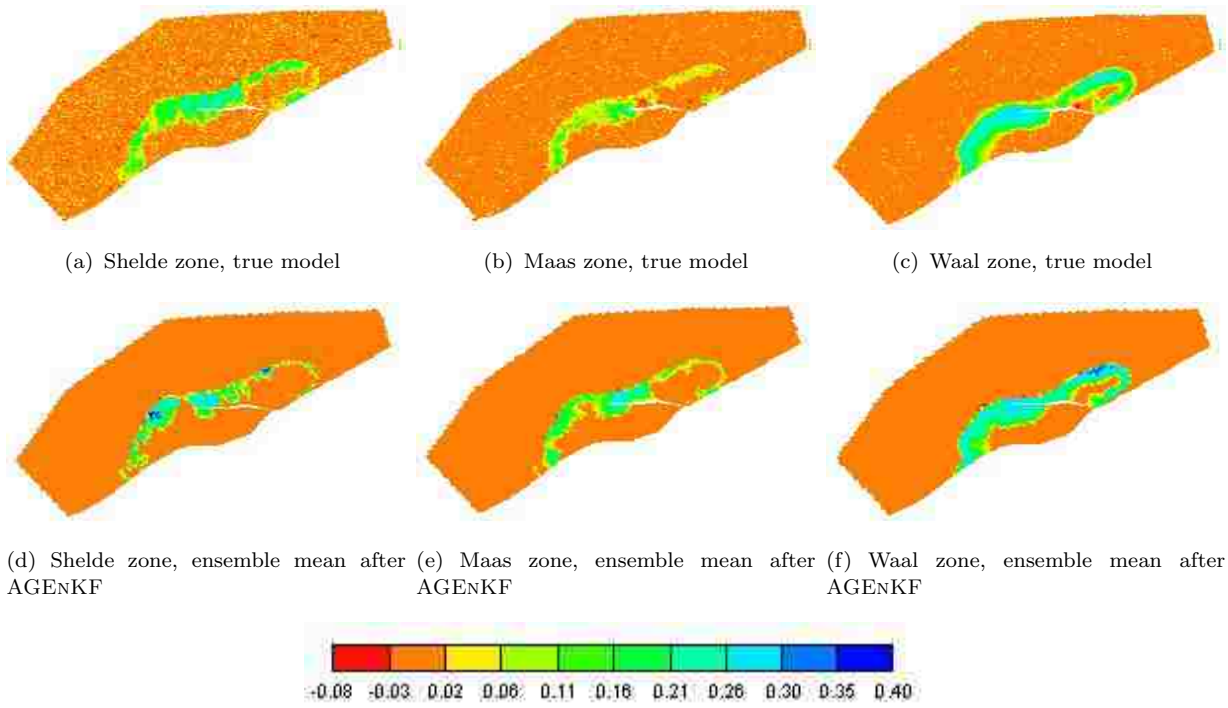

(a) Shelde zone, true model (b) Maas zone, true model (c) Waal zone, true model

(d) Shelde zone, ensemble mean after AGEnKF (e) Maas zone, ensemble mean after AGEnKF (f) Waal zone, ensemble mean after AGEnKF

Figure 5.3: Water saturation changes for selected formations. Upper graphs show the 4D inverted seismic data from true model. Lower graphs are the predictions of the updated ensemble for adaptively gathered EnKF. The saturation changes after adaptively gathered EnKF match the 4D seismic data well compared with the predictions from the initial ensemble (Fig. 4.7).

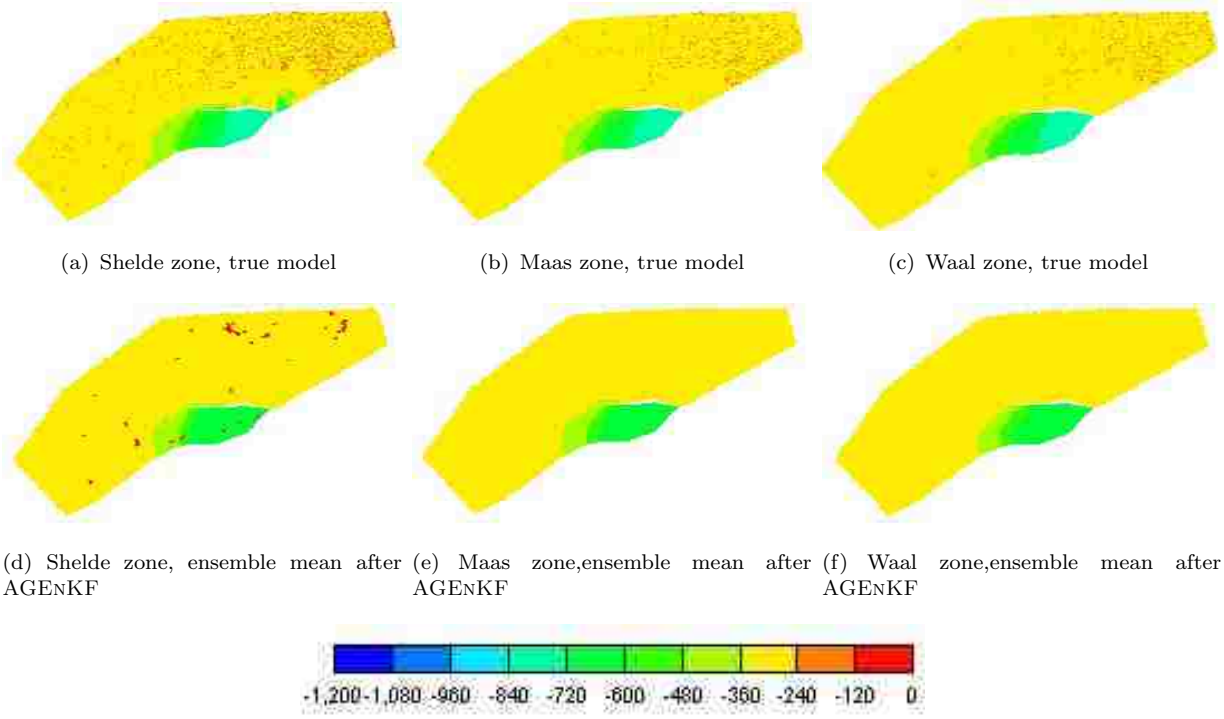

(a) Shelde zone, true model (b) Maas zone, true model (c) Waal zone, true model

(d) Shelde zone, ensemble mean after AGEnKF (e) Maas zone,ensemble mean after AGEnKF (f) Waal zone,ensemble mean after AGEnKF

Figure 5.4: Pressure changes (unit in psi) for selected formations. Upper graphs show the 4D inverted seismic data from true model. Lower graphs are the predictions of the updated ensemble for adaptively gathered EnKF. The pressure changes after adaptively gathered EnKF match the 4D seismic data well compared with the predictions from the initial ensemble (Fig. 4.8).

Table 5.3: Computation time (unit in hour) used for different methods. GEnKF and AGEnKF stand for gathered EnKF and adaptively gathered EnKF respectively.

	Time used for run simulations	Time used for Kalman gain	Time used for i/o, etc.	Total
Standard EnKF	14.19	0.37	1.55	16.11
GEnKF $N_g = 3$	7.17	0.23	0.68	8.08
GEnKF $N_g = 5$	5.75	0.40	0.56	6.71
GEnKF $N_g = 10$	5.02	1.06	0.01	6.09
AGEnKF $N_g \in \{2, 4, 8\}$	5.78	0.69	0.12	6.59

gain of each assimilation step also increases significantly (shown with blue in Fig. 5.6). For gather size $N_g = 1$, the calculation of Kalman gain at each time step only takes 30 seconds; but for $N_g = 10$, it takes about 900 seconds. When gather size reaches to a certain value, it becomes impractical to calculate the Kalman gain matrix. The total time used on Kalman gain calculation through out the history matching process first decreases and then increases with the increase of gather size (shown with red in Fig. 5.6). The reduction is caused by decreasing of total number of assimilation steps.

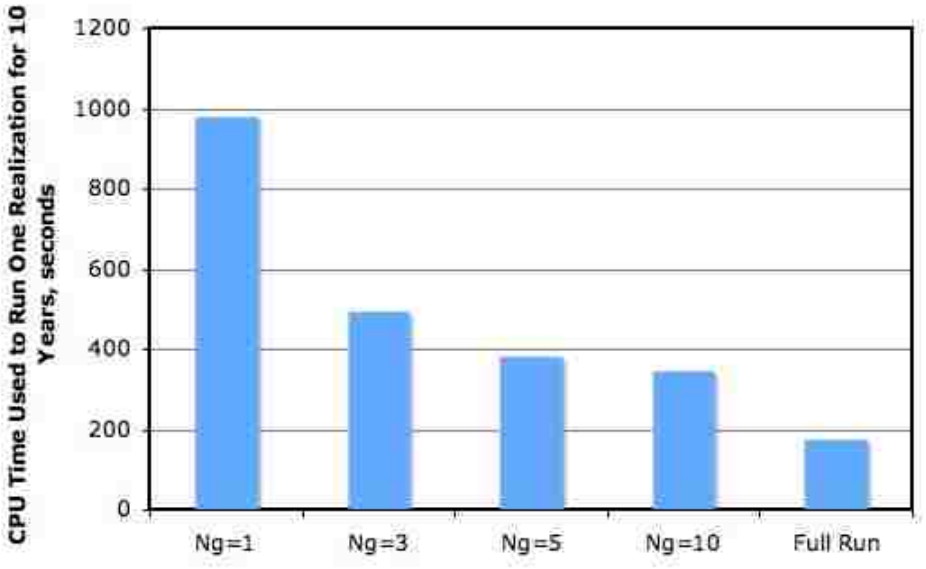

Figure 5.5: Total simulation time increases with number of restarts. Axis Y shows the total simulation time required to simulate the Brugge field for 10 years. Axis X shows cases with different number of simulation breakdown. Running 10 years in 40 restarts ($N_g = 1$) costs almost 5 times as an uninterrupted run (full run) does.

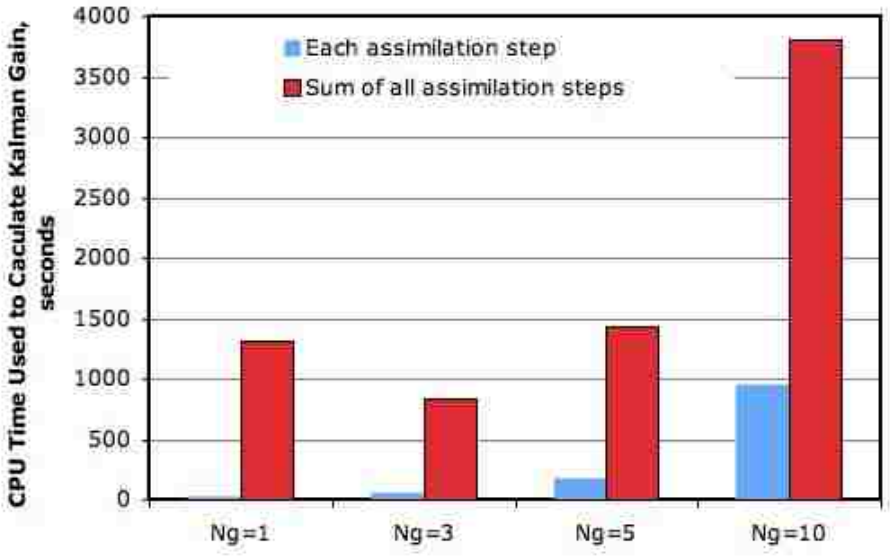

Figure 5.6: Time used to calculate Kalman gain for different senerios. Blue shows time used at each assimilation step, red shows the total time used on Kalman gain calculation for the whole history matching process. Time used on Kalman gain at each time step increases significantly with the increase of gather size. The total time used decreases and then increases with increase of gather size.

5.4 Discussion

Despite the appeal of ensemble Kalman filter, there is much yet to be learned before it reaches its full potential. As we mentioned in chapter 3, one substantial problem of EnKF is that the ensemble estimate of covariance tends to be overwhelmed with noise when the ensemble size is small, leading to unrealistic updating of the unknown variables. For the Brugge field, the size of ensemble (52) used is much smaller than the number of unknowns ($44{,}550 \times 7$). Thus, the estimated ensemble covariance is expected to exhibit strong spurious correlations. In the following two subsections, we discuss two methods that can reduce the noise in the estimated covariance. The first method is called distance localization in which the spurious correlations in the estimated ensemble covariance is filtered by multiplying the covariance matrix with a distance dependent correlation function. For the second method, we reduce the number of unknowns (size of the state vector) by using the correlations between reservoir gridblock properties.

5.4.1 Distance localization

Spurious correlations may arise in the estimated ensemble covariance when a limited ensemble size is used in an EnKF. When the gridblocks are far apart, correlations between the separated gridblock properties are small. Thus the spurious noise tends to dominate the estimated covariance. Houtekamer and Mitchell (1998) noted that by simply filtering (excluding) the observations greatly distant from the gridblock can improve the accuracy of EnKF method. Their method was further improved by filtering the estimated covariance using the *Schur product* of the estimated ensemble covariance matrix and a distance–dependent correlation function that varies from 1.0 at the observation location to 0 at some prespecified radial distance (Houtekamer and Mitchell 2001). They found that by incorporating this covariance localization not only the analysis errors are improved but also the analysis were smoother than when observations beyond a specified distance from the observation were excluded. Hamill and Whiteaker (2001) used numerical experiments to show that noise in the estimated covariance overwhelms the signal at relatively short distances from the observations, if the ensemble size is small; for larger ensembles, noise does not overwhelm until much further from the observations.

We use the distance–dependent correlation function described in Furrer and Bengtsson (2007) which is also applied by Chen (2008):

$$\rho(s) = \frac{1}{1 + (1 + f_c(0)^2/f_c(s)^2)/N_e}, \tag{5.4}$$

where N_e is the ensemble size. f_c is a covariance function used to calculate the covariance between different gridblock properties. The exponential form is used in this study,

$$f_c(s) = \exp\left(-(\frac{s}{L})^2\right), \tag{5.5}$$

with parameter L is the specified distance within which the observations is incorporated instead of filtered; s is the distance between two gridblocks.

The standard localization scheme applies the localization matrix $\rho(s)$ to the estimated Kalman gain K_e via Schur product (Chen 2008),

$$K_{loc} = \rho(s) \circ K_e, \tag{5.6}$$

with K_e calculated by Eq. 3.4. The Schur product matrices A and B is a matrix C of the same dimension, where $C_{i,j} = A_{i,j}B_{i,j}$.

The updated permeability distributions with and without localization for Brugge field are shown in Fig. 5.7. Without localization, unreasonable large changes happens in regions where permeabilities have small correlations with the observations. With localization, only permeabilities near the well locations are changed.

5.4.2 Using correlations between different properties

Spurious correlation become strong if ensemble size is small compared with the state vector. Either increasing the ensemble size or reducing the size of state vector should reduce the spurious correlations; however, increasing the ensemble size is computationally expensive, especially for complex reservoir models. Instead, the correlations between the gridblock properties can be used to reduce the uncertainty of the reservoir models, because this reduces the number of unknowns.

In general, correlations exist between porosity and permeability k_x, k_y and k_z. This is also true for the Brugge field. The initial information given by TNO shows that a linear relationship exists between porosity and ln horizontal permeabilities (see Fig. 5.8 upper two graphs and Fig. 4.3). In our previous numerical experiments, porosity and permeability k_x, k_y and k_z are assumed to be independent from each other. For these cases, after EnKF, the correlations are not well preserved due to spurious correlations (Fig. 5.8 lower two graphs).

In this subsection, reservoir model uncertainty is reduced using the relationship between the gridblock properties from the initial ensemble mean. Thus, only net-to-gross and porosity are the properties need to be updated. Permeability k_x is generated using equation $\hat{k}_x = 0.038 \exp(43\phi)$ (see Fig. 5.8 upper left graph). Since for the Brugge, $k_x = k_y$, same equation

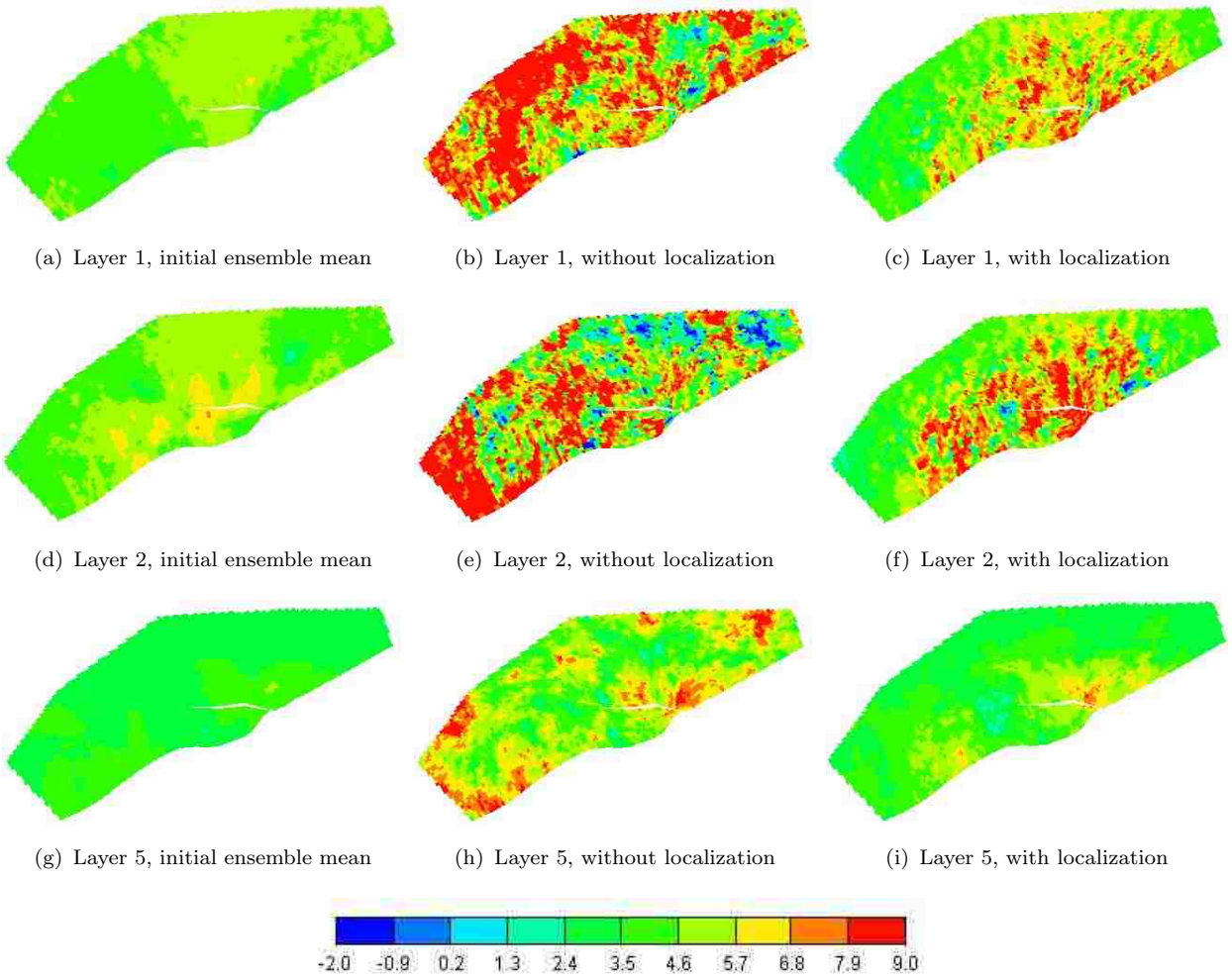

(a) Layer 1, initial ensemble mean (b) Layer 1, without localization (c) Layer 1, with localization

(d) Layer 2, initial ensemble mean (e) Layer 2, without localization (f) Layer 2, with localization

(g) Layer 5, initial ensemble mean (h) Layer 5, without localization (i) Layer 5, with localization

Figure 5.7: $\ln k$ distribution for selected layers. Left graphs are the $\ln k$ of the initial ensemble mean. Middle graphs are the updated $\ln k$ without localization; and the right graphs are the results with localization. With localization, only the permeabilities near the well locations are changed.

is used to generate k_y. k_z is generated using equation $\hat{k}_z = 0.00058 \exp(48\phi)$ (see Fig. 5.8 upper right graph). The two equations are obtained by applying reduced major axis (Jennings 1999) regression on the initial ensemble mean. By doing so, the correlations between porosity and permeabilities are better preserved without sacrificing the quality of history match. Fig. 5.9 shows EnKF with correlations matches the rate observations as good as the EnKF without correlations (and with more unknown model parameters). In addition, reducing the number of unknowns saves CPU time when calculating Kalman gain. For example, in this

case, for a gather size of $N_g = 8$, the CPU time used to calculate Kalman gain is reduced by half if correlations between different parameters are used.

However, one should be careful when using correlations between different parameters to reduce the uncertainty: inappropriate correlations may cause unreasonable updating of the unknowns and eventually lead to filter divergence.

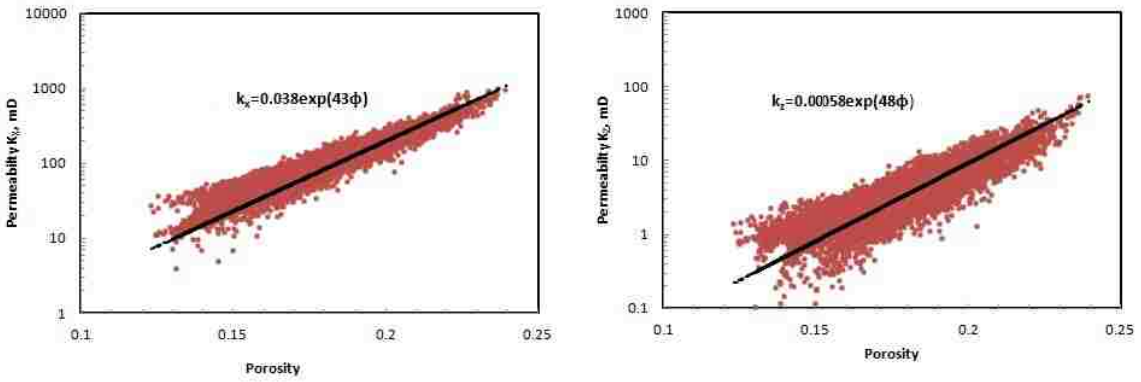

(a) PoroPerm(k_x) correlations of the initial ensemble mean (b) PoroPerm (k_z) correlations of the initial ensemble mean

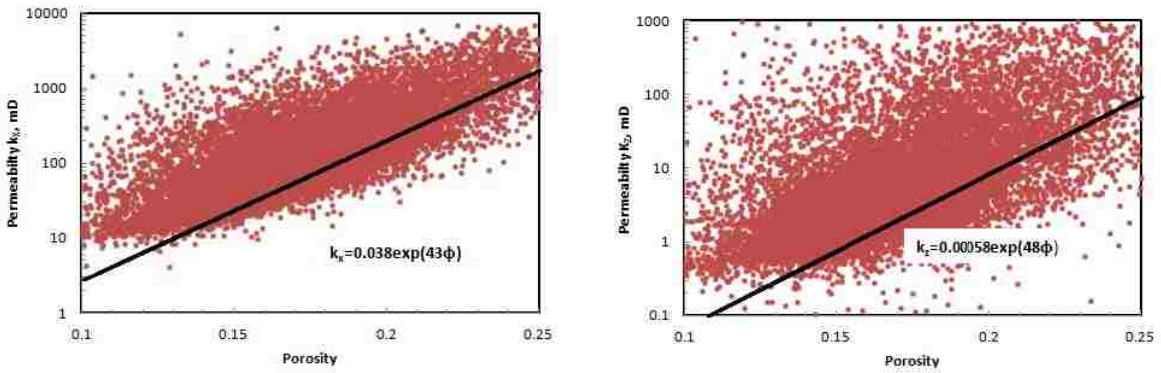

(c) PoroPerm(k_x) correlations of the ensemble mean after EnKF (d) PoroPerm(k_z) correlations of the ensemble mean after EnKF

Figure 5.8: Porosity and permeability correlations before and after EnKF. The correlations are not well preserved after EnKF due to spurious correlations.

5.5 Conclusions

An adaptively gathered EnKF is proposed in this chapter. The adaptively gathered EnKF is tested on Brugge field and compared with the standard EnKF. Our numerical experiments show that when the prior mean is not near the "truth", the gathered EnKF with a fixed

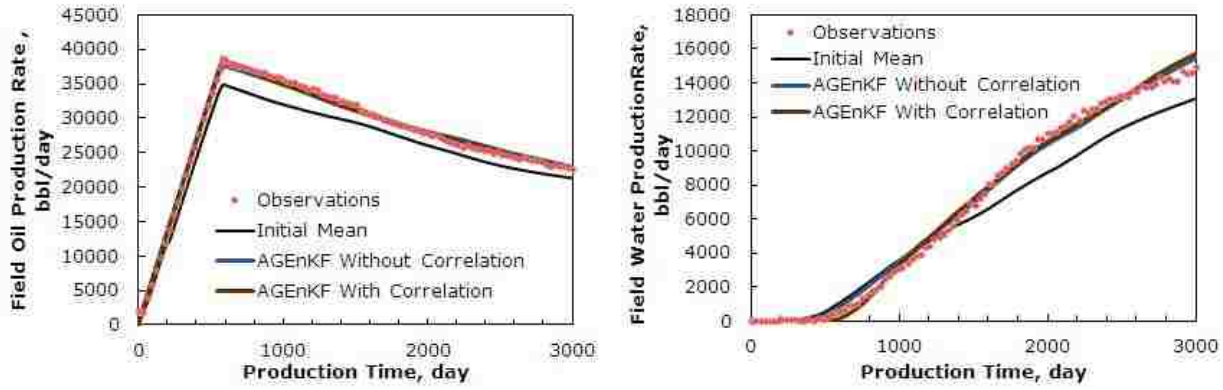

(a) Oil production rate

(b) Water production rate

Figure 5.9: History match of field oil and water production rates using EnKF with and without parameter correlation. EnKF with correlations works as good as EnKF without correlations.

gather size may not work well. In this case, an adaptively gathered EnKF is needed. Experiment shows the adaptively gathered EnKF is more efficient, accurate, and stable than the standard EnKF for the Brugge field. In addition, using distance–localization and parameter correlations improves the accuracy or efficiency of EnKF method. Distance–localization improves the accuracy by filtering spurious correlations in which the observation–parameter distance is large. Finally, using parameter corrections may better preserve relationships among parameters without sacrificing the quality of history match, and may yield savings in computation time.

Chapter 6

Closed–Loop Reservoir Management On Brugge Field, Including Price Uncertainty

6.1 Introduction

The closed–loop reservoir management is also known as i–field, e–field, smart field or digital oil field of the future. It uses interactive, complementary technologies and knowledge–management systems to allow company continuously optimize the field. New technologies including intelligent wells with fiber–optic sensors ensure constant stream of data about the well and its environment transferred to the remote office, enabling timely decision be made. The closed–loop reservoir management helps companies to reach previously off–limits reserves. It also helps the oil industry manage a shrinking labor force and rising oil demand.

From reservoir engineer of view, the closed–loop reservoir management has two major components: real–time reservoir model updating and model–based production optimization. The real–time reservoir model updating differs from traditional history matching in a way that it assimilates the observations in a sequential manner instead of a "batch type" in order to keep the reservoir model up–to–date. The primary goal of real–time model updating is to allow decision to be made to maximize the production potential based on the most recent updated reservoir models. When the geological model(s) are updated, model–based production optimization is used to simultaneously determine optimal operating parameters for the remaining expected life of the reservoir. The reservoir model updating and production optimization loop can be repeated over the life of the reservoir. The underlying hypothesis for closed–loop reservoir management is that by frequent life–cycle optimization based on frequently updated models we can increase the reservoir recovery significantly.

There is a large element of uncertainty in reservoir management, including technical uncertainty and economic uncertainty. Fariyibi (2006) defines technical uncertainty is the uncertainty "relates to whether or not the hydrocarbon volume estimated by geologists and

engineers exists in the ground and whether or not the reserves and recovery rates will be as projected by the engineers", and economic uncertainty is caused by "a lack of knowledge of future oil and gas prices, drilling and production costs, and other parameters affecting the economic performance of petroleum assets." Since uncertainty is inevitable, how to quantify those uncertainties is important in reservoir management. Quantification of uncertainty leads to better decision making and greater profitability; absent or inaccurate uncertainty quantification and forecasts can lead to suboptimal operations and poor economic performance. Previous works quantify technical uncertainty in closed–loop reservoir management; however, relatively little attention has been paid on addressing economic uncertainty.

This chapter demonstrates the closed–loop reservoir management concept in Brugge field. This demonstration includes oil price uncertainty in closed–loop reservoir management, and discusses the impact of price uncertainty on optimized well controls. The technical uncertainty is quantified via a set of realistic models using all known information and keeping these models up to date by conditioning the forecast model to new observations.

To better forecast and quantify the uncertainty of future oil price, the historical oil price is examined. Three price forecasting models–Conventional Forecast (CF) method, Bootstrap Sampling (BS) and Sequential Gaussian Simulation (SGS)–are used to forecast prices. The forecast oil prices are updated whenever new oil prices are available. The adaptively gathered EnKF is then used to update the reservoir models and multiscale regularized EnOpt is used to determine the optimal frequency for adjusting well controls. The effect of discount rate on optimized well control is also discussed.

6.2 Historical oil price

To predict the future behavior of crude oil, examination of the historical oil price is needed. The blue curve in Fig. 6.1 shows the historical monthly oil prices from year 1974 to year 2011. In the past 37 years, the crude oil prices adjusted have fluctuated wildly between a low price of about 6 $/bbl to a high price about 130 $/bbl with an average about 50 $/bbl. There are

many factors affecting crude oil prices, including supply and demand, petroleum reserves, world crises, natural and man made disasters, technical advances and so on. Because the forecasting methods are assumed to be stochastic, we give no explanation of events that lead to extreme oil price fluctuations.

The Brugge field is used as an example to illustrate the closed–loop reservoir management concept. To verify the accuracy of the forecast models, we assume Brugge field starts developing at January 2002. Therefore, only prices from January 1974 to December 2001 are treated as historical data and used in the price forecasting models after adjusting for inflation (red curve in Fig. 6.1). Oil prices from January 2002 to December 2011 are used as price observations which are assumed to be gradually available during reservoir development.

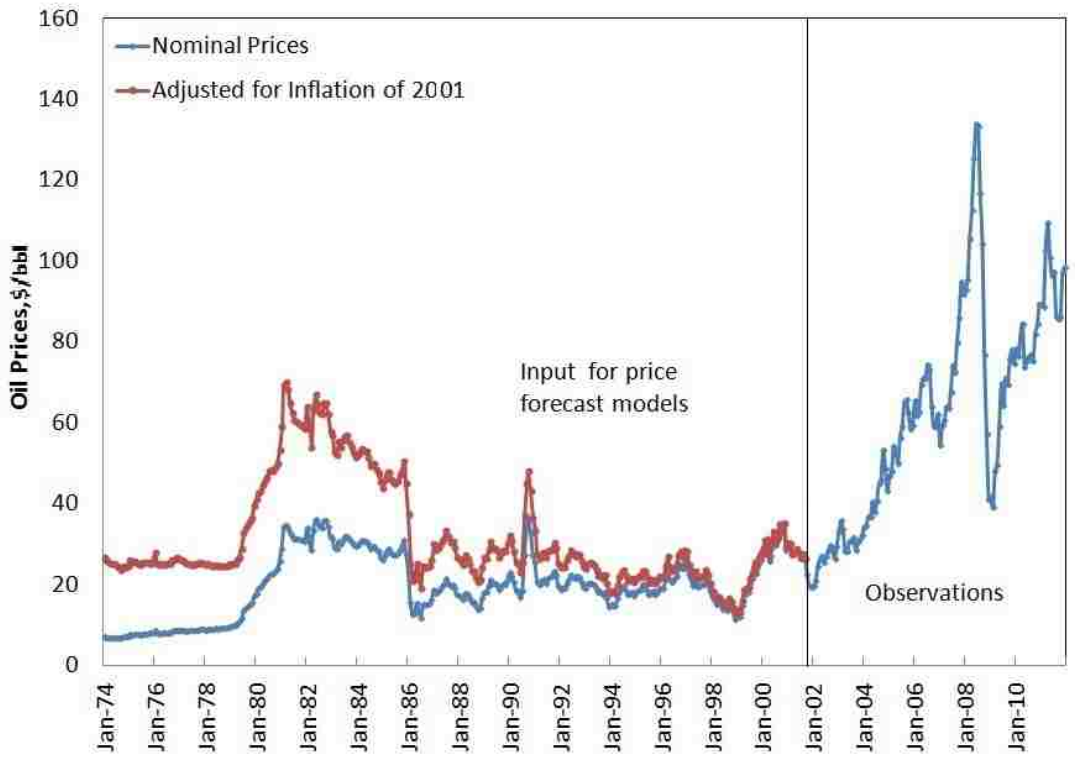

Figure 6.1: Monthly historical WTI oil prices from year 1974 to 2011 (Energy Information Administration 2012). Blue curve indicates the nominal oil prices; and the red curve indicates oil price adjusting for inflation of December 2001.

6.3 Price forecasting models

The impacts of the price uncertainty quantification models on optimized well controls are investigated using three different forecast models: conventional forecast method, bootstrap sampling method and sequential Gaussian simulation method. The workflow of these three methods are described in the following subsections.

6.3.1 Conventional forecast

The conventional method uses a range of forecasts representing the pessimistic, most likely and optimistic cases to quantify the uncertainty of oil prices. The pessimistic case is considered to be a P90 value and the optimistic case a P10 value. The spread between the pessimistic and optimistic cases is interpreted as 80 percent confidence interval. Conventional forecasts are commonly represented as monotonically increasing, having little resemblance to historical prices paths. As a result, conventional method fails to capture the full range and fluctuating character of price uncertainty (Fariyibi 2006; Holmes, Mendjoge, and McVay 2006; McMichael 1999)

Following McMichael (1999), the pessimistic case in this study assumes the oil prices remain at current oil price (20 $/bbl in December 2001) in the future. The most likely case assumes oil price increases with a constant annual rate which is determined from historical information, and the optimistic case assumes oil price raises with an annual rate twice as the mostly likely case. The average historical inflation rate (3 percent) is chosen as the annual increasing rate. In this dissertation, to generate multiple realizations, a normal distribution with mean 3 percent and standard deviation of 1.3 percent are used to generate annual increasing rates for different realizations. The forecast realizations are shown in Fig. 6.2. The price uncertainty is poorly captured by conventional forecast because all of the realizations are far lower than the true oil prices.

Figure 6.2: Conventional oil price forecasts from year 2002 to 2011. Black curves represent the forecast realizations and the green curve represents the forecast mean. The red curve represents the real observations

6.3.2 Bootstrap forecast

The basic idea behind bootstrap is simple and goes back at least two centuries (Faure and Grotjahn 2001). Given an original sample, which itself is assumed to be the best estimation of the population, bootstrap generates a sample set of size n by randomly sampling the original data with replacement. In this way, some numbers in the original data set may be taken several times while others may be excluded. The process can then be repeated as often as needed. The advantage of it is the simplicity. However, it requires each number must be statistically independent of the other number and does not preserve the correlation of oil prices in time (McMichael 1999; Fariyibi 2006).

Following Fariyibi (2006), the historical monthly fractional prices changes $(\frac{\Delta P_o}{P_o})_i$ of the crude oil without inflation are used to generate multiple forecasts

$$(\frac{\Delta P_o}{P_o})_i = \frac{P_{o,i} - P_{o,i-1}}{P_{o,i-1}}, \tag{6.1}$$

where $P_{o,i}$ is the price of oil for month i after adjusting for inflation.

Steps for generating the multiple price realizations for bootstrap method are summarized as below:

1. Remove inflation for historical nominal oil prices (present in 2001 December constant dollars). This is done by diving the inflation factor with nominal oil prices;

2. Calculate the historical fractional monthly oil price changes $((\frac{\Delta P}{P})_i)$ using Eq. 6.1;

3. Use the historical monthly oil prices changes $((\frac{\Delta P}{P})_i)$ as the population, forecasting fractional monthly oil price changes for the future using bootstrap sampling;

4. Calculate future oil price by multiplying current oil price $(P_{o,0})$ with cumulative fractional price change which is defined as

$$\frac{P_{o,i}}{P_{o,0}} = (1 + (\frac{\Delta P_o}{P_o})_i)(1 + (\frac{\Delta P_o}{P_o})_{i-1})(1 + (\frac{\Delta P_o}{P_o})_{i-2}) \cdots (1 + (\frac{\Delta P_o}{P_o})_1); \tag{6.2}$$

5. Adjust the forecasted oil prices for inflation (an annual inflation rate of 3 percent is used in this case);

6. Repeated all the above steps for multiply forecasts.

The forecast results of bootstrap method are shown in Fig. 6.3. Bootstrap forecasting captures uncertainty better than conventional method (Fig. 6.2).

6.3.3 Sequential Gaussian simulation forecast

Holmes, Mendjoge, and McVay (2006) applied sequential Gaussian simulation (SGS) method to quantify the uncertainty of future oil prices. Since the use of SGS requires the input

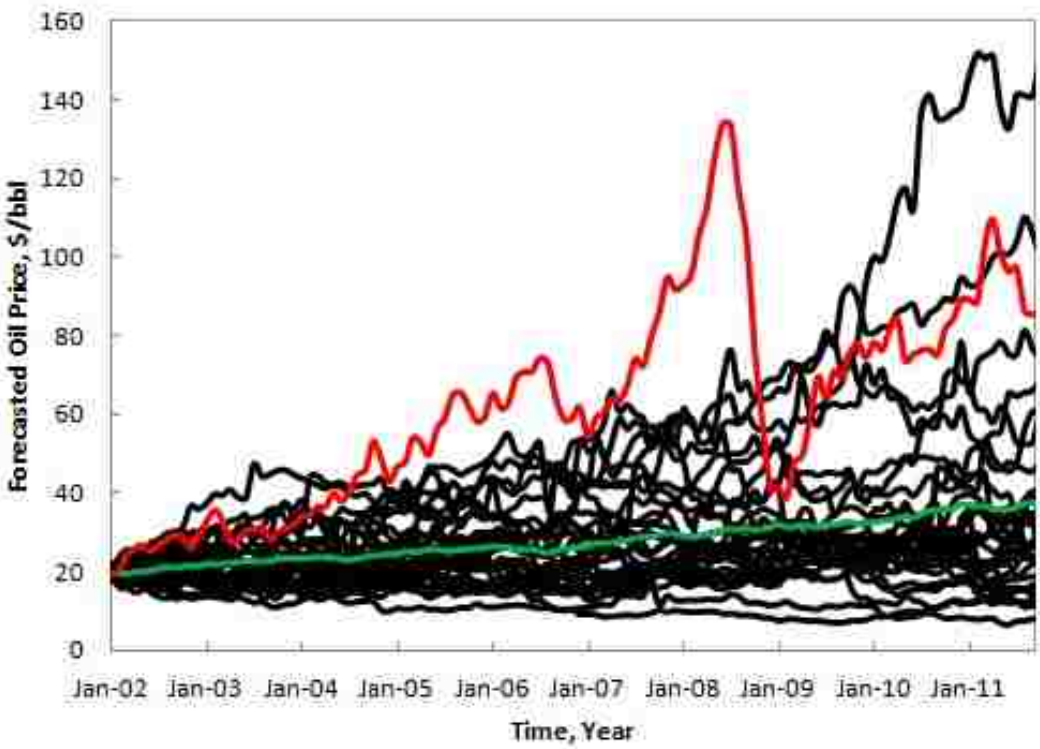

Figure 6.3: Bootstrap oil price forecasts from year 2002 to 2011. Black curves represent the forecast realizations and the green curve represents the forecast mean. The red curve represents the real observations.

data be normal distribution whereas the historical oil prices were not; they used a normal score transform, transferring the historical oil prices after removing inflation to a standard normal distribution. The transformed data was then used to model the correlation of the oil price in time by plotting out the semivariogram. Finally, the SGS method was used to generate multiple realizations consisting with both the frequency distribution and temporal variability of the historical price. A inverse normal score transform was then used to converts the forecasted normal score oil prices to regular oil prices. Comparing with bootstrap method, the advantage of SGS is that it preserves the correlations of the oil prices in time.

As shown in Fig. 6.4, even though the historical oil prices from year 1974–2011 are not normally distributed (shown in the left figure), their log values are approximately normal distributed (shown in the right figure). So, instead of using a normal score transform, we directly use the $\log(P_o)$ to develop the semivariogram. An exponential model is then used

to fit the semivariogram as shown in Fig. 6.5. The exponential model is used to generate multiply realizations using conditional sequential gaussian simulation. All these processes were performed using software R (Team 2008).

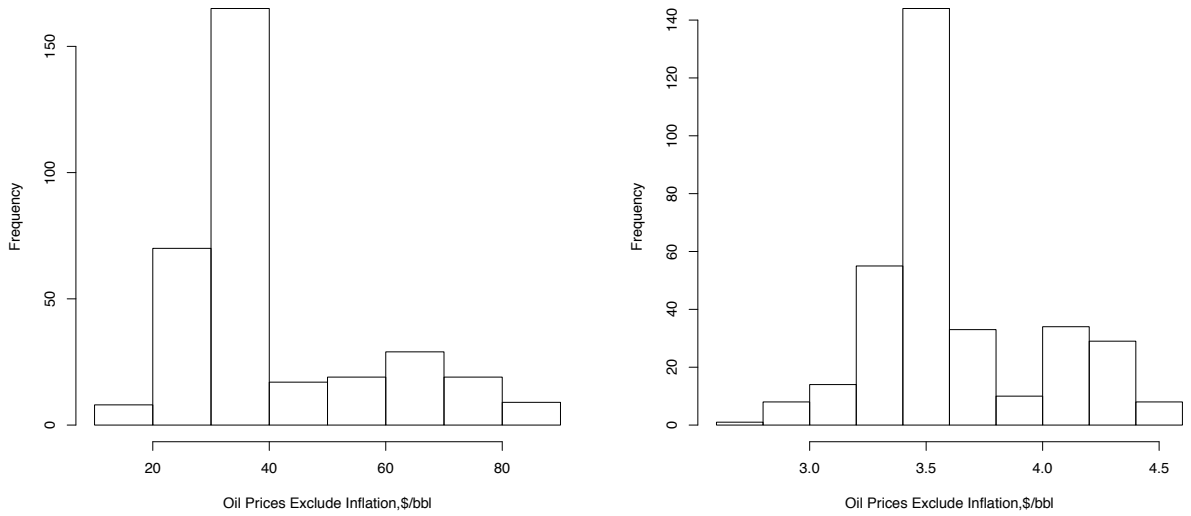

Figure 6.4: Histograms of historical oil price (left) and log historical oil prices (right), from year 1974–2001, excluding inflation. Historical oil prices are approximately normal distributed after log transform.

Steps for generating the multiple price realizations for sequential Gaussian simulation method are summarized as below:

1. Remove inflation for historical nominal oil prices (present in 2001 December constant dollars);

2. Generate the semivariogram of historical $\log(P_{o,i})$;

3. Use conditional (condition it to current oil price (December 2001)) sequential Gaussian simulation to generate multiple realization for $\log(P_{o,i})$. The generate realizations must be consistent with the historical semivariogram;

4. Adjust the forecasted oil prices for inflation (an annual inflation rate of 3 percent is used in this case).

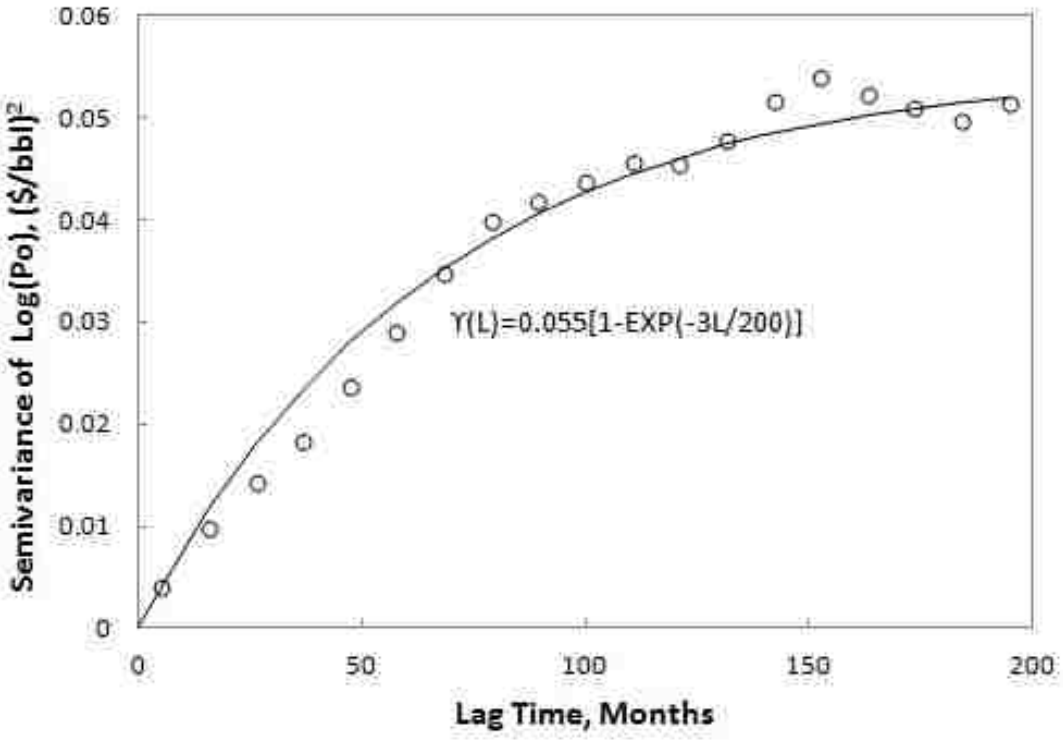

Figure 6.5: Semi-variogram of historical oil prices after log transform.The exponential model fits to the semi-variogram well.

Price forecasting results for sequential Gaussian simulation method are shown in Fig. 6.6. The uncertainty forecasted using sequential Gaussian simulation is higher than conventional method and lower than the bootstrap method. All these three methods underestimate the future oil prices in this particular case.

6.4 Optimization formulation and methods

Chapter 2 described production optimization methods on single reservoir model assuming known geology model and constant oil and water price. This chapter extends the optimization objective function and methods to multiple reservoir models and oil price realizations. Only the ensemble based optimization method is used in this chapter. The BOBYQA method is discarded because it is not as efficient as EnOpt when the number of unknowns is in the order of 100.

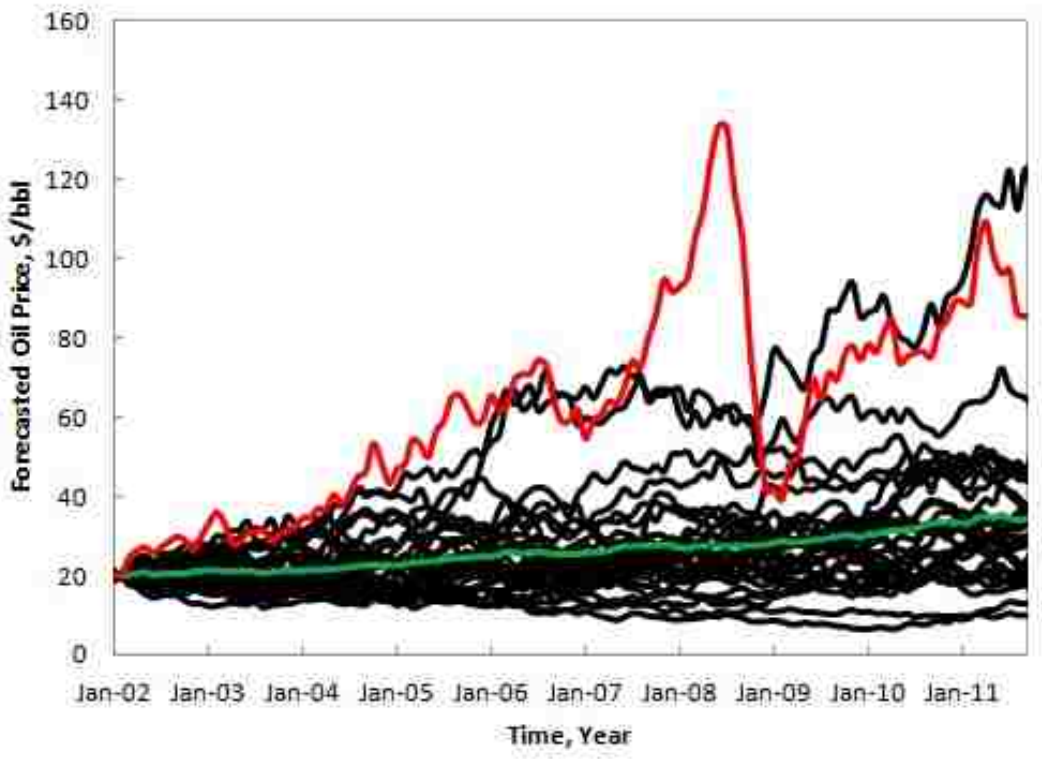

Figure 6.6: Sequential Gaussian simulation oil price forecasts from year 2002 to 2011. Black curves represent the forecast realizations and the green curve represents the forecast mean. The red curve represents the real observations.

6.4.1 Objective function

As in chapter 2, the net present value (NPV) is chosen as the objective function to be maximized. When optimizing considering geological and oil price uncertainty, the optimized NPV is not only affected by well controls, but also by reservoir properties and future oil prices. Therefore, the NPV of each realization j is calculated as

$$g_j(x, y_j, P_{o,j}) = \sum_{i=1}^{N_t} \frac{P_{o,i,j} Q_{o,i,j}(x, y_j) - P_w Q_{w,i,j}(x, y_j)}{(1 + r_\tau)^{\frac{t_i}{\tau}}}, \tag{6.3}$$

where x is the vector of well control variables; y indicates the vector of reservoir properties; N_e is the total number of reservoir model realizations; N_t is the total number of control time steps; $P_{o,i,j}$ is the forecast oil price at time t_i for realization j. P_w is the water disposal cost which assumed to be a constant. $Q_{o,i,j}$ and $Q_{w,i,j}$ represent the total production oil and water over time step Δt_i for realization j, respectively. r_τ is the discount rate in terms of time span

τ, t_i is the cumulative production time at time step i. The objective function $g_j(x, y_j, P_{o,j})$ gives NPV as a function of well control x, reservoir properties y and oil prices P_o.

The average NPV over all realizations is the objective function needed to be maximized

$$J(x) = \frac{1}{N_e} \sum_{j=1}^{N_e} g_j(x, y_j, P_{o,j}). \tag{6.4}$$

Only the well controls are adjusted during the optimization process. In closed–loop reservoir management, the reservoir properties y_j are updated after each data assimilation (reservoir history matching). The forecast oil prices $P_{o,j}$ are also updated when new oil prices are available.

6.4.2 Ensemble–based optimization under uncertainty

As in chapter 2, steepest ascent method is used to illustrate the methodology of EnOpt. The steepest ascent method is given as,

$$x_{l+1} = \frac{1}{\alpha_l} C_x G_l^T + x_l, \tag{6.5}$$

where x is a vector of the well control variables; l is the iteration index. C_x is the covariance matrix of the well control variables which is used as a preconditioner here (Chen 2008). α is the step size for the search direction, and G_l is the gradient of objective function with respective to x.

For the uncertain reservoir description represented by an ensemble,

$$C_x G^T \approx \frac{1}{N_e} \sum_{j=1}^{N_e} C_{x, g_j(x, y_j, P_{o,j})}, \tag{6.6}$$

where N_e is the ensemble size of reservoir models, iteration index l is dropped for simplicity.

As it is proven by Chen (2008), the cross-covariance $C_x G^T$ can be approximated

$$C_x G^T \approx \frac{1}{N_e} [\sum_{i=1}^{N_e} (x_j - \bar{x})(g_j(x_j, y_j, P_{o,j}) - \bar{g}(x, y, P_o)], \tag{6.7}$$

where

$$\bar{g}(x, y, P_o) = \frac{1}{N_e} \sum_{j=1}^{N_e} g_j(x_j, y_j, P_{o,j}), \tag{6.8}$$

and

$$\bar{x} = \frac{1}{N_e} \sum_{j=1}^{N_e} x_j. \tag{6.9}$$

6.5 Open–loop production optimization

In this section, we use open–loop production optimization to demonstrate (a) multiscale regularization application on finding optimal adjusting frequency for well control; (b) the effect of discount rate on optimized well control and (c) the effect of different forecast models on optimized well control. The open–loop optimization is an approach wherein the optimization is directly performed on the true reservoir model (Sarma 2006). Because, in reality, the true reservoir model is never known. Here, we use the history matched reservoir models from last chapter instead. We assume the history matched models are very close to the true model. In chapter 5, we history matched the reservoir models using production data from year 0–10. Here, we optimize the NPV of the field from year 10–20 using the history matched models. The optimization is carried out with only one inflow control valve (ICV) per well. Producers are producing under maximum fluid rate constraint (3000 stb/day) and the injectors are producing under maximum injection rate constraint (4000 bbl/day). If not otherwise specified, the cost for disposing produced water is 5 $/bbl and the oil price is 80 $/bbl. The liquid production rate of each producer and water injection rate of each injector are manipulated to maximize the NPV. These well controls are adjusted every half year for nonregularized case. There are 30 wells $\times$ 20 time steps = 600 unknowns. An ensemble size of 30 is used for all scenarios.

6.5.1 Sensitivity to discount rate

If the NPV is discounted, it assumes the early production phase is more important than the later years. Assuming a discount rate of 10 percent, one barrel of oil in 10 years later would be equivalent of $\frac{1}{(1+0.1)^{10}} = 0.385$ barrel today. In this subsection we test how the optimized well control strategies are affected by discount rate. Four different scenarios are considered: a

nondiscounted case (discount rate = 0) and three discounted cases with discount rate equal to 0.1, 0.2 and 0.3 respectively. Except the discount rate, other parameters are the same for these four scenarios. The effect of discount rate on the optimized well control strategy is clearly demonstrated in Fig. 6.7. When a higher discount rate is used, it implies a higher value for oil produced early, and very little value is attached to oil produced in later years or decades. As a result, less cumulative oil is usually produced at higher discount rates. If a discount rate of zero is used, the optimization target is equivalent to maximizing the cumulative field oil production rate while minimizing the cumulative water production.

6.5.2 The effect of multiscale regularization

Chapter 2 presented multiscale regularization for an ensemble based method. Here, multiscale regularization method is further tested on the Brugge field. For unregularized EnOpt, well controls are adjusted every half year; this gives a total of 600 unknowns. For multiscale regularized EnOpt, optimization starts with a coarse scale (well controls are adjusted every 10 years) and gradually refined until further refinement does not improve the NPV. Table. 6.1 compares the results of EnOpt with multiscale regularized EnOpt. Optimization has improved the NPV by more than 15 percent for both methods. Multiscale regularized EnOpt obtains slightly higher NPV than standard EnOpt while using a larger well control adjustment time interval. In addition, multiscale regularization saves computational cost by about 30 percent.

Table 6.1: Comparison of EnOpt and multiscale regularized EnOpt. MEnOpt stands for multiscale regularized EnOpt.

Methods	Time interval used for well control adjustment	Initial NPV[a]	optimized NPV[a]	CPU time used for optimization
EnOpt	6 months	3.0×10^9\$	3.45×10^9\$	31 hours
MEnOpt	15 months[b]	3.0×10^9\$	3.50×10^9\$	22 hours

[a]The NPV shown here is the mean value of the ensemble.
[b]This is the finest scale used in MEnOpt.

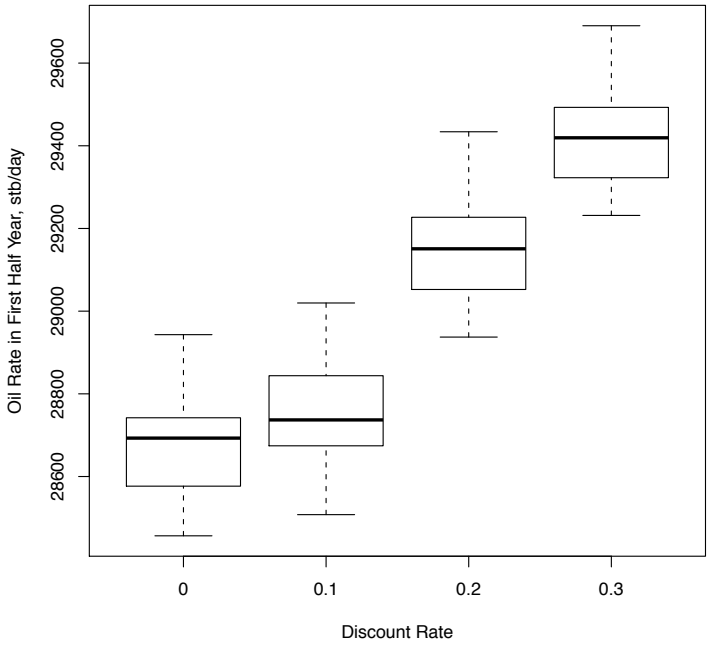

(a) First half year oil production rate

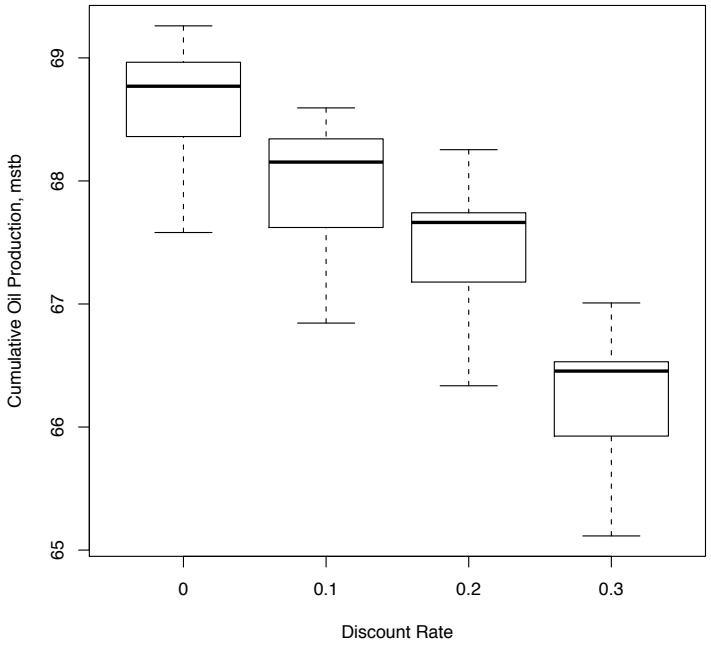

(b) Cumulative oil

Figure 6.7: The effect of discount rate on optimized well control strategy. When a higher discount rate is used, it implies a higher value for oil produced early, and very little value is attached to oil produced in later years or decades. As a result, less cumulative oil is usually produced at higher discount rates.

6.5.3 Optimization with price forecasting

This subsection test the impact of the price uncertainty quantification models on optimized well control strategies. Three different scenarios are compared:

1. Optimize with known prices: oil prices are assumed to be known without uncertainty and the production optimization is done based on the true prices use EnOpt method. This is used as a reference case.

2. Optimize with price forecast mean: oil prices are assumed to be unknown. Conventional, bootstrap and sequential Gaussian simulation methods are used to forecast the future oil prices. The forecast means are then used for each simulation model.

3. Optimize with multiple price realizations: the same as scenario 2 except instead of using forecast mean, different price realizations are used for different geology models.

When optimization is done under single price model (without uncertainty), the closer the forecast price to the true price, the higher the NPV is achieved. This is clearly demonstrated in Table 6.2. The normalized RMSE of forecast prices are used to quantify the accuracy of forecast price models. It is defined as

$$\delta_{Po} = \sqrt{\frac{1}{N_{Po}} \sum_{i=1}^{N_{Po}} (\frac{P_{o,i}^{fm} - P_{o,i}^{t}}{P_{o,i}^{t}})^2}, \tag{6.10}$$

where N_{Po} is the total number of prices used in optimizations. In this case $N_{Po} = 120$ (120 months $\times$ 1/ month). $P_{o,i}^{fm}$ is the forecast mean and $P_{o,i}^{t}$ is the true price. Among all these three forecast methods, bootstrap obtains the lowest RMSE and the conventional forecast obtains the highest. As a result, the realized NPV using bootstrap forecasting is \$70 million more than that of using conventional forecasting, and it is very close to the realized NPV of optimizing with known price (1 percent difference).

The forecast price mean for all these three methods increases monotonically; while the real oil prices fluctuated wildly (Figs. 6.2, 6.3 and 6.6). To demonstrate how the fluctuation in oil

Table 6.2: Comparison of different forecast models.

Methods	Normalized RMSE of forecast prices	Optimized NPV 10^9\$	Realized NPV[a] 10^9\$
Optimize with known price	0.00	2.20	2.20
Optimize with BS mean	0.52	0.92	2.18
Optimize with SGS mean	0.55	0.85	2.14
Optimize with CF mean	0.60	0.74	2.09

[a]The realized NPV is NPV achieved when applying true price to the optimized control strategies.

prices impacts the optimized well controls, semivariograms are generated using optimized well controls of all 20 producers for optimizations with bootstrap forecast mean and known price. The bootstrap forecast mean is used as a representative of monotonically increasing cases. As it is shown in Fig. 6.8, optimized well control with true prices has a larger semivariogram sill (i.e., control variability) than that with bootstrap forecast mean at the same lag-time. Thus, instability in the oil prices also causes fluctuation in optimized well controls. This is also clearly demonstrated in Fig. 6.9.

There is always uncertainty associated with future oil prices. In this study, like the geological uncertainty, the price uncertainty is represented by using an ensemble of price forecast models. Incorporating uncertainty in decision making can lower the risk and therefore may leads to cost reduction. Fig. 6.10 compares optimized NPV frequency distribution with and without uncertainty for three different forecasting models. The red curve represents the case of optimizing with multiple price realizations and the blue curve represents the case of optimizing with forecast mean but calculating optimized NPV with multiple price realizations. Optimizing without uncertainty obtains higher NPVs than optimizing under uncertainty for all three methods which is somewhat surprising. This is because the EnOpt uses Monte Carlo method to approximate the gradient. The approximation works well if the joint pdf is narrow. But if there is large uncertainty in the geological and price models, the optimization algorithm is more easier trapped at local optima. This could possibly be improved by increasing the size of ensemble.

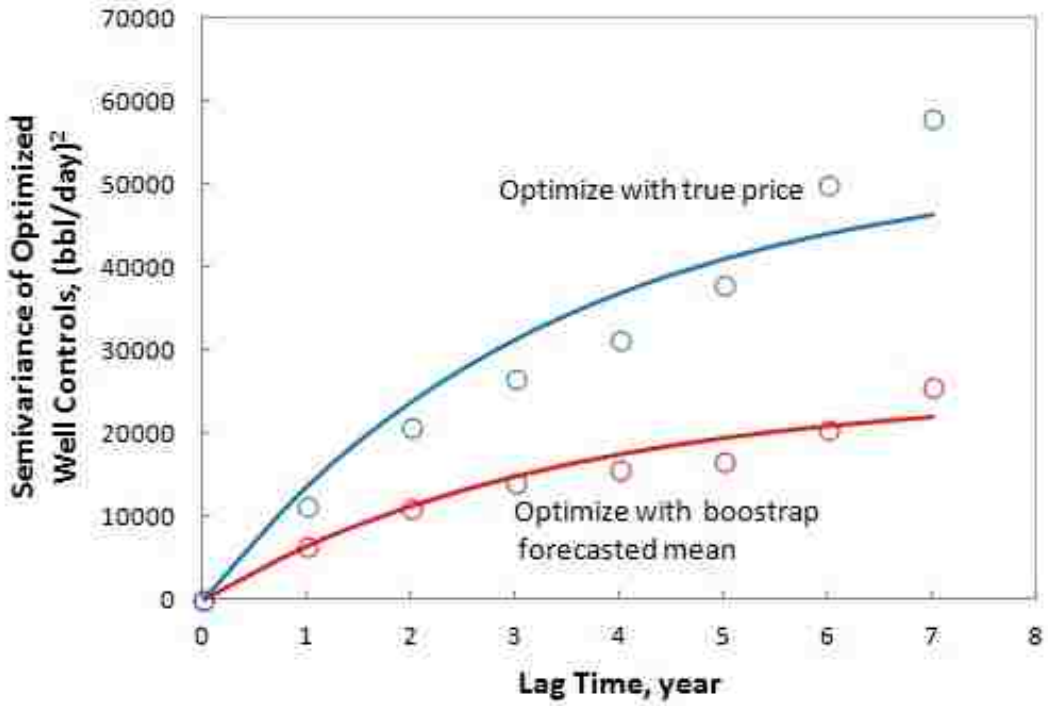

Figure 6.8: Semi-variogram of optimized well controls. Blue and red dots are the calculated semivariograms for optimized well controls with known price and bootstrap forecast mean, respectively. Instability in the oil prices also causes fluctuation in optimized well controls.

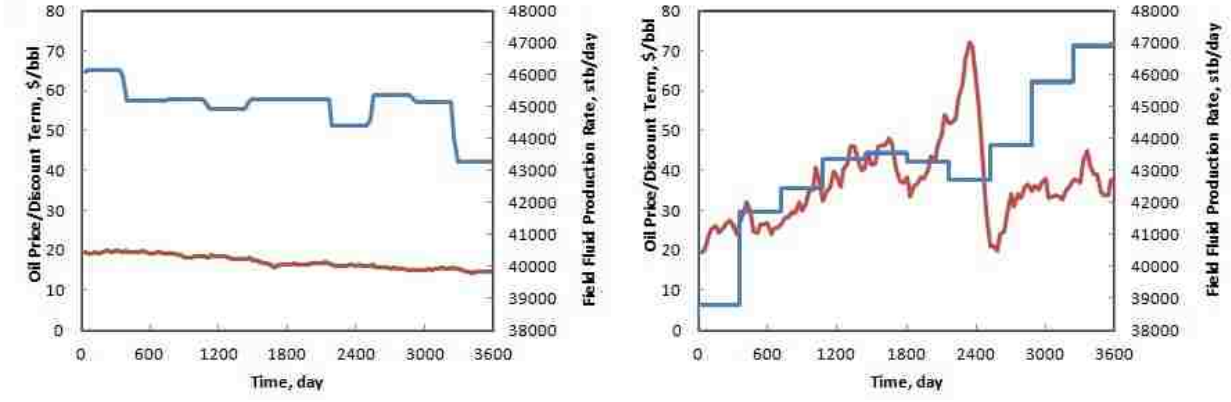

(a) Optimize with BS mean

(b) Optimize with known price

Figure 6.9: Optimized field liquid rate changes with oil price. Red curves represent bootstrap forecast mean (left) and real oil prices (right) changes with time after adjusting for discount rate; blue curves represent the optimized field liquid production rates of these two cases. Instability in the oil prices also causes fluctuation in optimized well controls.

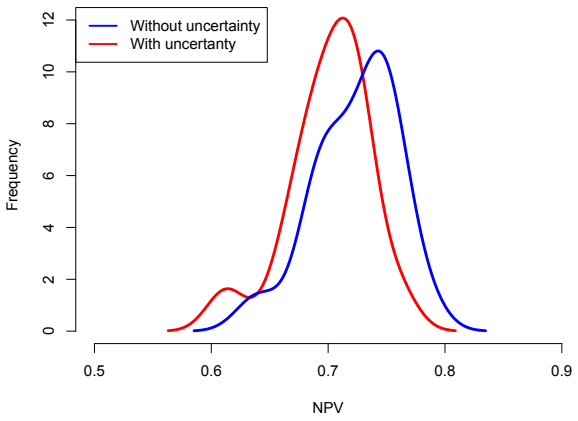

(a) Conventional forecast

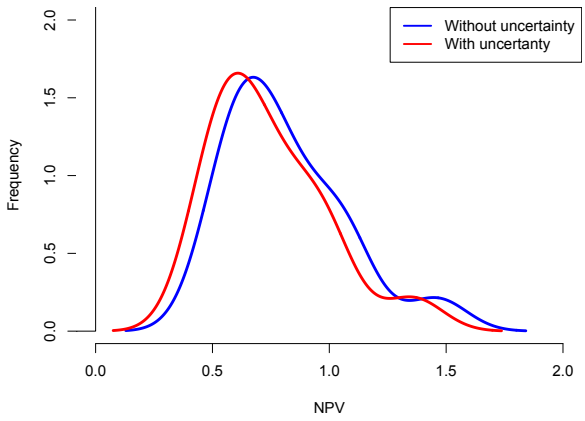

(b) Sequential Gaussian simulation

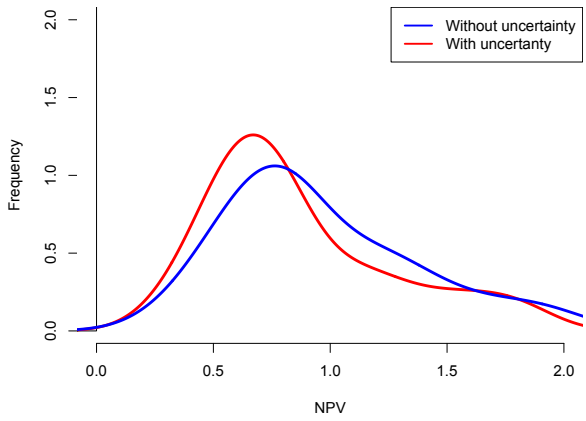

(c) Bootstrap sampling

Figure 6.10: Comparison of optimized NPV frequency distribution with and without uncertainty. The red curve represents the case of optimizing with multiple price realizations and the blue curve represents the case of optimizing with forecast mean but calculating optimized NPV with multiple price realizations.

6.6 Closed–loop production optimization

In this section, we access the closed–loop reservoir management concept with Brugge field. Because the true model is not available, one realization is randomly picked up from 104 realizations as the "true" field. We assume all the 30 wells are opened at time 0 and the production constraints are the same mentioned in the open–loop production optimization section. Production optimization starts at time zero and repeated after each data assimilation. Adaptively gathered EnKF is used to update the reservoir models. Four scenarios are examined in this section:

1. Optimization with true model: The reservoir geological properties and oil prices are assumed to be known. Production optimization is done based on the true model.

2. Nonoptimized case: Producers are producing at maximum fluid rate of 3000 stb/day and injectors are injecting at maximum injection rate constraint of 4000 bbl/day. Neither the oil price nor the geological model are updated.

3. Closed–loop optimization: The geological properties and oil prices are assumed to be unknown, 30 realizations are used to represent the uncertainty of the geological model. Those realizations are updated using adaptively gathered EnKF method. Forecast oil prices are also updated at each data assimilation step using bootstrap sampling method. Production optimization is done under geology uncertainty after each data assimilation using EnOpt. The forecast mean of oil prices instead of all the realizations is used for optimization. This is because the price uncertainty is generally large, so that the EnOpt algorithm trapped at local optimum easily when small ensemble is used. Gather sizes used in this cases are $N_g \in \{2, 4, 8\}$. We start with a gather size of 2 and gradually double the gather size if the prediction of the ensemble mean close to the truth. Otherwise, the gather size is reduced by half.

4. Optimization without model updating: Production optimization is done only at time zero with uncertain geological models and forecast oil price mean.

6.6.1 Data assimilation results

As more and more observations become available, the geological uncertainty is expected to be reduced. This is clearly demonstrated in Fig. 6.11. The predicted water cuts of all the realizations for the selected well gradually approach the "true" model after each data assimilation. In addition, the uncertainty reduces significantly after first two steps of gathering (after 1.5 years production). This is also demonstrated in Fig. 6.12. The estimation of net to gross improved significantly in the first two steps. Hence, it makes sense to update and optimize more frequently in the early stage than the later time if only geological uncertainty is considered.

Unlike geological uncertainty, which should decrease with production of a reservoir, price uncertainty does not decrease over the life of a petroleum reservoir (Fig. 6.13). The longer the forecast time, the higher the uncertainty. When price uncertainty is considered, how frequent shall we optimize the production becomes a complicate question which requires further research.

6.6.2 Production optimization results

Fig. 6.14 shows the optimized well controls for selected wells. Dished lines represent the evolution of optimized controls in closed–loop reservoir management as production proceeds. Black line represents the final well control obtained using closed–loop reservoir management. Red line is the optimized control on the "true" case. The optimized controls in closed–loop reservoir management at the beginning of production is far away from optimized controls obtained from the "true" model because the estimated reservoir models and oil prices are not near the truth. As the production proceeds, more and more observations become available and the updated reservoir models and forecasted oil prices become more and more close to

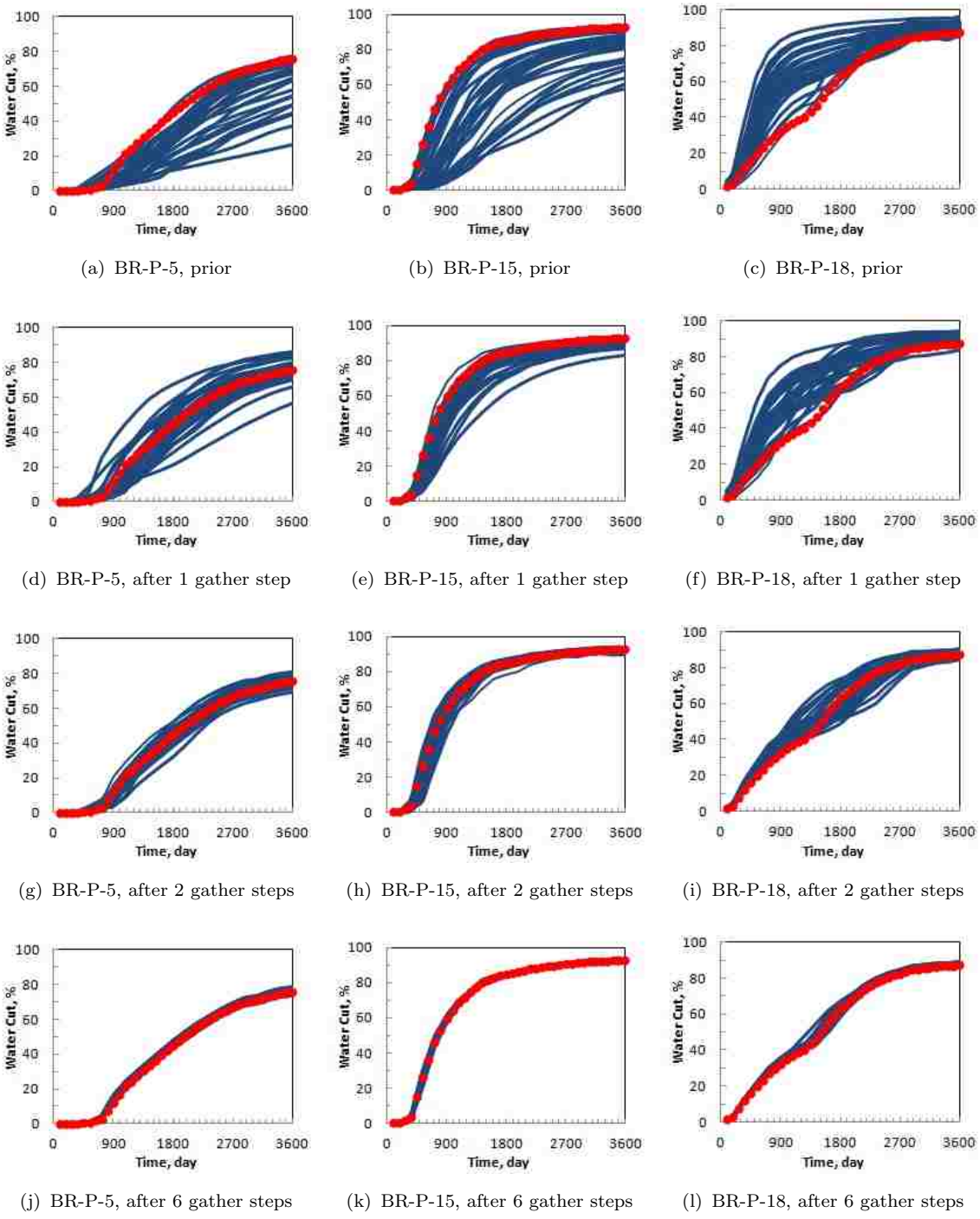

(a) BR-P-5, prior (b) BR-P-15, prior (c) BR-P-18, prior

(d) BR-P-5, after 1 gather step (e) BR-P-15, after 1 gather step (f) BR-P-18, after 1 gather step

(g) BR-P-5, after 2 gather steps (h) BR-P-15, after 2 gather steps (i) BR-P-18, after 2 gather steps

(j) BR-P-5, after 6 gather steps (k) BR-P-15, after 6 gather steps (l) BR-P-18, after 6 gather steps

Figure 6.11: Water cut matches for selected well in closed–loop reservoir management. Red dots indicate the observations from the true model. Blue curves are reruns with the updated realizations after data assimilation. Geological uncertainty reduces with production of a reservoir.

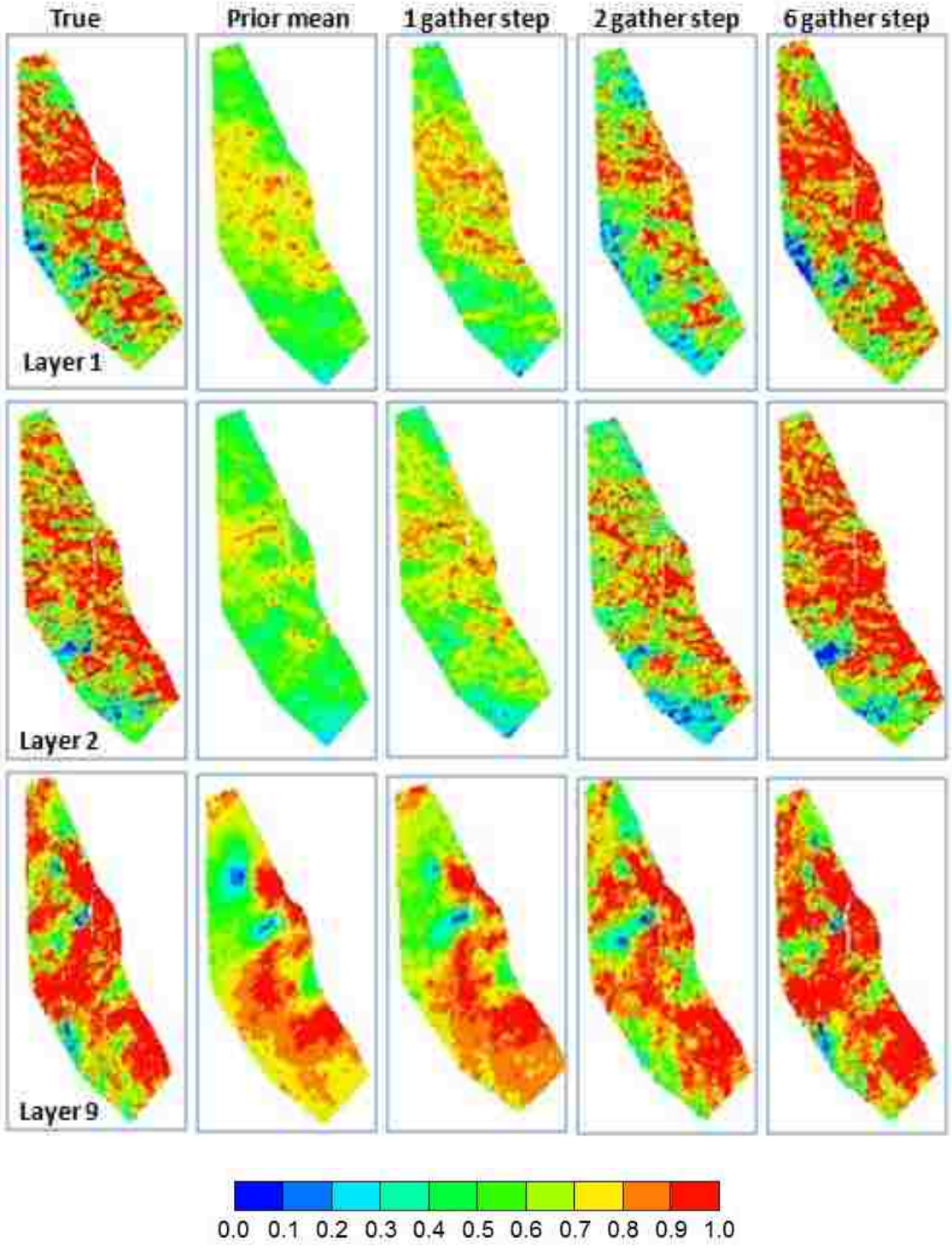

Figure 6.12: Updating of net-to-gross mean after each data assimilation. A good estimation of net-to-gross is obtained after 2 gathered steps.

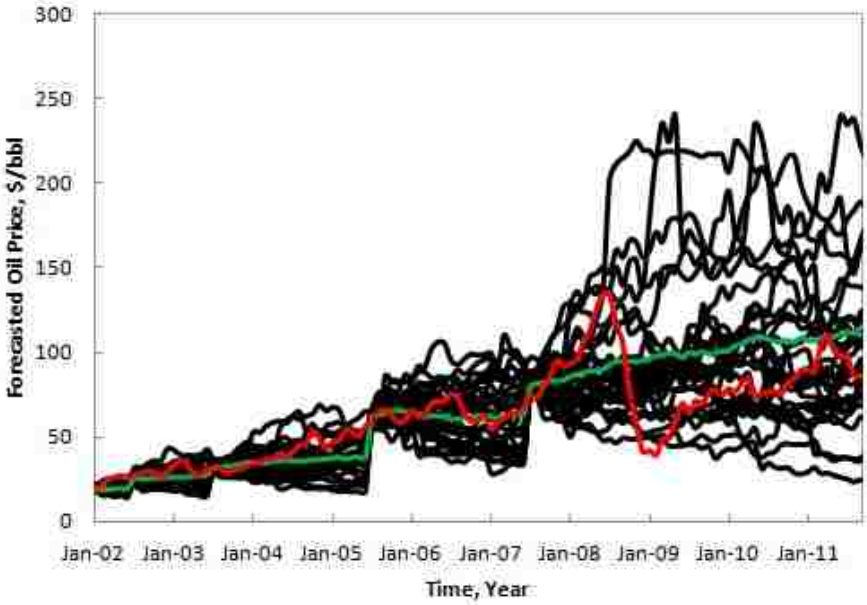

Figure 6.13: Oil price matches in closed-loop reservoir management. Black curves indicate the forecast realizations and the green curve is the ensemble mean. The red curve represents the real oil prices. Each shift of the green curve indicates an updating of the price forecast. Price uncertainty does not reduce with production of a reservoir.

the truth. As a result, the optimized controls are also approaching to the optimized controls obtained from the true case.

The realized NPVs for different scenarios are shown in Fig. 6.15. The black line indicates the realized NPVs with the true geological model and oil prices. The blue curve indicates the realized NPV of closed–loop reservoir management. The green dot indicates the realized NPV of optimization without model updating. The red dot shows the NPV for nonoptimized case. Closed–loop reservoir management obtains a NPV 8 percent higher than the nonoptimized case, 5 percent higher than optimization without model updating, and only 0.4 percent less than optimizing with the true case.

6.7 Conclusions

1. Three different price forecasting models are investigated: conventional forecast method, bootstrap sampling and sequential Gaussian simulation. They are used to forecast

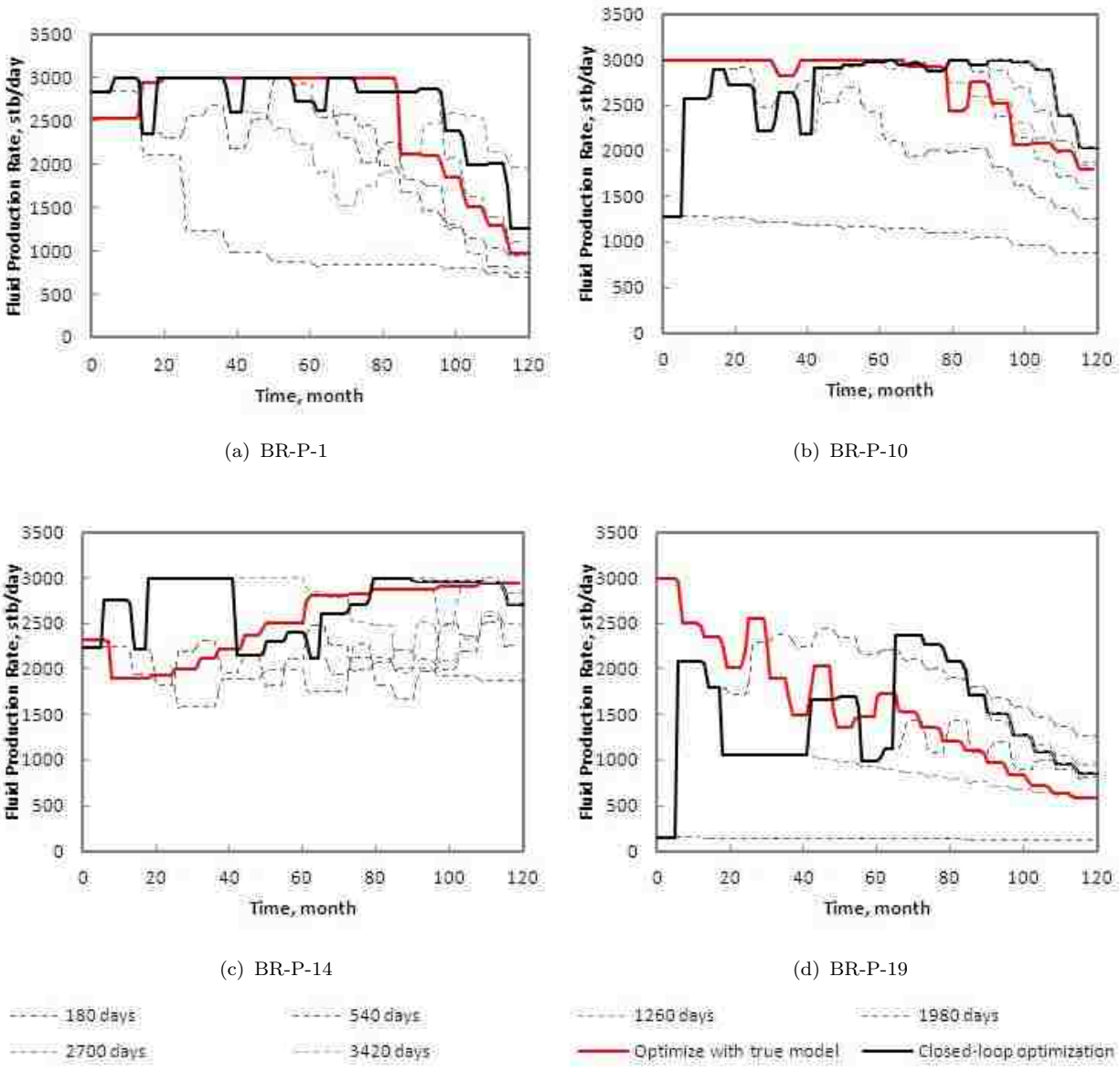

(a) BR-P-1

(b) BR-P-10

(c) BR-P-14

(d) BR-P-19

Figure 6.14: Optimized well controls for selected wells. Dished lines represent the evolution of optimized controls as production proceeds. Black line represents the final well control obtained using closed–loop reservoir management. Red line is the optimized control on the "true" case. As production proceeds, the optimized controls get more and more close to optimized controls on the "true" case.

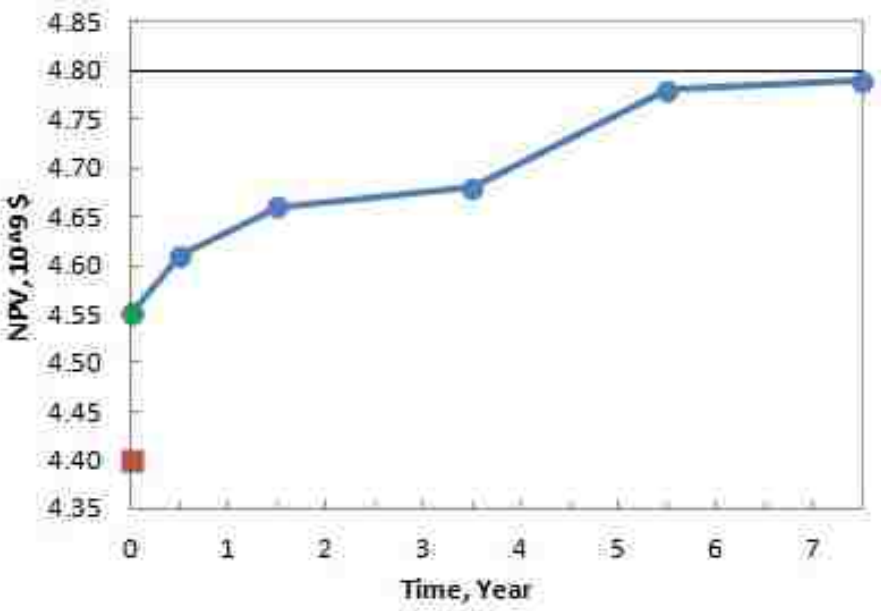

Figure 6.15: Realized NPV for different scenarios. The black line indicates the realized NPV with true geological and true price model. The blue curve indicates the realized NPV of closed–loop reservoir management. The green dot indicates the realized NPV without reservoir model updating. The red rectangular mark indicates the realized NPV of nonoptimized case. Closed–loop reservoir management obtains a NPV 8 percent higher than the nonoptimized case, 5 percent higher than optimization without model updating, and only 0.4 percent less than optimizing with the true case.

monthly oil prices from 2002 to 2011 using the historical data from year 1974 to 2001. None of these three methods captures the full range of price uncertainty. Among all these three methods, bootstrap sampling obtains a mean most close to the true oil price.

2. The forecast realizations and means are used in open–loop production optimization of the Brugge field from production year 10–20. It is shown that a better forecast model can improve NPV by more than 4 percent.

3. Optimization with price forecast means obtains higher NPVs than optimization with multiple realizations for all these three forecast models. This is because that EnOpt uses Monte Carlo method to approximate the gradient. The approximation works well

if the joint pdf is narrow. But if there is large uncertainty in the geological and price models, the optimization algorithm is more easier trapped at local optima.

4. The closed–loop reservoir management concept is also examined and compared with nonoptimized case, optimization without model updating and optimization with true geological model and oil prices. It is shown that the closed–loop reservoir management obtains a NPV 8 percent higher than the nonoptimized case, 5 percent higher than optimization without model updating, and only 0.4 percent less than optimization with the true reservoir model and oil prices.

Chapter 7
Concluding Discussion

Focused discussions have been presented in previous chapters. This chapter we first discuss some potential solutions to improve the efficiency of the current methods. We also propose a novel way to extend ensemble based methods for well placement optimization.

7.1 Karhunen–Loeve for gathered EnKF

One problem with gathered EnKF is that when the gather size becomes too big, it could be very time consuming or may not be practical to calculate the Kalman gain. Because the Kalman gain (Chapter 3) is a product of N_y by N_d^S matrix and N_d^S by N_d^S matrix, with N_y the dimension of augment vector y and N_d^s the total number of observations gathered at one assimilation step; the maximum gather size strongly depends on the dimension (N_y) of the augment vector (y). The smaller the N_y, the more the observations N_d^s can be assimilated before it becomes impractical to calculate the Kalman gain. To allow a big gather size for large scale reservoir simulation model updating, Karhunen-Loeve (K-L) expansion can be used to parameterize augment vector y to another vector ε which has a much smaller dimension than y (Huang, Quek, and Phoon 2001).

The discrete K-L expansion to generate realizations with the covariance C_y is given as (Sarma 2006),

$$y = E\Lambda^{1/2}\varepsilon \quad \equiv \quad y = f(\varepsilon), \tag{7.1}$$

where E is the matrix of eigenvectors of the covariance matrix C_y, Λ is a diagonal matrix of the eigenvalues of C_y, and ε is a set of uncorrelated, independent random variables. Since the matrix C_y has a dimension of $N_y \times N_y$, The maximum size of the matrices E and Λ is

also $N_y \times N_y$, and the dimension of vector ε is $N_y \times 1$. But the beauty of K-L expansion is that we can choose to retain only the largest N_K of the total N_y eigenvalues, in which case E is of size $N_y \times N_K$, Λ is of size $N_K \times N_K$, and ε is of size $N_K \times 1$. In fact, Sarma (2006) showed that the maximum number of nonzero eigenvalues is actually the minimum of N_y and the number of realizations N_e. Therefore, N_K could be much smaller than N_y for large scale model updating with moderate ensemble size N_e.

From above it is clear that K-L expansion is based on the eigen–decomposition of the covariance function. Singular value decomposition can be used to get the eigenvalues of the covariance matrix. But it is very computationally expensive when the covariance matrix is very large. Sarma (2006) suggested that using kernel formulation of the eigenvalue problem instead of directly performing an eigen-decompostion can solve this problem.

After K-L expansion, the data assimilation equation of EnKF can be written as

$$y(\varepsilon)_j^u = y(\varepsilon)_j^f + K(\varepsilon)_e(d_{obs,j} - d_j)\,. \tag{7.2}$$

Since ε has a much small dimension than y, calculation of Kalman gain $K(\varepsilon)_e$ could be much more efficient compared with the standard EnKF. Thus, more data can be gathered at each time assimilation step before it reaches to computational limits.

7.2 Optimize control with changing time interval

In chapter 2, ordinary multiscale regularization was used to find optimum frequency for well control adjustment with known reservoir model. In ordinary multiscale regularization, well controls are optimized using equal–length time interval for adjustment. Here, we propose an adaptive multiscale regularization method for closed–loop reservoir management. As it is shown in Fig. 7.1, the adaptive multiscale regularization method uses gradually increased time intervals for production optimization, at each optimization step. The time intervals are then gradually refined as production proceeds.

The step–wise procedure of using adaptive multiscale regularized EnOpt for closed–loop production optimization can be summarized as:

1. Well controls are optimized using the adjustment time intervals as Δt, $2\Delta t$, $4\Delta t$, $8\Delta t$, $\cdots$;

2. The optimized well controls are applied to next update time (say the field is produced for a time period of Δt), new observations are measured;

3. Reservoir models are updated with the new observations using adaptively gathered EnKF;

4. Production optimization is repeated for the rest of the reservoir life. The optimized well control from last optimization is used as the initial value for this step, and time intervals of this optimization step is obtained by slicing each of the last optimization' time interval to two. Thus the wells are adjusted at time intervals as: Δt, Δt, $2\Delta t$,$2\Delta t$, $4\Delta t$, $4\Delta t$, $8\Delta t$,$8\Delta t$,$\cdots$;

5. The procedure is repeated as the production going on.

Reasons for choosing gradually increased time intervals are: (1) if the NPV is discounted, early production phase is more important than the later years; (2) only the early years' well controls are implemented before the next production optimization, the later years' optimized well controls will be updated as the reservoir uncertainty reduces. (3) using gradually increased time intervals results in less number of unknowns comparing with using relatively fine equal-length time intervals. Therefore, the risk of the optimization algorithm been trapped at local optimum is reduced.

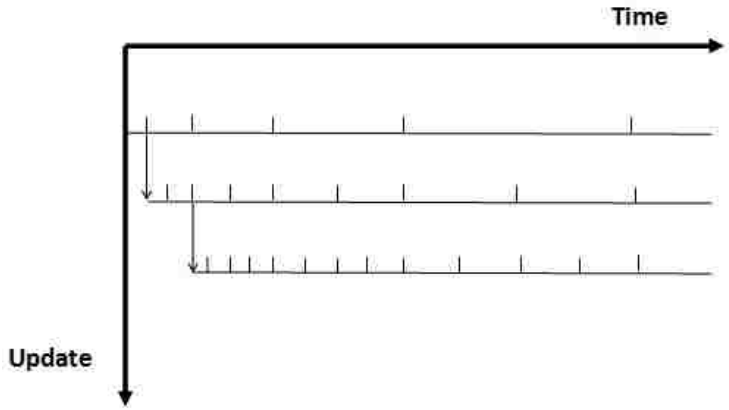

Figure 7.1: Adaptive multiscale regularization for closed–loop production optimization

7.3 EnOpt for well location optimization

As we mentioned in the introduction chapter, one of the crucial decisions in reservoir management is to determine the well locations. In this subsection, we discuss the possibility to extend ensemble–based method for well placement optimization.

The well placement optimization aims at finding the optimum locations of wells to maximize the reservoir performance. Here if we still use the NPV as the optimizing target, then the objective function g for a known reservoir model can be modified from Eq. 2.1,

$$g(x,u) = \sum_{i=1}^{N_t} \frac{P_o Q_{o_i}(x,u) - P_w Q_{w_i}(x,u)}{(1+r_\tau)^{\frac{t_i}{\tau}}}, \tag{7.3}$$

with u being a variable vector containing coordinates of each well. To simplify the problem, we assume the total number of wells, well types and well drilling cost are all fixed. Since the cost of drilling is assumed to be constant; it is not included into the objective function.

Well placement optimization is a challenge topic due to the discontinuity of the search space. With the standard commercial simulator, it is not possible to simulate off–center wells at arbitrary location accurately. That is to say, the well coordinates u can only be at the center of the well grid block. For the particular reason, evolution methods such as genetic algorithm(GA), simulated annealing (SA) and particle swarm (PS) optimization methods are commonly used for well placement optimization. For example, Montes, Repsol,

and Bartolome (2001) applied GA in a simple and a complex reservoir models. satisfactory results are obtained with both cases. However, global convergence and stability issues were observed. Combination of GA with other evaluation methods were recommended to improve the efficiency. Farshi (2008) generate a well placement optimization framework using continuous search engine to avoid generating invalid wells during reproduction. Onwunalu and Durlofsky (2009) applied PS for determine well location and type. Their study shows PS takes fewer function than GA to converge to global optimum. Even though such evolution methods are always claimed as global optimizations methods, they usually take large number of function evaluations to converge to global optimum. This could be a big issue for large scale complex reservoir model well placement optimization where function evaluation is very time–consuming and expensive.

While many authors are focusing on adapting the existing algorithms for discontinuous optimization; few efforts have been made to transform the discontinuous optimization problem to continuous fashion. If the off–center well can be simulate accurately in the reservoir simulator, the well placement optimization problems can then be treated as continuous optimization problems. Thus, many gradient–based methods such as EnOpt can directly be applied. Ding, Renard, and Weill (1998) shows how the off–center wells can be simulated in existing simulators by multiplying the conventional wellblock transmissibility with a correlation factor α. Their work is briefly summarized as following.

Considering an off–center well locates at arbitrary location of a grid block (Fig. 7.2), Ding, Renard, and Weill (1998) improved the fluid–flow calculations by using an equivalent transmissibility ($T_{eq,j}$) for the wellblock,

$$T_{eq,j} = kh\frac{\theta_i}{ln\frac{r_i}{r_o}}, i \in \{1,2,3,4\}, \tag{7.4}$$

where θ_i is the angle formed by the i-th wellblock interface view from the well, and r_i is the distance of the well to its i-th neighboring block center.

To simulate the off-center well in standard simulators, a correlation coefficient for wellblock transmissibility is introduced, it is calculated as

$$\alpha_i = \frac{T_{eq,i}}{T_i}, \tag{7.5}$$

where T_i is the conventional transmissibility, and it is defined as,

$$\begin{aligned} T_i &= kh\frac{\Delta b_0}{\Delta a_{\pm 1/2}}, \quad (i = 1, 3) \quad and \\ T_i &= kh\frac{\Delta a_0}{\Delta b_{\pm 1/2}}, \quad (i = 2, 4). \end{aligned} \tag{7.6}$$

For instance, α_1 is defined as,

$$\alpha_1 = \frac{\Delta a_{1/2}}{\Delta b_0}\frac{\theta_1}{ln(\frac{r_1}{r_0})}. \tag{7.7}$$

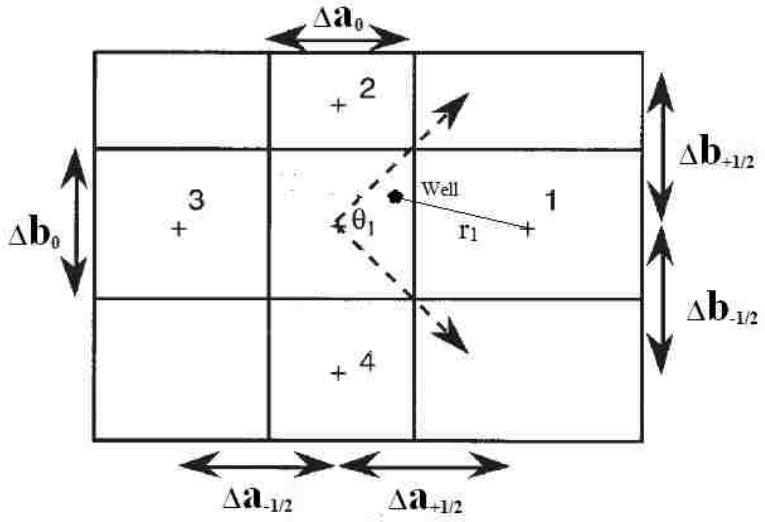

Figure 7.2: Representation of off–center well in numerical simulation, adapted from Ding, Renard, and Weill (1998).

Through this way, well placement optimization can be done using EnOpt by updating the gridblock transmissibility file, just like updating permeability file.

Chapter 8
Summary and Recommendations

8.1 Summary

Two simulator–independent methods are compared for production optimization: the ensemble–based optimization method (EnOpt) and the bound optimization by quadratic approximation (BOBYQA). EnOpt uses the steepest ascent method to iteratively update the well control vectors, and at each iteration uses a perturbed ensemble to approximate the gradients; whereas BOBYQA builds a local quadratic model to approximate the objective function by multivariate interpolation and updates the well controls using trust region technologies. Even though BOBYQA extracts a local second order Hessian information, whereas EnOpt only uses first order gradient information, our numerical experiments show that EnOpt converges to a higher NPV than BOBYQA for optimization problems with more than 100 of unknowns.

Multiscale regularization is applied to both EnOpt and BOBYQA to find out the optimum well control adjustment frequency. Multiscale regularized optimization starts from the coarsest control scale and refines successively using the coarse–scale solution as the initial guess of controls for next finer scale optimization. The refining process is terminated when no further improvement on the objective function is obtained. Result shows that multiscale regularized method is more efficient than direct fine–scale optimization because the coarse scale is less likely to be trapped at local optimum than the fine-scale. In addition, unlike the non–regularized EnOpt and BOBYQA methods, which are sensitive to the initial guess of well controls, the regularized methods converge to consistent, higher optima regardless of differences in the initial controls.

A gathered EnKF method, which can also be seen as a step–wise ensemble smoother method, is proposed to handle the high frequency data from permanent downhole sensors.

In this method, if there is no significant mismatch between the observations and the ensemble predictions, the observations are stored (or gathered) instead of being assimilated immediately. Model updating is done only if the gathered data volume exceeds a specified threshold, or if the observations diverge from prior ensemble predictions. It is proven that by gathering the observations, sampling errors introduced from the perturbed observations to the Kalman gain are reduced resulting in less biased ensemble covariance. Another benefit of gathering the observation is the reduction of computational cost by avoiding simulation restarts. However, gathered EnKF with a fixed gather size does not always work well due to the nonlinearity of the dynamic model. An adaptively gathered EnKF is then proposed to solve this problem. The adaptively gathered EnKF starts from a small gather size and gradually increases the gather size if the ensemble forecast converges to the true observations, otherwise, the gather size are reduced. Besides reducing the sampling errors and computational cost, the adaptively gathered EnKF can also be used to determine the optimal frequency for updating reservoir model and optimizing the production controls. It is reasonable to update the model more frequently at the beginning (when the mean is not near the truth and the uncertainty is relatively large). When the mean is near the truth and the uncertainty is small, corrections to the prior model are smaller, and high–frequency model updating may destroy ensemble diversity and cause filter divergence.

Besides reservoir model uncertainty, oil price uncertainty has also be incorporated into closed–loop reservoir management. Three price forecast models are used to demonstrate how the price forecast models affect optimized NPV. They are conventional forecast, sequential Gaussian simulation and bootstrap sampling methods. Among all these three methods, the bootstrap sampling forecast works best when they are used to forecast oil price from 2002–2011. As a result, it obtains a optimized NPV four percent higher than other methods. Our numerical experiments also show that EnOpt tends to trap at local optimum if there is large uncertainty in the forecasted oil prices. The closed–loop reservoir management concept is also examined and compared with nonoptimized case as well as optimization with known

geological model and oil prices. It is shown that the closed–loop reservoir management obtains a NPV eight percent higher than the nonoptimized case, and only 0.4 percent less than optimization with the true case.

8.2 Recommendations

- This dissertation only address well control optimization problems. It would be interesting to incorporate other optimization problems, for example, well count, well type, well location and trajectory, all together to one closed–loop reservoir management process.

- As it is mentioned earlier, the accuracy of ensemble based method strongly depends on the size of ensemble. In general, the ensemble size is recommended to be on the order of 100 to keep an adequate sampling. But running 100 simulations for model based production optimization is still every time consuming, especially for large scale complex reservoir models. Take the Brugge field for example, to optimize the field for 10 years costs about one and half days (100 simulations $\times$ 2 minutes per simulation $\times$ 10 iterations = 33.3 hours) if 100 realizations are used. Therefore, parallel simulation is strongly recommended.

- The LSU petroleum and geology departments have built up a sand tank experiment to mimic real–time reservoir management. Because the algorithms described in this dissertation are only tested with synthetic cases, further verifying them with the sandtank experiment is desirable.

- When price forecasting is included in closed–loop reservoir management, our objective function is not only affected by the reservoir model uncertainties but also by the price uncertainty and its fluctuations. How often should we update the price forecast and repeat the production optimization process has not yet been addressed. In principle, both the magnitude and frequency of the price fluctuations may impact optimized controls.

Bibliography

[1] Addiego-Guevara, E. A., M. D. Jackson, and M. A. Giddins. 2008, 20-23 April. "Insurance Value of Intelligent Well Technology Against Reservoir Uncertainty." *SPE/DOE Symposium on Improved Oil Recovery*. Tulsa, Oklahoma. SPE–113918–MS.

[2] Aitokhuehi, Inebenose. 2004, June. "Real–Time Optimization of Smart Wells." Master's thesis, Stanford University.

[3] Brouwer, D. R., J. D. Jansen, S. van der Starre, C. P. J. W. van Kruijsdijk, and C.W.J. Berentsen. 2001, 21-22 May. "Recovery Increase through Water Flooding with Smart Well Technology." *SPE European Formation Damage Conference*. SPE–68979–MS.

[4] Bukhamsin, Ahmed Y., Mohammad Moravvej Farshi, and Khalid Aziz. 2010. "Optimization of Multilateral Well Design and Location in a Real Field Using a Continuous Genetic Algorithm." *SPE/DGS Saudi Arabia Section Technical Symposium and Exhibition*. SPE–136944–MS.

[5] Burgers, Gerrit. 1998. "Analysis Scheme in the Ensemble Kalman Filter." *Monthly Weather Review* 126 (6): 1719.

[6] Chaudhri, Masroor M., Hemant A. Phale, Ning Liu, and Dean S. Oliver. 2009, 24-26 March. "An Improved Approach for Ensemble-Based Production Optimization." *SPE Western Regional Meething*. California. SPE–121305–MS.

[7] Chen, Chaohui, Yudou Wang, Gaoming Li, and Albert C. Reynolds. 2010. "Closed–Loop Reservoir Management on the Brugge Test Case." *Computational Geosciences* 14 (4): 691–703 (February).

[8] Chen, Yan. 2008. "Ensemble–based Closed–loop Production Optmization." Ph.D. diss., University of Oklahoma, Oklahoma.

[9] Chen, Yan, and Dean S. Oliver. 2010. "Ensemble–Based Closed–loop Optimization Applied to Brugge Field." *SPE Reservoir Evaluation & Engineering Engineering* 13 (February): 56–71.

[10] Chen, Yan, Dean S. Oliver, and Dongxiao Zhang. 2009. "Efficient Ensemble–based Closed–loop Production Optimization." *SPE Journal* 14 (4): 634–645. SPE–112873–PA.

[11] Ding, Yu, Gerard Renard, and Luce Weill. 1998. "Represetation of Wells in Numerical Reservoir Simulation." *SPE Reservoir Evaluation & Engineering Engineering*, February, 18–23.

[12] Dolle, Norbert, Prithipal Singh, Rob Turner, Myles Woodward, and Wan-Faisal Paino. 2006. "Bugan Field Gas Management Controls Four Producing Zones." *WorldOil* 227, no. 5.

[13] Energy Information Administration, U.S. Department of Energy. 2012. Crude Oil Spot Prices. http://www.eia.gov/dnav/pet/hist/LeafHandler.ashx?n=PET&s=RWTC&f=M.

[14] Evensen, Geir. 1994. "Sequential data assimilation with a non-linear quasi-geostrophic model using Monte Carlo methods to forecast error statistics." *Journal of Geophysical Research* 99 (C5): 10143–10162 (May).

[15] ———. 1997. "Advanced Data Assimilation for Strongly Nonlinear Dynamics." *Monthly Weather Review* 125:1342–1354.

[16] ———. 2009. *Data Assimilation — The Ensemble Kalman Filter*. Second Edition. Springer Dordrecht Heidelberg.

[17] Evensen, Geir, and Peter Jan van Leeuwen. 2000. "An Ensemble Kalman Smoother for Nonlinear Dynamics." *Monthly Weather Review* 128:1852–1867.

[18] Fariyibi, Festus L. 2006, August. "Application of Price Uncertainty Quantification Models And Their Impacts on Project Evaluations." Master's thesis, Texas A&M University, Texas.

[19] Farshi, Mohammad Moravvej. 2008, June. "Improving Genetic Algorithms for Optimum Well Placement." Master's thesis, Stanford University.

[20] Faure, Ghislain, and Richard Grotjahn. 2001, March. "Forecast Guidance of Significant Weather Events in Sacaramento Area Using Historical Analogs." Technical Report, UCDavis Atmospheric Science Program.

[21] Fowler, M.L., M.A. Young, E.L. Cole, and M.P. Madden. 1996, October. "Some Practical Aspects of Reservoir Management." *SPE Eastern Region Meeting*. SPE–37333–MS.

[22] Furrer, Reinhard, and Thomas Bengtsson. 2007. "Estimation of High–dimensional Prior and Posterior Covariance Matrices in Kalman Filter Variants." *Journal of Multivariate Analysis* 98 (February): 227–255.

[23] Gao, Changhong, T. Rajeswaran, and Edson Nakagawa. 2007, 31 March-3 April. "A Literature Review on Smart Well Technology." *SPE Production and Operation Symposium*. Oklahoma. SPE–106011–MS.

[24] Gringarten, Alian C. 1998. "Evolution of Reservoir Management Techniques: From Independent Methods to an Integrated Methodology. Impact on Petroleum Engineering Curriculum, Graduate Teaching and Competitive Advantage of Oil Companies." *SPE Asia Pacific Conference on Integrated Modeling for Asset Management*. SPE–39713.

[25] Gu, Yaqing, and Dean S. Oliver. 2006. "The Ensemble Kalman Filter for Continuous Updating of Reservoir Simulation Models." *Journal of Energy Resources Technology* 128 (March): 79–87.

[26] Hamill, Thomas M., and Jeffery S. Whiteaker. 2001. "Distance–dependent Filtering of Background Error Covariance Estimates in an Ensemble Kalman Filter." *American Meteorological Society* 129 (May): 2776–2790.

[27] Harding, T .J., N. J. Radcliffe, and P. R. King. 1996, 16-17 April. "Optimization of Production Strategies Using Stochastic Search Methods." *European 3-D Reservoir Modeling Conference*. Stavanger, Norway. SPE–35518–MS.

[28] Holmes, Jay C., Ashish V. Mendjoge, and Duane A. McVay. 2006. "Quantification of Oil Price Uncertainty in Economic Evaluation Using Sequential Gaussian Simulation." *Petroleum Science and Technology* 24:943–962.

[29] Houtekamer, P.L., and Herschel L. Mitchell. 1998. "Data Assimilation Using an Ensemble Kalman Filter Technique." *American Meteorological Society* 126 (March): 796–811.

[30] ———. 2001. "A Sequential Ensemble Kalman Filter for Atmospheric Data Assimilation." *American Meteorological Society* 123 (January): 123–137.

[31] Huang, S. P., S. T. Quek, and K. K. Phoon. 2001. "Convergence Study of The Truncated Karhunen–Loeve Expansion for Simulation of Stochastic Processes." *International Journal for Numerical Methods in Engineering* 52:1029–1043.

[32] Huang, XuRi, and M.G. Kelkar. 1994. "Application of Combinatorial Algorithms for Description of Reservoir Properties." *SPE Ninth Symposium on Improved Oil Recovery*. SPE–27803–MS.

[33] Isebor, Obiajulu Joseph. 2009, June. "Constrainted Production Optimization with an Emphasis on Derivative-Free Methods." Master's thesis, Stanford University.

[34] Jansen, J. D., A. M. Wagenvoort, V. S. Droppert, R. Daling, and C. A. Glandt. 2002, 8–10 October. "Smart Well Solutions for Thin Oil Rims: Inflow Switching and the Smart Stinger Completion." *SPE Asia Pacific Oil and Gas Conference and Exhibition*. Melbourne, Australia. SPE–77942–MS.

[35] Jennings, J.W. 1999. "How Much Core-Sample Variance Should a Well–log Model Reproduce?" *SPE Reservoir Evaluation & Engineering Engineering* 2 (5): 442–470. SPE–57477.

[36] Kalnay, Eugenia. 2006. *Ensemble Forecasting and Data Assimilation: Two Problems with the Same Solution ?* Predictability of Weather and Climate. Cambridge University Press.

[37] Leeuwen, Peter Jan Van, and Geir Evensen. 1996. "Data Assimilation and Inverse Methods in Terms of a Probabilistic Formulation." *Monthly Weather Review* 124 (December): 2898–2913.

[38] Li, Xin. 2008, Aug. "Continuous Reservoir Model Updating By Ensemble Kalman Filter on Grid Computing Architectures." Ph.D. diss., Louisiana State University, Baton Rouge, LA.

[39] Lien, M., D.R. Brouwer, T. Mannseth, and J.D. Jansen. 2008. "Multiscale Regularization of Flooding Optimization for Smart Feild Management." *SPE Journal* 13 (2): 195–204 (June). SPE–99728–PA.

[40] Maschio, C., and D. J. Schiozer. 2005. "Development and Application of Methodology for Assisted History Matching." *SPE Latin American and Caribean Petroleum Engneering*. SPE–94882.

[41] MathWorks Inc. 2010. *MATLAB User's Manual, version 7.10.0 (R2010a)*. Natick, Massachusetts: MathWorks Inc.

[42] McMichael, Claude. 1999, October. "The Fallacy of the Hockey Stick Projection." *SPE Annual Technical Conference and Exhibition*. Houston, Texas. SPE–56454.

[43] Meshioye, Oluwafisayo, Eric Mackay, E. Ekeoma, and Martinez Chukuwezi. 2010, 31 July-7 August. "Optimization of Waterflooding Using Smart Well Technology." *Nigeria Annual International Conference and Exhibition*. Tinapa - Calabar, Nigeria. SPE–136996–MS.

[44] Montes, Guillermo, Fundacion Repsol, and Pablo Bartolome. 2001, March. "The Use of Genetic Algorithms in Well Placement Optimization." *SPE Latin American and Caribean Petroleum Engneering*. SPE–69439.

[45] Moré, Jorge J., and Stefan M. Wild. 2009. "Benchmarking Derivative–Free Optimization Algorithms." *SIAM J. Optimization* 20 (1): 172–191.

[46] Nævdal, Geir, Liv Merethe Johnsen, Sigurd Ivar Aanonsen, and Erlend H. Vefring. 2005. "Reservoir Monitoring and Continuous Model Updating Using Ensemble Kalman Filter." *SPE Journal* 10 (1): 66–74 (March). SPE–84372–PA.

[47] Nwaozo, Jude. 2006. "Dynamic Optimization of a Water Flooding Reservoir." Master's thesis, University of Oklahoma, Norman, Oklahoma.

[48] Oliver, Dean S., and Yan Chen. 2008. "Improved Initial Sampling for the Ensemble Kalman Filter." *Computational Geosciences* 13:13–27.

[49] Oliver, Dean S., Albert C. Reynolds, and Ning Liu. 2008. *Inverse Theory for Petroleum Reservoir Characterization and History Matching*. ISBN 978-0-521-88151-7. Cambridge University Press.

[50] Onwunalu, Jerome E., and Louis J. Durlofsky. 2009. "Application of A Particle Swarm Optimization Algorithm for Determining Optimum Well Location and Typend Type." *Computational Geosciences* 14:183–198.

[51] Onwunalu, Jérôme E., and Louis J. Durlofsky. 2010. "Application of A Particle Swarm Optimization Algorithm for Determining Optimum Well Location and Type." *Computational Geosciences* 14 (1): 183–198.

[52] Peters, Lies, Rob Arts, Geert Brouwer, and Cees Gee. 2009, June. "Results of the Brugge Benchmark Study for Flooding Optimisation and History Matching." *SPE Reservoir Simulation Symposium*. SPE–119094–MS.

[53] Powell, M.J.D. 2009. "The BOBYQA Algorithm for Bound Constrained Optimization Without Derivatives." *Report DAMTP 2009/NA06*. Centre for Matchematical Sciences, University of Cambridge, UK.

[54] Quenes, Ahmed, Srinivasa Bhagavan, and B.J Travis. 1994. "Application of Simulated Annealing and Other Global Optimization Methods to Reservoir Description: Myths and Realities." *SPE Annual Technical Conference and Exhibition*. SPE–28415–MS.

[55] Quenes, Ahmed, B. Brefort, G. Meunier, and S. Dupere. 1993. "A New Algorithm for Automatic History Matching: Application of Simulated Annealing Methods (SAM) to Reservoir Inverse Modeling." *SPE Journal*. SPE–26297–MS.

[56] Ramakrishnan, T.S. 2007. "On Reservoir Fluid-Flow Control With Smart Completions." *SPE Production and Operation* 22 (1): 4–12 (February). SPE–84219–PA.

[57] Sacher, Willam, and Peter Bartello. 2008. "Sampling Errors in Ensemble Kalman Filtering. Part I: Theory." *Monthly Weather Review* 136 (8): 3035 (August).

[58] Sarma, Pallav. 2006. "Efficient Closed-loop Optimal Control of Petroleum Reservoir Under Uncertainty." Ph.D. diss., Stanford University.

[59] Skjervheim, J.-A., G. Evensen, J. Hove, and J. G. Vabø. 2011, February. "An Ensemble Smoother for Assisted History Matching." *SPE Reservoir Simulation Symposium*. The Woodlands, Texas, USA. SPE–141929–MS.

[60] Steinhubl, Andrew, and Glenn Klimchuk. 2008. "The Digital Oil Field Advantage." Technical Report, Booz & Company Inc.

[61] Team, R Development Core. 2008. *R: A Language and Environment for Statistical Computing*. Vienna, Austria: R Foundation for Statistical Computin.

[62] Thakur, Ganesh C. 1996. "What is Reservoir Management?" *SPE Distinguish Author Series* 48, no. 6 (June). SPE–26289–PS.

[63] van Essen, G. M., J. D. Jansen, D. R. Brouwer, S. G. Douma, M. J. Zandvliet, K. I. Rollett, and D. P. Harris. 2010. "Optimization of Smart Wells in the St. Joseph Field." *SPE Reservoir Evaluation & Engineering Engineering* 13 (4): 588–595 (August). SPE–123563–PA.

[64] van Essen, G. M., M. J. Zandvliet, P. M. J. Van den Hof, O. H. Bosgra, and J.D. Jansen. 2009. "Robust Waterflooding Optimization of Multiple Geological Scenarios." *SPE Journal* 14 (1): 202–210 (March). SPE–102913–PA.

[65] van Leeuwenan, Peter Jan. 1998. "Comment on "Data Assimilation Using an Ensemble Kalman Filter Technique"." *Monthly Weather Review*, vol. 127.

[66] Verma, Vidya B, and Raymond E Cline. 2005. "Realtime Reservoir Management for Achieving Better Asset Value." *Exploration & Production: The Oil & Gas Review*, vol. .

[67] Wang, Chunhong, Gaoming Li, and Albert C. Reynolds. 2009. "Production Optimization in Closed–Loop Reservoir Management." *SPE Journal* 14 (3): 506–523 (September). SPE–109805–PA.

[68] Wen, Xian-Huan, and Wen H. Chen. 2007. "Some Practical Issues on Real–time Reservoir Model Updating Using Ensemble Kalman Filter." *SPE Journal* 12 (2): 156–166 (June). SPE–111571–PA.

[69] Yang, C., L. Nghiem, and C. Card. 2007. "Reservoir Model Uncertainty Quantification Through Computer-Assisted History Matching." *SPE Annual Technical Conference and Exhibition*. SPE–109825.

[70] Yeten, Burk, Louis J. Durlofsky, and Khalid Aziz. 2002, 4-7 November. "Optimization of Smart Well Control." *SPE International Thermal Operations and Heavy Oil Symposium and International Horizontal Well Technology Coference*. Calgary, Alberta, Canada. SPE–79031–MS.

AppendixA: Comparing Sequential And Simultaneous Data Assimilation

If only sampling errors in the initial ensemble ϵ ($y^f_{\epsilon,1} = y^f_1 + \epsilon$ with subscript 1 denoting the first assimilation step) is considered, and for the linear case, sequential data assimilation should get identical results to simultaneous data assimilation. We prove this below. If the two data sets are assimilated sequentially, say $d_{obs,1}$ followed by $d_{obs,2}$, then after assimilation of the data set $d_{obs,1}$, the updated state vector $y^u_{\epsilon,1}$ can be written as

$$\begin{aligned} y^u_{\epsilon,1} &= y^f_{\epsilon,1} + C^f_{Y\epsilon,1}H_1^T(H_1C^f_{Y\epsilon,1}H_1^T + C_{D1})^{-1}(d_{obs,1} + \xi_1 - H_1y^f_{\epsilon,1}) \\ &= y^f_{\epsilon,1} + (H_1^TC_{D1}^{-1}H_1 + (C^f_{Y_{\epsilon,1}})^{-1})H_1^TC_{D1}^{-1}(d_{obs,1} + \xi_1 - H_1y^f_{\epsilon,1}). \end{aligned} \tag{8.1}$$

The updated covariances after assimilating $d_{obs,1}$ is calculated as,

$$\begin{aligned} C^u_{Y\epsilon,1} &= \left\langle \left(y^u_{\epsilon,1} - \left\langle y^u_{\epsilon,1}\right\rangle\right)\left(y^u_{\epsilon,1} - \left\langle y^u_{\epsilon,1}\right\rangle\right)^T \right\rangle \\ &= C^f_{Y\epsilon,1} - C_{Y\epsilon,1}H_1^T(H_1C_{Y\epsilon,1}H_1^T + C_{D1})^{-1}H_1^TC_{Y\epsilon,1} \\ &= [H_1^TC_{D1}H_1 + (C^f_{Y\epsilon,1})^{-1}]^{-1}. \end{aligned} \tag{8.2}$$

When incorporating the new data set $d_{obs,2}$, a forward step is taken. Assuming the forward model is linear, that is to say $y^f_{\epsilon,2} = Ay^u_{\epsilon,1}$, then the augment vector can be calculated as,

$$\begin{aligned}
y^u_{\epsilon,2} &= y^f_{\epsilon,2} + C^f_{Y\epsilon,2}H_2^T(H_2C^f_{Y\epsilon,2}H_2^T + C_{D2})^{-1}(d_{obs,2} + \xi_2 - H_2y^f_{\epsilon,2}) \\
&= A[y^u_{\epsilon,1} + C^u_{Y\epsilon,1}A^TH_2^T(H_2AC^u_{Y\epsilon,1}A^TH_2^T + C_{D2})^{-1} \\
&\quad (d_{obs,2} + \xi_2 - H_2Ay^u_{\epsilon,1})] \\
&= A\{y^u_{\epsilon,1} + [A^TH_2^TC_{D2}^{-1}H_2A + H_1^TC_{D1}^{-1}H_1 + (C^f_{Y_{\epsilon,1}})^{-1}]^{-1} \\
&\quad AH_2^TC_{D2}^{-1}(d_{obs,2} + \xi_2 - H_2y^f_{\epsilon,2})\} \\
&= A\{y^f_{\epsilon,1} + C^f_{Y\epsilon,1}H_1^T(H_1C^f_{Y\epsilon,1}H_1^T + C_{D1})^{-1}(d_{obs,1} + \xi_1 - H_1y^f_{\epsilon,1}) \\
&\quad +[A^TH_2^TC_{D2}^{-1}H_2A + H_1^TC_{D1}^{-1}H_1 + (C^u_{Y_{\epsilon,1}})^{-1}]^{-1} \\
&\quad AH_2^TC_{D2}^{-1}(d_{obs,2} + \xi_2 - H_2y^f_{\epsilon,2})\} \\
&= A\{y^f_{\epsilon,1} + [A^TH_2^TC_{D2}^{-1}H_2A + H_1^TC_{D1}^{-1}H_1 + (C^f_{\epsilon,1})^{-1}]^{-1} \\
&\quad [A^TH_2^TC_{D2}^{-1}(d_{obs,2} + \xi_2 - H_2Ay^f_{\epsilon,1}) \\
&\quad +H_1^TC_{D1}^{-1}(d_{obs,1} + \xi_1 - H_1y^f_{\epsilon,1})]\}\,, \qquad (8.3)
\end{aligned}$$

with the updated ensemble covariance

$$C^u_{Y\epsilon,2} = [A^TH_2^TC_{D2}^{-1}H_2A + H_1^TC_{D1}^{-1}H_1 + (C^f_{Y\epsilon,1})^{-1}]^{-1}. \qquad (8.4)$$

If the two data set are assimilated simultaneously,

$$\begin{aligned}
y^u_\epsilon &= A\{y^f_{\epsilon,1} + [A^TH_2^TC_{D2}^{-1}H_2A + H_1^TC_{D1}^{-1}H_1 + (C^f_{\epsilon,1})^{-1}] \\
&\quad [A^TH_2^TC_{D2}^{-1}(d_{obs,2} + \xi_2 - H_2Ay^f_{\epsilon,1}) \\
&\quad +H_1^TC_{D1}^{-1}(d_{obs,1} + \xi_1 - H_1y^f_{\epsilon,1})]\}\,, \qquad (8.5)
\end{aligned}$$

with the updated ensemble covariance

$$C_{Y,\epsilon} = [A^TH_2^TC_{D2}^{-1}H_2A + H_1^TC_{D1}^{-1}H_1 + (C^f_{Y\epsilon,1})^{-1}]^{-1}.$$

Hence

$$y^u_\epsilon = y^u_{\epsilon,2} \quad and \quad C^u_{Y,\epsilon} = C^u_{Y\epsilon,2}. \qquad (8.6)$$

Similar proof can also be found in (49).

Appendix B: Calculation of $K_{2,e}$ and $C^u_{Y_2,e}$

Substituting $C^f_{YE,2} = C^f_{Y\epsilon,2} + \eta$ to the Kalman gain,

$$\begin{aligned} K_{E,2} &= C^f_{YE,2} H_2^T (H_2 C^f_{YE,2} H_2^T + C_{D2})^{-1} \\ &= (C^f_{Y\epsilon,2} + \eta) H_2^T (H_2 C_{Y\epsilon,2} H_2^T + H_2 \eta H_2^T + C_{D2})^{-1} \\ &= (K_{\epsilon,2} + \kappa_\eta)(I + H_2 \kappa_\eta)^{-1} \\ &= K_{\epsilon,2} + (I - K_{\epsilon,2} H_2)[\kappa_\eta (I + H_2 \kappa_\eta)^{-1}]. \end{aligned} \tag{8.7}$$

Following Sacher and Bartello (57), if $\| \ H_2 \kappa_\eta \ \| \ll \| \ I \ \|$, then the Taylor expansion for $(I + H_2 \kappa_\eta)^{-1}$ is

$$\begin{aligned} (I + H_2 \kappa_\eta)^{-1} &= I - H_2 \kappa_\eta + (H_2 \kappa_\eta)^2 + \cdots + (-1)^n (H_2 \kappa_\eta)^n \\ &\quad + O(\| \ H_2 \kappa_\eta \ \|^n) \, . \end{aligned} \tag{8.8}$$

This leads to

$$\begin{aligned} K_{E,2} &= K_{\epsilon,2} + L_{\epsilon,2} \sum_{i=0}^{n} (-1)^i \kappa_\eta (H_2 \kappa_\eta)^i + O(\| \ (\kappa_\eta H_2)^n \kappa_\eta \ \|) \\ &= K_{\epsilon,2} + L_{\epsilon,2} (\kappa_\eta - \kappa_\eta H_2 \kappa_\eta) + O(\| \ \kappa_\eta H_2 \kappa_\eta \ \|). \end{aligned} \tag{8.9}$$

Using Eq. 3.21 $C^u_{YE,2}$ can be calculated as,

$$\begin{aligned} C^u_{YE,2} &= (I - K_{E,2} H_2) C^f_{YE,2} (I - H_2^T K_{E,2}^T) \\ &\quad + K_{E,2} (C_{D2} + \rho_2) K_{E,2}^T \\ &= C^f_{YE,2} - K_{E,2} H_2 C^f_{YE,2} - C^f_{YE,2} H_2^T K_{E,2}^T \\ &\quad + K_{E,2} (H_2 C^f_{YE,2} H_2^T + C_{D2}) K_{E,2}^T + K_{E,2} \rho_2 K_{E,2}^T \\ &= (I - K_{E,2} H_2) C^f_{YE,2} + K_{E,2} \rho_2 K_{E,2}^T \, . \end{aligned} \tag{8.10}$$

Substituting Eq. 8.9 into Eq. 8.10,

$$
\begin{aligned}
C^u_{YE,2} &= (I - K_{E,2}H_2)C^f_{YE,2} + K_{E,2}\rho_2 K^T_{E,2} \\
&= \{I - K_{\epsilon,2}H_2 - (I - K_{\epsilon,2}H_2)[\kappa_\eta(I + H_2\kappa_\eta)^{-1}]H_2\} \\
&\quad (C^f_{Y\epsilon,2} + \eta) + K_{E,2}\rho_2 K^T_{E,2} \\
&= (I - K_{\epsilon,2}H_2)[I - \kappa_\eta(I + H_2\kappa_\eta)^{-1}H_2](C^f_{Y\epsilon,2} + \eta) \\
&\quad + K_{E,2}\rho_2 K^T_{E,2} \\
&= L_{\epsilon,2}[I - \kappa_\eta(I + H_2\kappa_\eta)^{-1}H_2](C^f_{Y\epsilon,2} + \eta) \\
&\quad + K_{E,2}\rho_2 K^T_{E,2} \\
&= L_{\epsilon,2}C^f_{Y\epsilon,2} + L_{\epsilon,2}[\eta - \sum_{i=0}^{n-1}(-1)^i(\kappa_\eta H_2)^i\kappa_\eta\Phi_\epsilon^{-1}\kappa_\eta^T]L^T_{\epsilon,2} \\
&\quad + K_{E,2}\rho_2 K^T_{E,2} + O(\parallel (\kappa_\eta H_2)^n\eta \parallel) \\
&= C^u_{Y\epsilon,2} + L_{\epsilon,2}(\eta - \kappa_\eta\Phi_\epsilon^{-1}\kappa_\eta^T)L^T_{\epsilon,2} + K_{E,2}\rho_2 K^T_{E,2} \\
&\quad + O(\parallel (\kappa_\eta\Phi_\epsilon^{-1}\kappa_\eta^T \parallel). \qquad (8.11)
\end{aligned}
$$

Appendix C: Historical Oil Prices From Year 1974-2011

Month	Nominal oil prices($)[3]	CPI index[4]	Inflation index, adjusted to Dec,2001	Adjusted oil prices ($) adjusted to Dec,2001
Jan-74	7.0	46.6	0.26	26.6
Feb-74	6.9	47.2	0.26	26.0
Mar-74	6.8	47.8	0.27	25.3
Apr-74	6.8	48.0	0.27	25.1
May-74	6.9	48.6	0.27	25.2
Jun-74	6.9	49.0	0.27	24.9
Jul-74	6.8	49.4	0.28	24.5
Aug-74	6.7	50.0	0.28	23.9
Sep-74	6.7	50.6	0.28	23.6
Oct-74	7.0	51.1	0.29	24.3
Nov-74	7.0	51.5	0.29	24.1
Dec-74	7.1	51.9	0.29	24.4
Jan-75	7.6	52.1	0.29	26.0
Feb-75	7.5	52.5	0.29	25.4
Mar-75	7.6	52.7	0.30	25.6
Apr-75	7.6	52.9	0.30	25.4
May-75	7.5	53.2	0.30	25.2
Jun-75	7.5	53.6	0.30	24.9
Jul-75	7.8	54.2	0.30	25.5
Aug-75	7.7	54.3	0.30	25.4
Sep-75	7.8	54.6	0.31	25.3
Oct-75	7.8	54.9	0.31	25.4
Nov-75	7.8	55.3	0.31	25.1
Dec-75	7.9	55.5	0.31	25.5
Jan-76	8.6	55.6	0.31	27.7
Feb-76	7.9	55.8	0.31	25.1
Mar-76	7.8	55.9	0.31	24.8
Apr-76	7.9	56.1	0.31	25.0
May-76	7.9	56.5	0.32	24.9
Jun-76	8.0	56.8	0.32	25.1
Jul-76	8.0	57.1	0.32	25.1
Aug-76	8.0	57.4	0.32	24.9
Sep-76	8.4	57.6	0.32	26.0
Oct-76	8.5	57.9	0.32	26.1
Nov-76	8.6	58.0	0.33	26.5
Dec-76	8.6	58.2	0.33	26.4
Jan-77	8.5	58.5	0.33	25.9
Feb-77	8.6	59.1	0.33	25.9
Mar-77	8.5	59.5	0.33	25.3
Apr-77	8.4	60.0	0.34	25.0

May-77	8.5	60.3	0.34	25.1
Jun-77	8.4	60.7	0.34	24.8
Jul-77	8.5	61.0	0.34	24.8
Aug-77	8.6	61.2	0.34	25.1
Sep-77	8.6	61.4	0.34	25.1
Oct-77	8.7	61.6	0.35	25.2
Nov-77	8.7	61.9	0.35	25.1
Dec-77	8.8	62.1	0.35	25.2
Jan-78	8.7	62.5	0.35	24.8
Feb-78	8.8	62.9	0.35	25.1
Mar-78	8.8	63.4	0.36	24.7
Apr-78	8.8	63.9	0.36	24.6
May-78	8.8	64.5	0.36	24.4
Jun-78	9.1	65.2	0.37	24.7
Jul-78	9.0	65.7	0.37	24.3
Aug-78	9.1	66.0	0.37	24.4
Sep-78	9.2	66.5	0.37	24.5
Oct-78	9.2	67.1	0.38	24.4
Nov-78	9.2	67.4	0.38	24.3
Dec-78	9.5	67.7	0.38	24.9
Jan-79	9.5	68.3	0.38	24.7
Feb-79	9.7	69.1	0.39	25.0
Mar-79	9.8	69.8	0.39	25.1
Apr-79	10.3	70.6	0.40	26.1
May-79	10.7	71.5	0.40	26.7
Jun-79	11.7	72.3	0.41	28.9
Jul-79	13.4	73.1	0.41	32.7
Aug-79	14.0	73.8	0.41	33.8
Sep-79	14.6	74.6	0.42	34.8
Oct-79	15.1	75.2	0.42	35.8
Nov-79	15.5	75.9	0.43	36.5
Dec-79	17.0	76.7	0.43	39.6
Jan-80	17.9	77.8	0.44	40.9
Feb-80	18.8	78.9	0.44	42.5
Mar-80	19.3	80.1	0.45	43.1
Apr-80	20.3	81.0	0.45	44.7
May-80	21.0	81.8	0.46	45.8
Jun-80	21.5	82.7	0.46	46.4
Jul-80	22.3	82.7	0.46	48.0
Aug-80	22.6	83.3	0.47	48.4
Sep-80	22.6	84.0	0.47	47.9
Oct-80	23.2	84.8	0.48	48.8
Nov-80	23.9	85.5	0.48	49.9
Dec-80	25.8	86.3	0.48	53.3
Jan-81	28.9	87.0	0.49	59.1
Feb-81	34.1	87.9	0.49	69.3

Mar-81	34.7	88.5	0.50	69.9
Apr-81	34.1	89.1	0.50	68.1
May-81	32.7	89.8	0.50	64.9
Jun-81	31.7	90.6	0.51	62.4
Jul-81	31.1	91.6	0.51	60.6
Aug-81	31.1	92.3	0.52	60.1
Sep-81	31.1	93.2	0.52	59.6
Oct-81	31.0	93.4	0.52	59.2
Nov-81	31.0	93.7	0.53	59.0
Dec-81	30.7	94.0	0.53	58.3
Jan-82	33.9	94.3	0.53	64.0
Feb-82	31.6	94.6	0.53	59.5
Mar-82	28.5	94.5	0.53	53.7
Apr-82	33.5	94.9	0.53	62.8
May-82	35.9	95.8	0.54	66.9
Jun-82	35.1	97.0	0.54	64.5
Jul-82	34.2	97.5	0.55	62.5
Aug-82	34.0	97.7	0.55	62.0
Sep-82	35.6	97.9	0.55	64.9
Oct-82	35.7	98.2	0.55	64.8
Nov-82	34.2	98.0	0.55	62.1
Dec-82	31.7	97.6	0.55	57.9
Jan-83	31.2	97.8	0.55	56.9
Feb-83	29.0	97.9	0.55	52.7
Mar-83	28.6	97.9	0.55	52.1
Apr-83	30.6	98.6	0.55	55.4
May-83	30.0	99.2	0.56	53.9
Jun-83	31.0	99.5	0.56	55.6
Jul-83	31.7	99.9	0.56	56.5
Aug-83	31.9	100.2	0.56	56.8
Sep-83	31.1	100.7	0.56	55.1
Oct-83	30.4	101.0	0.57	53.7
Nov-83	29.8	101.2	0.57	52.6
Dec-83	29.2	101.3	0.57	51.5
Jan-84	29.7	101.9	0.57	52.0
Feb-84	30.2	102.4	0.57	52.6
Mar-84	30.8	102.6	0.58	53.5
Apr-84	30.6	103.1	0.58	52.9
May-84	30.7	103.4	0.58	52.9
Jun-84	29.9	103.7	0.58	51.3
Jul-84	28.7	104.1	0.58	49.2
Aug-84	29.2	104.5	0.59	49.9
Sep-84	29.4	105.0	0.59	49.9
Oct-84	28.6	105.3	0.59	48.4
Nov-84	28.0	105.3	0.59	47.4
Dec-84	26.7	105.3	0.59	45.1

Jan-85	25.9	105.5	0.59	43.7
Feb-85	27.3	106.0	0.59	46.0
Mar-85	28.5	106.4	0.60	47.8
Apr-85	28.6	106.9	0.60	47.7
May-85	27.6	107.3	0.60	45.9
Jun-85	27.1	107.6	0.60	45.0
Jul-85	27.2	107.8	0.60	45.0
Aug-85	27.6	108.0	0.61	45.5
Sep-85	28.5	108.3	0.61	47.0
Oct-85	29.5	108.7	0.61	48.5
Nov-85	30.9	109.0	0.61	50.5
Dec-85	27.5	109.3	0.61	44.8
Jan-86	22.9	109.6	0.61	37.3
Feb-86	15.5	109.3	0.61	25.2
Mar-86	12.6	108.8	0.61	20.7
Apr-86	12.8	108.6	0.61	21.1
May-86	15.4	108.9	0.61	25.2
Jun-86	13.4	109.5	0.61	21.9
Jul-86	11.6	109.5	0.61	18.9
Aug-86	15.1	109.7	0.62	24.5
Sep-86	14.9	110.2	0.62	24.1
Oct-86	14.9	110.3	0.62	24.1
Nov-86	15.2	110.4	0.62	24.6
Dec-86	16.1	110.5	0.62	26.0
Jan-87	18.7	111.2	0.62	29.9
Feb-87	17.8	111.6	0.63	28.4
Mar-87	18.3	112.1	0.63	29.1
Apr-87	18.7	112.7	0.63	29.6
May-87	19.4	113.1	0.63	30.6
Jun-87	20.1	113.5	0.64	31.5
Jul-87	21.3	113.8	0.64	33.4
Aug-87	20.3	114.4	0.64	31.7
Sep-87	19.5	115.0	0.64	30.3
Oct-87	19.9	115.3	0.65	30.7
Nov-87	18.9	115.4	0.65	29.1
Dec-87	17.3	115.4	0.65	26.7
Jan-88	17.1	115.7	0.65	26.4
Feb-88	16.8	116.0	0.65	25.8
Mar-88	16.2	116.5	0.65	24.8
Apr-88	17.9	117.1	0.66	27.2
May-88	17.4	117.5	0.66	26.4
Jun-88	16.5	118.0	0.66	25.0
Jul-88	15.5	118.5	0.66	23.3
Aug-88	15.5	119.0	0.67	23.3
Sep-88	14.5	119.8	0.67	21.6
Oct-88	13.8	120.2	0.67	20.4

Nov-88	14.1	120.3	0.67	21.0
Dec-88	16.4	120.5	0.68	24.2
Jan-89	18.0	121.1	0.68	26.5
Feb-89	17.9	121.6	0.68	26.3
Mar-89	19.5	122.3	0.69	28.4
Apr-89	21.1	123.1	0.69	30.5
May-89	20.1	123.8	0.69	29.0
Jun-89	20.1	124.1	0.70	28.8
Jul-89	19.8	124.4	0.70	28.4
Aug-89	18.6	124.6	0.70	26.6
Sep-89	19.6	125.0	0.70	27.9
Oct-89	20.1	125.6	0.70	28.5
Nov-89	19.9	125.9	0.71	28.1
Dec-89	21.1	126.1	0.71	29.8
Jan-90	22.9	127.4	0.71	32.0
Feb-90	22.1	128.0	0.72	30.8
Mar-90	20.4	128.7	0.72	28.2
Apr-90	18.4	128.9	0.72	25.5
May-90	18.2	129.2	0.72	25.1
Jun-90	16.7	129.9	0.73	22.9
Jul-90	18.5	130.4	0.73	25.2
Aug-90	27.3	131.6	0.74	37.0
Sep-90	33.5	132.7	0.74	45.0
Oct-90	36.0	133.5	0.75	48.1
Nov-90	32.3	133.8	0.75	43.1
Dec-90	27.3	133.8	0.75	36.4
Jan-91	25.2	134.6	0.75	33.4
Feb-91	20.5	134.8	0.76	27.1
Mar-91	19.9	135.0	0.76	26.3
Apr-91	20.8	135.2	0.76	27.5
May-91	21.2	135.6	0.76	27.9
Jun-91	20.2	136.0	0.76	26.5
Jul-91	21.4	136.2	0.76	28.0
Aug-91	21.7	136.6	0.77	28.3
Sep-91	21.9	137.2	0.77	28.4
Oct-91	23.2	137.4	0.77	30.1
Nov-91	22.5	137.8	0.77	29.1
Dec-91	19.5	137.9	0.77	25.2
Jan-92	18.8	138.1	0.77	24.3
Feb-92	19.0	138.6	0.78	24.5
Mar-92	18.9	139.3	0.78	24.2
Apr-92	20.2	139.5	0.78	25.9
May-92	21.0	139.7	0.78	26.8
Jun-92	22.4	140.2	0.79	28.5
Jul-92	21.8	140.5	0.79	27.6
Aug-92	21.3	140.9	0.79	27.0

Sep-92	21.9	141.3	0.79	27.6
Oct-92	21.7	141.8	0.80	27.3
Nov-92	20.3	142.0	0.80	25.5
Dec-92	19.4	141.9	0.80	24.4
Jan-93	19.0	142.6	0.80	23.8
Feb-93	20.1	143.1	0.80	25.0
Mar-93	20.3	143.6	0.81	25.2
Apr-93	20.3	144.0	0.81	25.1
May-93	20.0	144.2	0.81	24.7
Jun-93	19.1	144.4	0.81	23.6
Jul-93	17.9	144.4	0.81	22.1
Aug-93	18.0	144.8	0.81	22.2
Sep-93	17.5	145.1	0.81	21.5
Oct-93	18.2	145.7	0.82	22.2
Nov-93	16.6	145.8	0.82	20.3
Dec-93	14.5	145.8	0.82	17.8
Jan-94	15.0	146.2	0.82	18.3
Feb-94	14.8	146.7	0.82	18.0
Mar-94	14.7	147.2	0.83	17.8
Apr-94	16.4	147.4	0.83	19.9
May-94	17.9	147.5	0.83	21.6
Jun-94	19.1	148.0	0.83	23.0
Jul-94	19.7	148.4	0.83	23.6
Aug-94	18.4	149.0	0.84	22.0
Sep-94	17.5	149.4	0.84	20.8
Oct-94	17.7	149.5	0.84	21.1
Nov-94	18.1	149.7	0.84	21.5
Dec-94	17.2	149.7	0.84	20.4
Jan-95	18.0	150.3	0.84	21.4
Feb-95	18.6	150.9	0.85	21.9
Mar-95	18.5	151.4	0.85	21.8
Apr-95	19.9	151.9	0.85	23.4
May-95	19.7	152.2	0.85	23.1
Jun-95	18.5	152.5	0.86	21.6
Jul-95	17.3	152.5	0.86	20.3
Aug-95	18.0	152.9	0.86	21.0
Sep-95	18.2	153.2	0.86	21.2
Oct-95	17.4	153.7	0.86	20.2
Nov-95	18.0	153.6	0.86	20.9
Dec-95	19.0	153.5	0.86	22.1
Jan-96	18.9	154.4	0.87	21.8
Feb-96	19.1	154.9	0.87	22.0
Mar-96	21.3	155.7	0.87	24.4
Apr-96	23.5	156.3	0.88	26.8
May-96	21.2	156.6	0.88	24.1
Jun-96	20.4	156.7	0.88	23.2

Jul-96	21.3	157.0	0.88	24.2
Aug-96	21.9	157.3	0.88	24.8
Sep-96	24.0	157.8	0.89	27.1
Oct-96	24.9	158.3	0.89	28.0
Nov-96	23.7	158.6	0.89	26.7
Dec-96	25.2	158.6	0.89	28.4
Jan-97	25.1	159.1	0.89	28.2
Feb-97	22.2	159.6	0.90	24.8
Mar-97	21.0	160.0	0.90	23.4
Apr-97	19.7	160.2	0.90	21.9
May-97	20.8	160.1	0.90	23.2
Jun-97	19.3	160.3	0.90	21.4
Jul-97	19.7	160.5	0.90	21.8
Aug-97	20.0	160.8	0.90	22.1
Sep-97	19.8	161.2	0.90	21.9
Oct-97	21.3	161.6	0.91	23.5
Nov-97	20.2	161.5	0.91	22.3
Dec-97	18.3	161.3	0.90	20.3
Jan-98	16.7	161.6	0.91	18.4
Feb-98	16.1	161.9	0.91	17.7
Mar-98	15.1	162.2	0.91	16.6
Apr-98	15.4	162.5	0.91	16.8
May-98	14.9	162.8	0.91	16.3
Jun-98	13.7	163.0	0.91	15.0
Jul-98	14.2	163.2	0.92	15.5
Aug-98	13.5	163.4	0.92	14.7
Sep-98	15.0	163.6	0.92	16.4
Oct-98	14.5	164.0	0.92	15.7
Nov-98	13.0	164.0	0.92	14.1
Dec-98	11.4	163.9	0.92	12.3
Jan-99	12.5	164.3	0.92	13.6
Feb-99	12.0	164.5	0.92	13.0
Mar-99	14.7	165.0	0.93	15.9
Apr-99	17.3	166.2	0.93	18.6
May-99	17.7	166.2	0.93	19.0
Jun-99	17.9	166.2	0.93	19.2
Jul-99	20.1	166.7	0.93	21.5
Aug-99	21.3	167.1	0.94	22.7
Sep-99	23.8	167.9	0.94	25.3
Oct-99	22.7	168.2	0.94	24.1
Nov-99	25.0	168.3	0.94	26.5
Dec-99	26.1	168.3	0.94	27.7
Jan-00	27.3	168.8	0.95	28.8
Feb-00	29.4	169.8	0.95	30.8
Mar-00	29.8	171.2	0.96	31.1
Apr-00	25.7	171.3	0.96	26.8

May-00	28.8	171.5	0.96	29.9
Jun-00	31.8	172.4	0.97	32.9
Jul-00	29.7	172.8	0.97	30.6
Aug-00	31.3	172.8	0.97	32.3
Sep-00	33.9	173.7	0.97	34.8
Oct-00	33.1	174.0	0.98	33.9
Nov-00	34.4	174.1	0.98	35.3
Dec-00	28.4	174.0	0.98	29.1
Jan-01	29.6	175.1	0.98	30.1
Feb-01	29.6	175.8	0.99	30.0
Mar-01	27.3	176.2	0.99	27.6
Apr-01	27.5	176.9	0.99	27.7
May-01	28.6	177.7	1.00	28.7
Jun-01	27.6	178.0	1.00	27.6
Jul-01	26.4	177.5	1.00	26.5
Aug-01	27.4	177.5	1.00	27.5
Sep-01	26.2	178.3	1.00	26.2
Oct-01	22.2	177.7		
Nov-01	19.6	177.4		
Dec-01	19.4	176.7		
Jan-02	19.7	177.1		
Feb-02	20.7	177.8		
Mar-02	24.5	178.8		
Apr-02	26.2	179.8		
May-02	27.0	179.8		
Jun-02	25.5	179.9		
Jul-02	27.0	180.1		
Aug-02	28.4	180.7		
Sep-02	29.7	181.0		
Oct-02	28.8	181.3		
Nov-02	26.4	181.3		
Dec-02	29.5	180.9		
Jan-03	33.0	181.7		
Feb-03	35.8	183.1		
Mar-03	33.5	184.2		
Apr-03	28.2	183.8		
May-03	28.1	183.5		
Jun-03	30.7	183.7		
Jul-03	30.8	183.9		
Aug-03	31.6	184.6		
Sep-03	28.3	185.2		
Oct-03	30.3	185.0		
Nov-03	31.1	184.5		
Dec-03	32.1	184.3		
Jan-04	34.3	185.2		
Feb-04	34.7	186.2		

Mar-04	36.7	187.4
Apr-04	36.8	188.0
May-04	40.3	189.1
Jun-04	38.0	189.7
Jul-04	40.8	189.4
Aug-04	44.9	189.5
Sep-04	45.9	189.9
Oct-04	53.3	190.9
Nov-04	48.5	191.0
Dec-04	43.2	190.3
Jan-05	46.8	190.7
Feb-05	48.2	191.8
Mar-05	54.2	193.3
Apr-05	53.0	194.6
May-05	49.8	194.4
Jun-05	56.4	194.5
Jul-05	59.0	195.4
Aug-05	65.0	196.4
Sep-05	65.6	198.8
Oct-05	62.3	199.2
Nov-05	58.3	197.6
Dec-05	59.4	196.8
Jan-06	65.5	198.3
Feb-06	61.6	198.7
Mar-06	62.7	199.8
Apr-06	69.4	201.5
May-06	70.8	202.5
Jun-06	71.0	202.9
Jul-06	74.4	203.5
Aug-06	73.0	203.9
Sep-06	63.8	202.9
Oct-06	58.9	201.8
Nov-06	59.1	201.5
Dec-06	62.0	201.8
Jan-07	54.5	202.4
Feb-07	59.3	203.5
Mar-07	60.4	205.4
Apr-07	64.0	206.7
May-07	63.5	207.9
Jun-07	67.5	208.4
Jul-07	74.1	208.3
Aug-07	72.4	207.9
Sep-07	79.9	208.5
Oct-07	85.8	208.9
Nov-07	94.8	210.2
Dec-07	91.7	210.0

Jan-08	93.0	211.1
Feb-08	95.4	211.7
Mar-08	105.5	213.5
Apr-08	112.6	214.8
May-08	125.4	216.6
Jun-08	133.9	218.8
Jul-08	133.4	220.0
Aug-08	116.7	219.1
Sep-08	104.1	218.8
Oct-08	76.6	216.6
Nov-08	57.3	212.4
Dec-08	41.1	210.2
Jan-09	41.7	211.1
Feb-09	39.1	212.2
Mar-09	47.9	212.7
Apr-09	49.7	213.2
May-09	59.0	213.9
Jun-09	69.6	215.7
Jul-09	64.2	215.4
Aug-09	71.1	215.8
Sep-09	69.4	216.0
Oct-09	75.7	216.2
Nov-09	78.0	216.3
Dec-09	74.5	215.9
Jan-10	78.3	216.7
Feb-10	76.4	216.7
Mar-10	81.2	217.6
Apr-10	84.3	218.0
May-10	73.7	218.2
Jun-10	75.3	218.0
Jul-10	76.3	218.0
Aug-10	76.6	218.3
Sep-10	75.2	218.4
Oct-10	81.9	218.7
Nov-10	84.3	218.8
Dec-10	89.2	219.2
Jan-11	89.2	220.2
Feb-11	88.6	221.3
Mar-11	102.9	223.5
Apr-11	109.5	224.9
May-11	100.9	226.0
Jun-11	96.3	225.7
Jul-11	97.3	225.9
Aug-11	86.3	226.5
Sep-11	85.5	226.9
Oct-11	86.3	226.4

Nov-11	97.2	226.2
Dec-11	98.6	225.7

[3] Monthly nominal oil prices are adapted from http://www.eia.gov/dnav/pet/hist/LeafHandler.ashx?n=PET&s=RWTC&f=M

[4] CPIs are adapted from http://www.bls.gov/cpi/

Vita

Yuanyuan Shuai was born in Jiangxi Province, People's Republic of China in 1984. She received a bachelor of science degree in marine and offshore engineering from China University of Petroleum (Dongying) in July 2005. She earned her master degree from China University of Geosciences (Beijing) as a reservoir engineering student in January 2008. She is currently a candidate for the degree of Doctor of Philosophy in Petroleum Engineering at Louisiana State University, which is expected to be awarded in August 2012.